



# Transportation Research Division



## Technical Report 14-14

*Splicing and Local Reinforcement of Concrete Filled FRP Tubes*

Technical Report Documentation Page

1. Report No. ME 14-14	2.	3. Recipient's Accession No.	
4. Title and Subtitle Splicing and Local Reinforcement of Concrete Filled FRP Tubes		5. Report Date January 2014	
		6.	
7. Author(s) Heather Parry, Graduate Research Assistant Xenia Rofes, P.E. Roberto Lopez-Anido, Ph.D., P.E.		8. Performing Organization Report No. 14-12-1023A	
9. Performing Organization Name and Address University of Maine		10. Project/Task/Work Unit No. Project 17891.00	
		11. Contract © or Grant (G) No. Contract # 20111223*2878	
12. Sponsoring Organization Name and Address Maine Department of Transportation 16 State House Station Augusta, Maine 04333		13. Type of Report and Period Covered	
		14. Sponsoring Agency Code	
15. Supplementary Notes			
16. Abstract (Limit 200 words)			
<p>This report includes fulfillment of Task 1 of a multi-task contract to further enhance concrete filled FRP tubes, or the Bridge in a Backpack. Task 1 investigates and develops a feasible solution for splicing the concrete filled FRP tubes. This will allow use of this bridge type in longer spans.</p> <p>A splicing solution using a combination of internal rebar reinforcing and an outer FRP collar to connect the two sides of the arch is developed and tested. The outer collar sustains the loads during filling of the arch with concrete. The internal rebar provides the long term load carrying capacity with all dead and live loads.</p> <p>Results from the laboratory tests and analysis show the splice detail is structurally adequate but is conservative.</p>			
17. Document Analysis/Descriptors Concrete filled fiber reinforced polymer tubes, arch bridge, splicing		18. Availability Statement	
19. Security Class (this report)	20. Security Class (this page)	21. No. of Pages 153	22. Price

**SPLICING AND LOCAL REINFORCEMENT OF  
CONCRETE FILLED FRP TUBES (CFFTS)**

**Prepared for:**

**Dale Peabody**

Maine Department of Transportation  
Office of Safety, Training, and Research  
16 State House Station  
Augusta, ME 04333  
(207) 624-3305

**Advanced Structures and Composites Center**

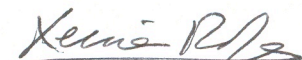
**Report Number: 14-12-1023A**

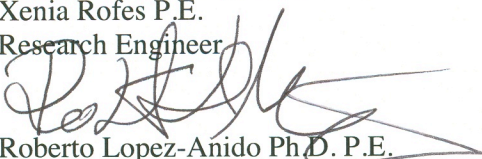
January 17, 2014

This report shall not be reproduced, except in full, without the written approval of  
**Advanced Structures and Composites Center.**

**Prepared by:**

Heather Parry  
Graduate Research Assistant

  
Xenia Rofes P.E.  
Research Engineer

  
Roberto Lopez-Anido Ph.D. P.E.  
Professor of Civil and Environmental Engineering

**Reviewed by:**



Keenan Goslin P.E.  
Structural Engineer



William Davids Ph.D. P.E.  
Professor of Civil and Environmental  
Engineering

*An ISO 17025 accredited testing laboratory  
Accredited by international Accreditation Service*



## **EXECUTIVE SUMMARY**

Research is currently underway to create a feasible solution for splicing concrete-filled fiber-reinforced polymer (FRP) tubes (CFFTs). This technology is used in bridge construction where tubular FRP arches are placed parallel to the roadway, and filled with a self-consolidating concrete (SCC) mix on site. The tubes have an FRP deck fastened on the top side, a granular backfill, and a bituminous pavement. The FRP tubes act as exoskeletal reinforcement for the concrete. The advantages over typical steel or concrete bridges can include speed of construction, low maintenance costs, and cost reduction for the appropriate site conditions. AASHTO specifications for these arches were approved in the summer of 2012. One current limitation of the technology is the ability to ship longer arches. A splice design is described in this report, which facilitates use of long-span arches.

A splicing solution using a combination of internal rebar reinforcing and an outer FRP collar to connect the two sides of the arch is considered. The internal solution is being evaluated using three different types of reinforcement: 1) Steel rebar (baseline material); 2) E-glass fiber reinforced rebar; and 3) Carbon fiber composite cable (CFCC). The goal is to develop an all FRP composite bridge solution. The internal reinforcing will carry all of the loads during the bridge service life. The external reinforcing for the splice will consist of an FRP composite collar attached with mechanical fasteners and will sustain the loads due to erection, concrete filling of the tubes, and associated construction live loads. The mechanically fastened splice eliminates the need for surface preparation and adhesive bonding in the field, speeding construction and enabling efficient quality control of the installation process.

This report investigates a splice design that will be used for implementation in construction of longer span arch bridges. The tested splice design incorporates a steel rebar cage for internal reinforcing and a mechanically fastened external reinforcing collar. The experimental work included: collar fastener bearing strength, internal rebar pullout strength, and hollow CFFT beam spliced with the external reinforcing collar. The full-scale splice with internal and external reinforcing was experimentally validated in CFFT beam tests and arch tests. From the experimental results it can be concluded that the splice is structurally adequate, but is conservative. Further testing and analysis should be conducted to improve on the proposed splice design.

## TABLE OF CONTENTS

EXECUTIVE SUMMARY .....	iv
LIST OF TABLES .....	ix
LIST OF FIGURES .....	x
CHAPTER 1	
1.1 Background .....	1
1.2 Significance of Research and Objectives.....	2
1.3 Design Approach and Construction Sequence .....	3
1.3.1. Temporary Loads (Construction).....	3
1.3.2. Bridge Service Loads .....	4
1.3.3. Collar Design .....	5
1.3.4. Internal Reinforcing Design .....	5
1.4 Literature Review .....	6
CHAPTER 2	
2.1 Introduction .....	8
2.2 Testing Materials and Equipment.....	8
2.3 Material Level Joint Tests.....	9
2.3.1. Single Fastener Lap Shear Testing of Hybrid Material Individual Layers.....	10
2.3.2. Single Fastener Lap Shear Testing of Braided Collar Material.....	24
2.3.3. Multi Fastener Lap Shear Tests .....	30
2.4 Fastener Testing Summary & Conclusion .....	37
CHAPTER 3	
3.1 Introduction .....	38

3.2	Testing Materials and Specimen Fabrication .....	38
3.3	Test Configuration .....	41
3.4	Estimation of Embedment Lengths Used in Test Program.....	42
3.5	Carbon Fiber Composite Cable (CFCC) Pullout Tests.....	46
3.6	CFCC Embedment Length Results and Conclusions .....	50
CHAPTER 4		
4.1	Introduction .....	52
4.2	Design of External Reinforcing Collar .....	53
4.3	Beam and Collar Manufacturing.....	56
4.4	Installation of the External Collar .....	57
4.5	Fill Load Testing (Hollow Beam Testing).....	60
4.6	Arch Manufacturing.....	66
4.7	Summary of Results and Recommendations .....	70
CHAPTER 5		
5.1	Introduction .....	71
5.2	Splice Design for Long-Term and Live Loads .....	71
5.3	Spliced Beam Tests (Concrete Filled) .....	74
5.4	Summary of Beam Test Results and Recommendations .....	97
CHAPTER 6		
6.1	Introduction .....	99
6.2	Arch Filling.....	99
6.3	Spliced Arch Testing.....	100

6.4	Summary of Arch Test Results .....	110
CHAPTER 7		
7.1	Conclusions.....	111
7.2	Recommendations.....	113
7.3	Future Work.....	114
REFERENCES.....		115
Appendix A: Pull out test for Steel/GFRP.....		117
Appendix B: Calculations for the CFCC Pullout Test .....		129
Appendix C: Moment-%strain plots .....		134
Biography of the Author .....		<b>Error! Bookmark not defined.</b>

## LIST OF TABLES

Table 2.1: Material Layups Tested .....	9
Table 2.2: Summary of single fastener tests with metal back plate .....	17
Table 2.3: Summary of single fastener hybrid coupons .....	29
Table 2.4: Multi-fastener test summary .....	35
Table 3.1: CFCC pullout test matrix .....	45
Table 3.2: Summary of CFCC pullout test.....	50
Table 3.3: % Strain in gauges down the bar line of CFCC specimens.....	50
Table 3.4: CFCC Test Summary.....	51
Table 4.1: Summary of manufactured beam specimens.....	60
Table 4.2: Summary of Hollow Beam Tests .....	66
Table 5.1: Summary of beam specimens tested .....	80
Table 5.2: Summary of the CFFT beam test .....	98
Table 6.1: Summary of the CFFT Arch tests.....	111
Table A.1: Summary of the rebar development lengths tested.....	118
Table A.2: Summary of E-glass fiber coupler tensions test.....	124
Table A.3: Summary of steel and E-glass fiber embedment length test.....	128

## LIST OF FIGURES

Figure 2.1: Fastener test configurations.....	10
Figure 2.2: Edge distances tested .....	12
Figure 2.3: A hybrid coupon in the single fastener test setup.....	13
Figure 2.4: 45 mm Hybrid coupon test setup on the 100kN Instron machine .....	15
Figure 2.5: Typical bearing failure of hybrid coupon (32 mm edge distance specimen)....	16
Figure 2.6: 1 Layer E-Glass fiber Load vs. Deformation plot .....	19
Figure 2.7: Two layer carbon fiber Load vs. Deformation plot.....	20
Figure 2.8: Hybrid (2 layer carbon, 1 layer E-glass). .....	20
Figure 2.9: Comparison of the three materials tested with same edge distance .....	21
Figure 2.10: Typical Load vs. Deformation plot for three different collar options .....	21
Figure 2.11: Hybrid specimen attached to E-glass fiber collar material .....	24
Figure 2.12: Two unbonded stacked composite shells for the collar in the bearing test setup.....	26
Figure 2.13: Comparison of rivet. Left - Rivet using washer .....	28
Figure 2.14: Two stacked collar layers tested against the hybrid composite .....	29
Figure 2.15: Failure of actual layup used in connection. Left- Collar layers peeling up, .....	30
Figure 2.16: Two fastener specimen .....	31
Figure 2.17: 2 Fastener specimen. Left- Specimen speckle pattern for digital image correlation. Right- Typical bearing failure of 2 fastener coupon.....	32
Figure 2.18: Strain distribution field for multi_5 two fastener specimen. ....	32
Figure 2.19: Three fastener specimen.....	34
Figure 2.20: Three fastener strain field for multi_9 specimen .....	35

Figure 2.21: Typical Load vs. Deformation for varying number of fasteners ..... 36

Figure 3.1: 1x7 CFCC strands, Left – 17 mm (0.677-in) CFCC used in pullout test, Right – 8 mm (0.295-in) CFCC spiral ..... 40

Figure 3.2: Pullout specimen before filling with concrete..... 40

Figure 3.3: Pullout test setup ..... 41

Figure 3.4: Strain gauge layout for pullout test..... 42

Figure 3.5: Example of embedment length in CFFT ..... 44

Figure 3.6: CFCC 36-in embedment length specimen. Top left- Specimen at beginning of test, Top right- Specimen being pulled from concrete at initial failure, some concrete cracking observed, Bottom left- Continued pullout after initial failure capacity reached, Bottom right- Final bar pullout..... 47

Figure 3.7: CFCC load vs. deformation comparison for the four development lengths ..... 49

Figure 4.1: RISA Model, 21 Nodes, 20 Elements ..... 54

Figure 4.2: Cross-section of fastener spacing around circumference of specimen. .... 55

Figure 4.3: Two sections of carbon fiber CFFT and the E-glass fiber collar..... 57

Figure 4.4: Beam manufacturing sequence. Top: Collar placed on half the beam, Middle: Left- Marking out the fastener placement, Middle- Collar attached to one side, Right- Attaching the rest of the rivets, Bottom: Fully attached collar with rivets..... 59

Figure 4.5: Shear and moment diagrams to determine fill test conditions..... 62

Figure 4.6: Hollow beam offset three point bend setup ..... 62

Figure 4.7: Load-deflection plot for Tube A tested to failure ..... 64

Figure 4.8: Buckling failure at location of load application..... 64

Figure 4.9: Load-deformation plot for Tube G..... 65

Figure 4.10: Arch manufacturing sequence, Top: Left – Arch with collar on,..... 68

Figure 4.11: Completed unfilled, spliced arches ..... 69

Figure 5.1: Cross-section of the connection..... 74

Figure 5.2: Elevation view of the complete splice design ..... 74

Figure 5.3: Shear and moment diagram for the filled beam test ..... 76

Figure 5.4: Offset three-point beam test setup..... 77

Figure 5.5: Location of the strain gauges on the beam cross-section..... 77

Figure 5.6: Strain gauge placement on the length of the beam specimen ..... 78

Figure 5.7: Gauge placement on outside edge of tension rebar, ..... 78

Figure 5.8: Top – Tube E with collar intact, Bottom – Tube D with collar cut  
circumferentially..... 79

Figure 5.9: Load-deformation plot for the Control specimen ..... 81

Figure 5.10: Control beam specimen before and after test,..... 82

Figure 5.11: Moment-% strain plot for the Control specimen North End gauges..... 82

Figure 5.12: Moment-% strain plot for the Control specimen North Rebar End gauges ..... 83

Figure 5.13: Moment-% strain plot for the Control specimen Mid-span gauges..... 83

Figure 5.14: Moment-% strain plot for the Control specimen South Rebar End gauges ..... 84

Figure 5.15: Moment-% strain plot for the Control specimen South End gauges..... 84

Figure 5.16: Load- deformation plot for beam specimens with the collar intact..... 86

Figure 5.17: Failed Tube F..... 86

Figure 5.18: Failed Tube G with collar removed, bearing failure of rivets through the CFFT  
and concrete section separated at centerline..... 87

Figure 5.19: Moment-% strain for Tube E North End ..... 88

Figure 5.20: Moment- % strain for Tube E North Rebar End..... 88

Figure 5.21: Moment-%Strain for Tube E Mid-span on collar..... 89

Figure 5.22: Moment-%Strain for Tube E South Rebar End..... 89

Figure 5.23: Moment-%Strain Tube E South End ..... 90

Figure 5.24: Load-deformation plot for #6 rebar tested in tension..... 91

Figure 5.25: Moment-% Strain for tension rebar in Tube E ..... 91

Figure 5.26: Load-deformation of beams with cut collar..... 93

Figure 5.27: Tube B cut collar section with some collar still attached after failure..... 93

Figure 5.28: Moment- % Strain for Tube D North End ..... 94

Figure 5.29: Moment-% Strain for Tube D North Rebar end ..... 94

Figure 5.30: Moment-%Strain Tube D South Rebar End ..... 95

Figure 5.31: Moment-%Strain Tube D South End..... 95

Figure 5.32: Load-deformation comparison of three specimen types tested. .... 96

Figure 6.1: Arch setup for filling with concrete from the side..... 100

Figure 6.2: Arch Instrumentation setup (looking East)..... 101

Figure 6.3: Actuator Load-Displacement relationship for each Arch ..... 102

Figure 6.4: Arch#1 Failure Mechanism..... 103

Figure 6.5: Arch#2 Splice behavior at crown with Closeup of Spreading Cut Collar..... 104

Figure 6.6: Applied Load vs. Vertical Deformation for Spliced Arches ..... 105

Figure 6.7: Applied Load vs. End Rotation for Spliced Arches..... 106

Figure 6.8: Applied Load versus Cross Section Strain North (N) and South (S) of the Splice  
for Arch#1..... 107

Figure 6.9: Applied Load versus Cross Section Strain North (N) and South (S) of the Splice  
for Arch#2..... 107

Figure 6.9: Applied Load versus Cross Section Strain at Crown Tension Rebar for Arch#1  
..... 108

Figure 6.10: Applied Load versus Cross Section Strain at North Shoulder ..... 109

Figure A.1: Steel T-plate to rebar connection..... 120

Figure A.2: Failure of steel rebar at welded connection..... 120

Figure A.3: Load vs deformation plot for steel rebar pullout test..... 121

Figure A.4: Left- Coupler attachment to E-glass bar ..... 123

Figure A.5: Mechanical coupler using two steel plates and a garolite..... 123

Figure A.6: 457 mm (18-in) E-glass fiber specimen..... 125

FigureA.7: Load vs deformation plot for E-glass bar specimens ..... 126

Figure C.8: Moment- % Strain plot for Tube C south end rebar gauges ..... 137

Figure C.9: Moment- % Strain plot for Tube C south end gauges..... 138

Figure C.10: Moment- % Strain plot for Tube F north end gauges ..... 138

Figure C.11: Moment- % Strain plot for Tube F north end rebar gauges..... 139

Figure C.12: Moment- % Strain plot for Tube F centerline (collar) gauges ..... 139

Figure C.13: Moment- % Strain plot for Tube F south end rebar gauges..... 140

Figure C.14: Moment- % Strain plot for Tube F south end gauges ..... 140

## **CHAPTER 1 INTRODUCTION**

### **1.1 Background**

Concrete-filled fiber-reinforced polymer (FRP) tubes (CFFTs) are used in bridge construction where tubular FRP arches are placed parallel to the roadway and filled with Self-Consolidating Concrete (SCC) on site. The FRP tubes act as the exo-skeletal longitudinal reinforcing, protection, and confinement for the concrete, increasing its durability and strength. The thin-walled hybrid composite tubes developed at the University of Maine are fabricated from a combination of E-glass and carbon fiber braid infused with vinyl ester resin (Dagher et al. 2012). The tubes have an FRP deck fastened on the topside, a granular backfill, and a bituminous pavement. The arch bridges are designed by Advanced Infrastructure Technologies, a company based in Orono, Maine, which also oversees arch fabrication and bridge construction.

In the arch bridge construction, longer spans are limited due to transportation constraints. The road width bounds the maximum size arch that can be shipped because wide loads require a police escort and can increase the bridge cost. This research investigates a feasible long-span solution by field-splicing concrete filled FRP tubes. The splice design followed the published AASHTO Guide Specification for CFFTs (AASHTO 2012). The AASHTO Guide Specification includes provisions for the analysis and design of CFFTs to be used as structural components in bridges. Advantages to using CFFTs in bridge construction versus traditional

materials include low maintenance costs, and for appropriate site conditions, increased speed of construction and price competitive on a first-cost basis.

## **1.2 Significance of Research and Objectives**

The goal of this research is to develop longer span composite arch bridges by investigating CFFT joining and load transfer at the joint. The splice design was separated into two loading conditions. The design loads include both temporary and service loads. The proposed splice solution incorporates an outer FRP shell or collar to connect the two arch sides and internal rebar reinforcing. The design is conservative because this is a proof of concept, and our goal is to develop a structurally adequate, easily fabricated and constructed solution that is ready for implementation.

The first loading condition experienced by the composite arch is the temporary or construction load case. The external reinforcing will carry the loads due to erection, concrete filling of the tubes, and the associated construction live loads. An external FRP collar used to join two sections of arch is investigated to be attached with mechanical fasteners. The mechanically fastened splice eliminates the need for surface preparation and adhesive bonding in the field, speeding construction and enabling efficient quality control of the installation process. Additional dead load due to soil and decking and live load are the second condition. To reinforce the concrete arch during this condition, an internal rebar cage is proposed. The internal cage was evaluated using three different types of reinforcement: 1) Steel rebar (baseline material); 2) E-glass fiber reinforced rebar; and 3) Carbon fiber composite cable (CFCC). The internally reinforced splice is

designed to carry all of the loads during the bridge service life. The design reinforcement combination of external collar and internal rebar was manufactured, tested, and then implemented to create longer span composite arch bridges.

### **1.3 Design Approach and Construction Sequence**

The design approach and construction sequence for the development of the CFFT joint connection were based on two load conditions, temporary construction loads, and permanent dead and live loads.

#### **1.3.1. Temporary Loads (Construction)**

The temporary loads acting on the splice will be carried by external collar reinforcement. The collar will be used to join the two sides of the arch before it is filled with concrete. Rows of 8 mm (5/16-in) blind mechanical fasteners will be used as the load transfer mechanism to carry the load from CFFT shell to the collar to the other CFFT shell. A design parameter for the collar and fasteners, bolt bearing capacity, was investigated. Using the LRFD Final Pre-standard for Pultruded Sections, fasteners were tested with varying bolt placement and material type. The bearing capacity of the braided arch material was tested. The first round of testing was done with a single fastener attached at varying edge distances. The specimens were tested in a single fastener lap shear configuration based on a modified version of ASTM D953. The materials tested were two layers of braided carbon fiber, a single layer constraint E-glass, and a hybrid material with two layers of carbon fiber and one layer of constraint E-glass. The hybrid material is currently used in the composite arch technology. After the single fastener tests were completed and the

fastener edge distance established, a row of fasteners with two and three bolts were tested in tension in the same lap shear configuration attached to a collar-like material. Recommendations for the collar layup were made based on results from the fastener bearing tests conducted.

Following fastener testing, three hollow CFFT specimens were manufactured and tested in a three-point offset bend test. The beams were tested to determine the nominal capacity of the external splice design during construction and concrete fill, and to ensure large permanent deflections did not occur when the beams were filled with concrete.

### **1.3.2. Bridge Service Loads**

Internal reinforcing bars and a spiral cage will be used inside the CFFTs to carry the service loads. The internal reinforcing is designed to carry the loads during the bridge's lifetime. The reinforcing design incorporates a spiral of the material (steel, E-glass, and CFCC, respectively), with six longitudinal bars placed circumferentially around the inside of the spiral. While the spiral maintains the proper bar spacing, spacers attached to the outer diameter maintain proper concrete clear cover. Embedment lengths were tested to determine the length of bar needed in either side of the CFFT connection and the bar material to be used for the splice. The load transfer mechanism is the bar embedment length in concrete. The length was determined by using the factored design loads provided by AIT and using ACI equations based on the stress in the bottom bar of the spiral cage. The design parameter for the internal reinforcing was the development length required to carry the design load. The reinforcing materials tested were steel (baseline

material), E-glass rebar, and CFCC. Bar pull out tests were completed using the three different materials with concentric bars sticking out either end. The specimens incorporated different embedment lengths and contained a spiral of the same material. After the specimens were tested a full splice was designed for use in straight beam and arch testing.

### **1.3.3. Collar Design**

The external reinforcing collar is to be placed at the location of the splice, in this case the apex or centerline of the arch. Designed to mimic the strength of an unspliced arch, the collar will carry a factored design moment of 4.9 kN-m (3.6 ft.-kips). Bearing test results from specimens of flat plate collar and tube material attached with a single fastener were used to determine the fastener bearing capacity and determine the number of fasteners to be used around the circumference and attach the collar to tube. The E-glass fiber collar overlaps the joint connecting two separate arch segments. The collar is made up of two un-bonded composite shells each with one layer of structural E-glass fiber and one layer constraint E-glass fiber. The length of the collar section is dependent on the number of fasteners used and required spacing. A minimum length collar of 254 mm (10-in) was deemed sufficient; the proposed design uses a 610 mm (24-in) collar for additional safety and stability the first round of testing.

### **1.3.4. Internal Reinforcing Design**

The internal reinforcing for the connection was designed to carry the bridge service loads. The design began by considering the dead and live loads that the

bridge would experience through its lifetime. The arch shape causes shear, axial, and moment reactions at the apex of the arch, directly affecting the splice. The goal was to design the embedment length for the rebar and spiral into each side of the tube. An interaction diagram was created using ACI 440 and ACI 318 to design the internal reinforcing for the section. Each of the three materials considered (steel, E-glass, and CFCC) had to be analyzed differently to find the number of bars and appropriate development length. ACI has equations to relate force or load carried to embedment length in concrete for both steel and E-glass. There have been few tests conducted using CFCC in concrete, and therefore a modified ACI 440 equation was used to predict the development length in concrete. The recommended embedment lengths were then tested in CFFT specimens and the actual values compared to predicted values. The strength of one bar in concrete was determined and then a conservative design was used based on the test results. Steel was chosen as the internal reinforcing material due to its availability, lower material costs, and predictability. The bars will transfer the permanent dead and live loads carried by the arch from one side of the arch to the other.

#### **1.4 Literature Review**

Splicing of CFFTs was investigated previously by Zhu (2006) comparing different techniques. Internal reinforcing for the splice-included post-tensioned steel bar, FRP bar, and external reinforcing with an FRP socket. The socket spliced the section similar to how two pipes fit together with a male and female end. The internal spliced longitudinal bars were grouted into the system, and failure occurred in the grout. The four splice systems tested lower than the control CFFT specimen,

and the post-tensioned specimen performed best. Zhu suggests that the splicing system benefits from FRP continuity and the system could be improved by combining methods, internal and external reinforcing (Zhu 2006).

An all FRP bridge system was suggested for design of this spliced connection to be consistent with current applications of the technology. Carbon fiber composite cable (CFCC), typically used to replace traditional steel in pre-stressed bridge systems, was investigated to be used as rebar due to its durability, lightweight, and ease of installation. Previous work conducted by Grace (2006) on the material used in concrete box beam bridges showed the CFCC is a suitable material for bridge applications (Grace 2006). The Maine Department of Transportation has started to implement the non-metallic, non-corrosive material, by installing CFCC strands in the Penobscot-Narrows cable-stayed bridge (Berube et al. 2008) and by building a post-tensioned concrete slab bridge incorporating CFCC (MaineDOT 2013). Since CFCC is fairly new to the market here in Maine, and using the material, as straight rebar has not been thoroughly investigated, further research was conducted using the CFCC in the splice design.

This research focuses on determining a conservative solution to be used to field splice long span arches. The splice incorporates a combination of internal and external reinforcing. The internal reinforcing can be made from steel, E-glass fiber rebar, or CFCC.

## **CHAPTER 2 MECHANICAL FASTENER BEARING STRENGTH TESTS**

### **2.1 Introduction**

The mechanical fastener bearing strength tests were conducted to determine the key parameters for the external reinforcing collar design for the splice. The activities to study the parameters adopted for the test were characterizing the bearing strength of the material, determining the edge distance for the fastener in the braided FRP, and determining the number of fasteners. Single fastener tests were conducted to characterize the bearing strength of the material and the edge distance. Two and three fasteners were tested in a row to characterize the bearing strength of multiple fasteners. These parameters studied were taken into account to determine the design strength of the splice connection as detailed later in Chapter 4.

### **2.2 Testing Materials and Equipment**

The fastener tests were performed using a lap shear configuration with tension loading. The specimens incorporated five materials combined in different configurations to mimic the collar attachment to the existing CFFT. The CFFT braided fiber materials used for this testing were an E-glass fiber constraint, E-glass fiber structural, carbon fiber structural, and a hybrid coupon material using the structural carbon fiber and constraint E-glass fiber. The potential collar braided fiber materials were made from structural E-glass fiber and constraint E-glass fiber. These potential collar materials were chosen based on manufacturing feasibility and cost, and included a single layer of E-glass structural braid combined with an E-glass constraint layer; three layers of E-glass structural braid combined with an E-glass

constraint layer; and two separate, un-bonded composite shells each consisting of a single layer of E-glass structural braid infused with an E-glass constraint layer. All materials are summarized in Table 2.1, and were infused and flat plates were manufactured using the Vacuum Assisted Resin Transfer Molding (VARTM) process and Derakane 610C vinyl ester resin. The flat plate layups of the different materials were water jet cut to 254 mm (10-in) long by 101 mm (4-in) wide specimens. Huck Blind Oversized Mechanically (BOM) locked fasteners, 8 mm (5/16-in) diameter, 18 mm (0.695-in) long unclamped, were utilized for testing. The specimens were connected with single or multiple fasteners and then tested in tension using a 100 kN (22 kip) servo-hydraulic Instron machine (AS 108 & 269 load cell).

Table 2.1: Material Layups Tested

<b>Arch (CFFT) Materials</b>	<b>Collar Materials</b>
1 Layer E-glass Constraint	1 Layer E-glass Constraint 1 Layer E-glass Structural
2 Layers Carbon Fiber Structural	2 stacked composite shells (un-bonded): 1 Layer E-glass Constraint 1 Layer E-glass Structural
<i>Hybrid:</i> 1 Layer E-glass Constraint 2 Layers Carbon Fiber Structural	1 Layer E-glass Constraint 3 Layer E-glass Structural

### 2.3 Material Level Joint Tests

The material level joint tests utilized reinforcing materials that are typical in CFFT construction for bridge applications. Different numbers of bolts in a row were tested to determine the effect of multiple fasteners. The progression of fastener

testing from one fastener, which incorporated different materials and edge distances, to multiple fasteners can be seen in Figure 2.1. Single fastener configurations were used to determine the material bearing strengths and effect of fastener edge distance. The hybrid materials were then used to test multiple (2 and 3) fasteners in a row. A modified version of ASTM D 953 was adopted as a guideline to conduct the single and multi-fastener testing, and is explained more in detail in Section 2.3.1. The samples were then tested using the 100 kN (22 kip) servo-hydraulic Instron machine.

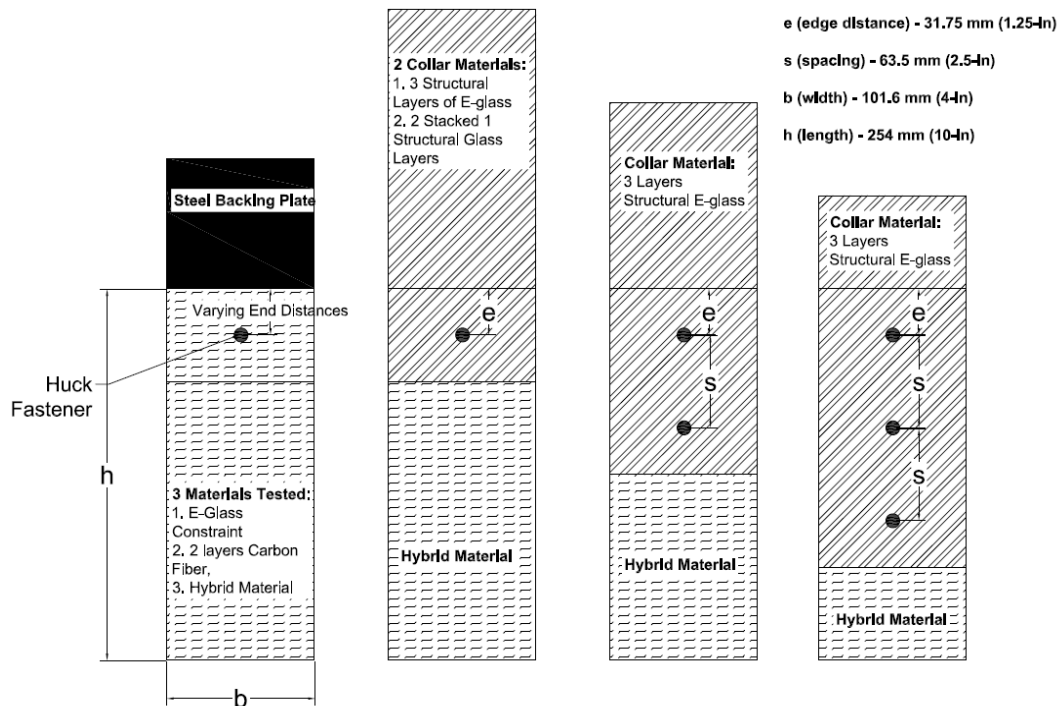


Figure 2.1: Fastener test configurations.

### 2.3.1. Single Fastener Lap Shear Testing of Hybrid Material Individual Layers

The single fastener tests were conducted to characterize the bearing strength of the material and the required edge distance. According to ASTM D 953 the edge

distance is the distance from the center of the bearing hole to the edge of the specimen in the direction of the principal stress.

The fastener tests were conducted using three different material types associated with arch manufacturing to determine the bearing strength of the hybrid composite and the relative contributions of the components. One layer of E-glass fiber, two layers of carbon fiber, and a hybrid material consisting of one layer of E-glass fiber, and two layers of carbon fiber were tested for bearing strength and edge distance. The braid angle of the E-glass constraint layer is 75 degrees and the material is about 11.7 N/m (0.80 lb./ft.), the braid angle of the carbon fiber was 22 degrees and the material weighs about 6.7 N/m (0.46lb/ft.). 10 mm (0.375-in) holes were drilled in the specimens at varying edge distances. The edge distances used for testing were four times the fastener diameter 32 mm (1.25-in), 45 mm (1.75-in), and 57 (2.25-in) as shown in Figure 2.2 based on the design requirements given by the Pre-standard for Load & Resistance Factor Design (LRFD) of Pultruded Fiber Reinforced Polymer (FRP) Structures *Table 8.1 Minimum requirements for bolted connection geometries* (ASCE 2010). The edge distance ratios chosen for testing were  $4d$  (minimum),  $5.5d$ , and  $7d$ , where  $d$  is the fastener diameter.

The specimens were attached to a 5 mm (3/16-in) thick steel backing plate using the Huck blind fasteners and a pneudraulic rivet gun. The steel backing plate ensured a bearing failure in the FRP material. An 18 gauge steel washer or washer plate was placed under the head of the blind fastener to protect the FRP material from fracturing during impact from the rivet gun. The specimens were tested in tension using a 100 kN (22 kip) Instron servo-hydraulic testing frame. The steel

plate was lined up in the top grips and the grips tightened. The free FRP specimen was then lined up with the bottom grips to ensure no torsion was introduced in the specimen while testing and the grips were tightened and the specimen loaded. The coupon in the test setup can be seen in Figure 2.3.

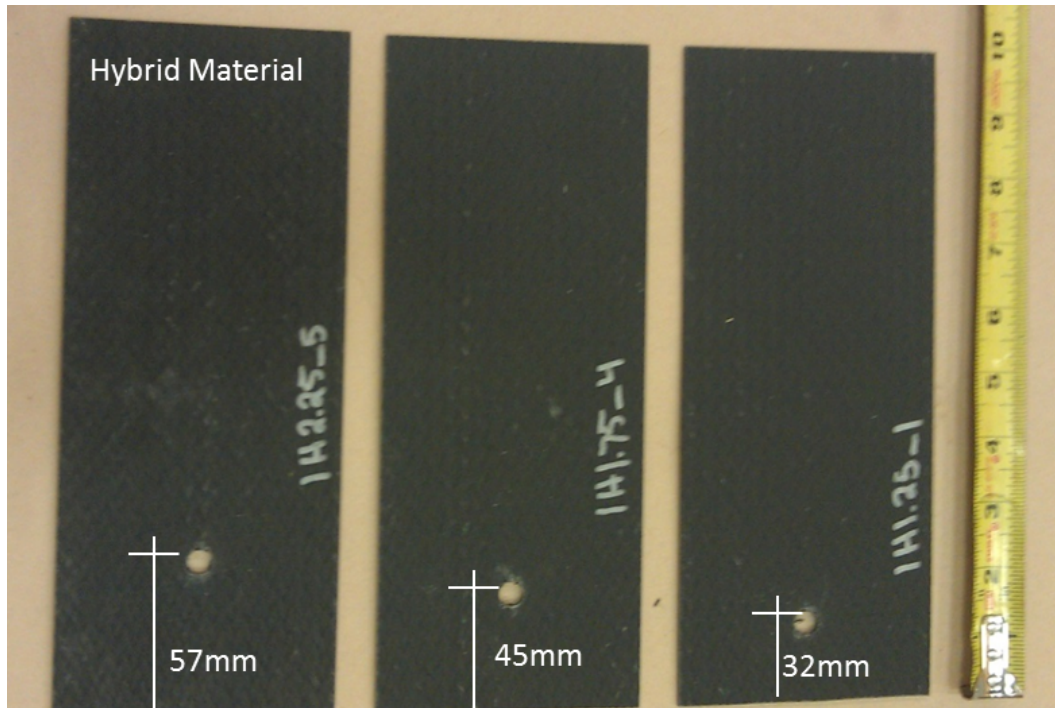


Figure 2.2: Edge distances tested.

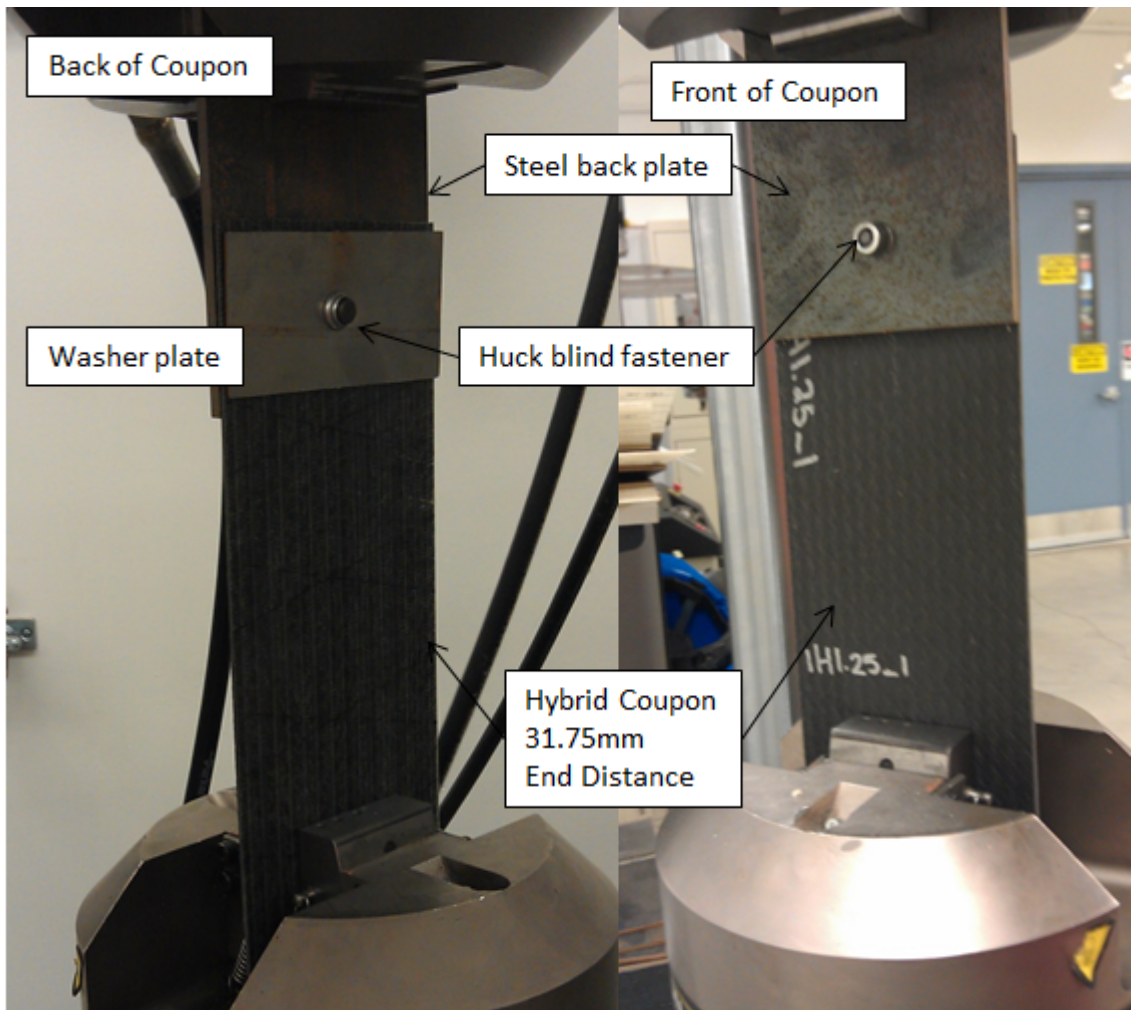


Figure 2.3: A hybrid coupon in the single fastener test setup.

The single fastener test was based on a modified version of the ASTM D 953 test procedure. ASTM D 953 provided guidance for the loading rate and the test configuration. The standard specifies a fixture where the FRP material is sandwiched between two steel plates; however, the single fastener test conducted used one steel plate and one FRP laminate to mimic the unsymmetrical load transfer the collar connection would see in the field. With the braided materials used in the arch a greater width and length were used to engage a sufficient number of fiber tows in load transfer.

According to ASTM D 953, the minimum dimensions when testing bearing strength are: 25 mm (1-in) width, 19 mm (0.75-in) edge distance, 111 mm (4 3/4-in) length, and 3 mm (1/8-in) thickness. The geometric parameters adopted for this test, as previously stated were a 102 mm (4-in) width, three edge distances, and a 254 mm (10-in) length to engage more tows through the section. The nominal thickness of the laminate was 1 mm (0.04-in) for E-glass fiber, 2 mm (0.06-in) for the two layers of carbon fiber, and 3 mm (0.1-in) for the hybrid layup. Each material sample set incorporated the three different edge distances. Five samples of one layer of E-glass braid with an average thickness of 1 mm (0.04-in) were tested using the three specified edge distances. Five samples of two-layer carbon fiber with an average thickness of 2 mm (0.06-in) were tested with the three different edge distances. The two materials were combined in a hybrid layup as is done for arch construction with an average thickness of 3 mm (0.1-in) and the three edge distances tested again. The three layups were tested separately to determine the capacity of individual components of a hybrid arch and to determine if there were synergistic effects with the hybrid layup. The samples were loaded in tension at a rate of 1 mm/mm (0.05-in/min), the recommended value from ASTM D 953. The complete test setup can be seen in Figure 2.4. Table 2.2 summarizes the characteristics of all specimens.

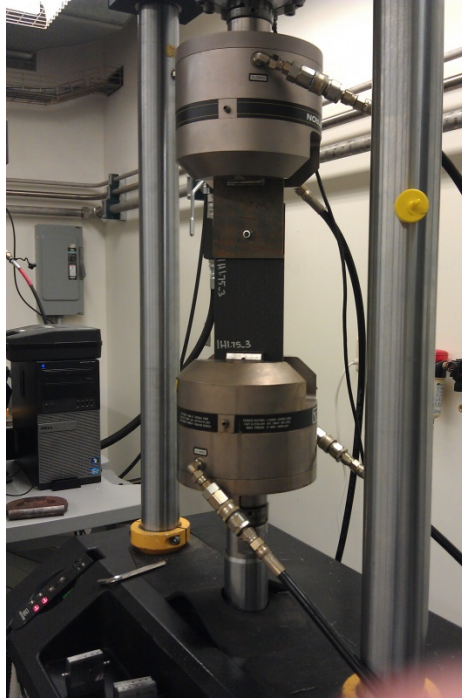


Figure 2.4: 45 mm Hybrid coupon test setup on the 100kN Instron machine.

The test results in Table 2.2 showed that edge distance for the hybrid material did not have a significant effect on the fastener bearing capacity. The maximum bearing strength of the material is determined from the maximum load sustained by the specimen, divided by the bearing area. The hybrid coupons failed in bearing as shown in Figure 2.5, and had a mean ultimate load of 10 kN (2225 kips) (COV = 6.5%). Based on these results, it was decided to continue with the 32 mm (1.25-in) edge distance for all future tests.

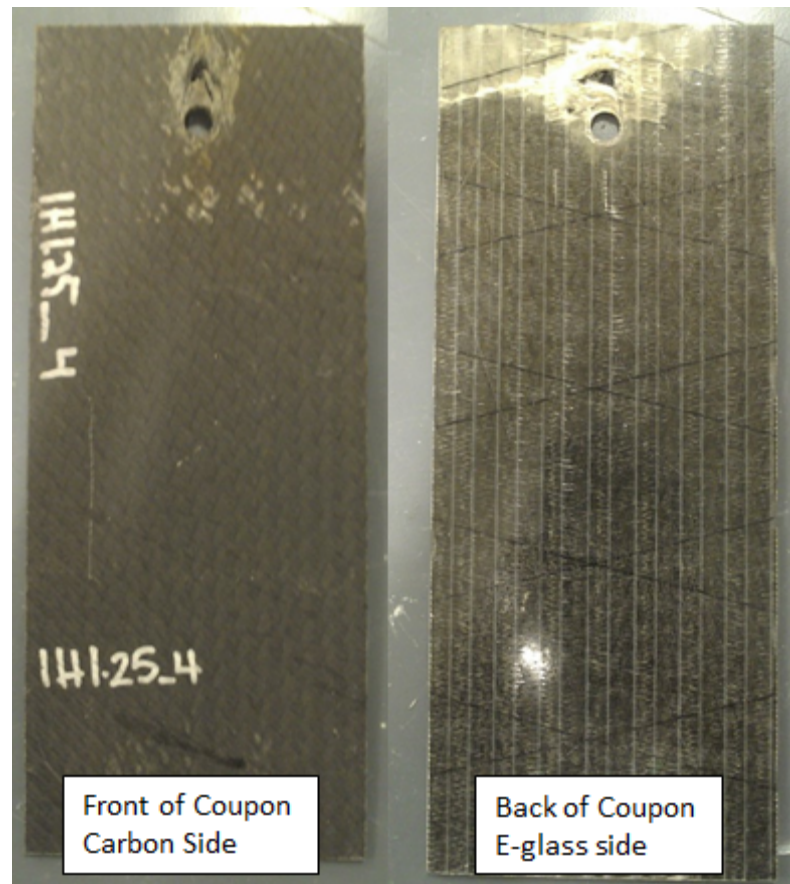


Figure 2.5: Typical bearing failure of hybrid coupon (32 mm edge distance specimen).

Table 2.2: Summary of Single Fastener Tests with Metal Back Plate

Coupon	Laminate Layup	Edge Distance mm(in)	Average Width mm(in) [cov]	Average Thickness mm(in) [cov]	Average Maximum Load kN(lb)	Bearing Strength MPa (ksi)	Failure Mode
Carbon	2 Layer C	32 (1.25)	101 (3.9889) [0.07]	2 (0.0592) [1.02]	5.035 (1132)	396 (57.4)	Bearing
		45 (1.75)	101 (3.9885) [0.05]	2 (0.0597) [2.20]	5.889 (1324)	466 (67.1)	Bearing
		57 (2.25)	101 (3.887) [0.04]	2 (0.0579) [4.71]	5.605 (1260)	455 (65.9)	Bearing
E-glass	1 layer G	32 (1.25)	101 (3.9870) [0.04]	1 (0.0417) [2.59]	2.326 (523)	-	Tension
		45 (1.75)	101 (3.9800) [0.37]	1 (0.0424) [1.52]	2.464 (554)	-	Tension
		57 (2.25)	101 (3.9793) [0.43]	1 (0.0415) [3.48]	2.455 (552)	-	Tension
Hybrid	2 layer C 1 layer G	32 (1.25)	101 (3.9915) [0.05]	3 (0.0952) [2.98]	9.987 (2225)	486 (70.5)	Bearing
		45 (1.75)	101 (3.9921) [0.05]	3 (0.0970) [2.52]	10.56 (2375)	510 (74.0)	Bearing
		57 (2.25)	101 (3.9918) [0.08]	3 (0.0986) [1.62]	9.906 (2227)	471 (68.3)	Bearing

From the typical load-deformation plot for the single fastener tests for the E-glass fiber constraint layer, Figure 2.6, it can be seen that the variation in edge distance increased the maximum load by 10%. The deformation in this context is the change in position recorded by the Instron machine. The constraint E-glass fiber maximum strength ranged from 2.3 kN (517 lb) to 2.5 kN (562 lb). It is also

observed that the material had a large, about 40%, decrease in load after the ultimate strength was achieved and after about 1 mm (0.04-in) deformation. The material consistently failed in tension at the bolt line and along the fibers. The two layers of structural carbon fiber, Figure 2.7, had capacities ranging from 4.8 kN (1080 lb) to 5.8 kN (1300 lb). The carbon fiber maintained approximately 80% of the maximum load as the deformation increased. The load-deformation plot for the hybrid material made up of one layer of E-glass constraint and two layers of structural carbon fiber can be seen in Figure 2.8. The material had a maximum load range from 9.8 kN (2200 lb) to 10.5 kN (2360 lb), a difference of 7% between fastener edge distances.

A comparison of the combined effects between the E-glass fiber constraint layer and the carbon fiber structural layers to the hybrid material can be seen in Figure 2.9. At the 32 mm (1.25-in) edge distance, by adding the E-glass fiber reinforcement, the maximum bearing strength is doubled. This shows that there is a synergistic effect achieved by combining the materials since the strength of the hybrid composite is greater than the sum of the strengths of the individual layers. The two materials combined work together to create a stronger hybrid material that performs better than the two materials individually. The 32 mm (1.25-in) carbon fiber only specimens had an average bearing strength of 396 MPa (ksi), when combined with E-glass the hybrid coupons had an average bearing strength of 486 MPa (ksi). The average strength increased 23%. One possible reason for this is that the largely longitudinal carbon tows bind the largely transverse E-glass tows to each

other, permitting the E-glass tows to bunch behind the fastener without rupturing, increasing both strength and apparent ductility.

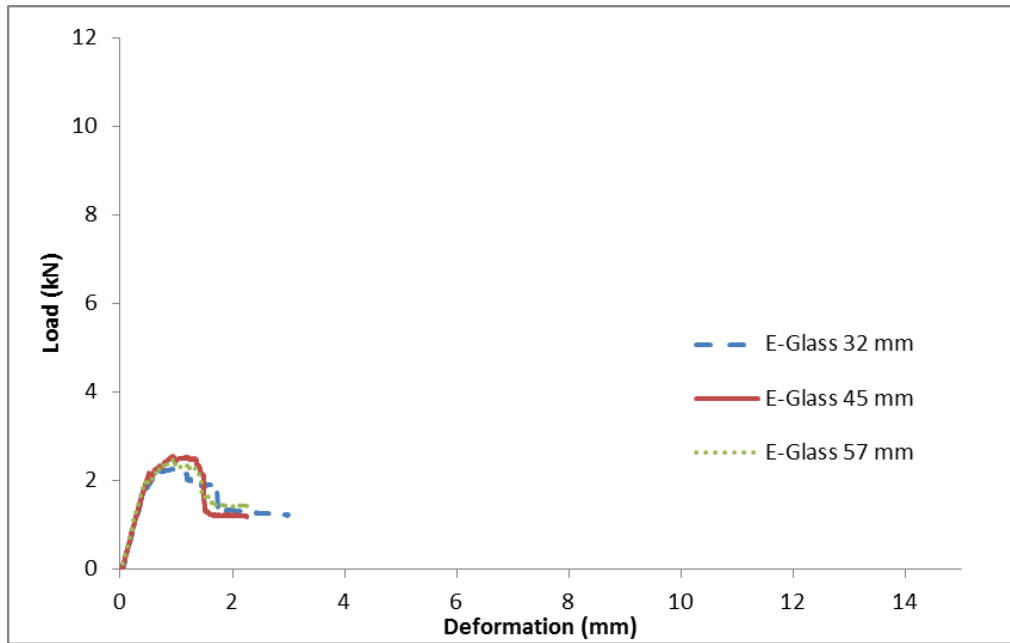


Figure 2.6: 1 Layer E-Glass fiber Load vs. Deformation plot for the three different edge distances.

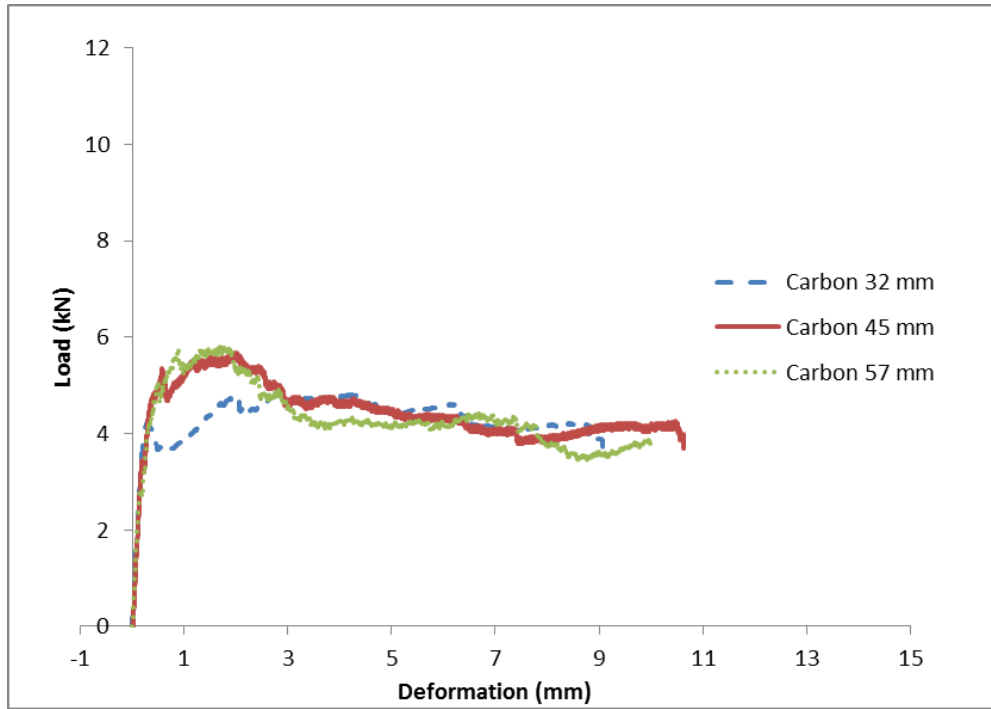


Figure 2.7: Two-layer carbon fiber Load vs. Deformation plot for the three different edge distances.

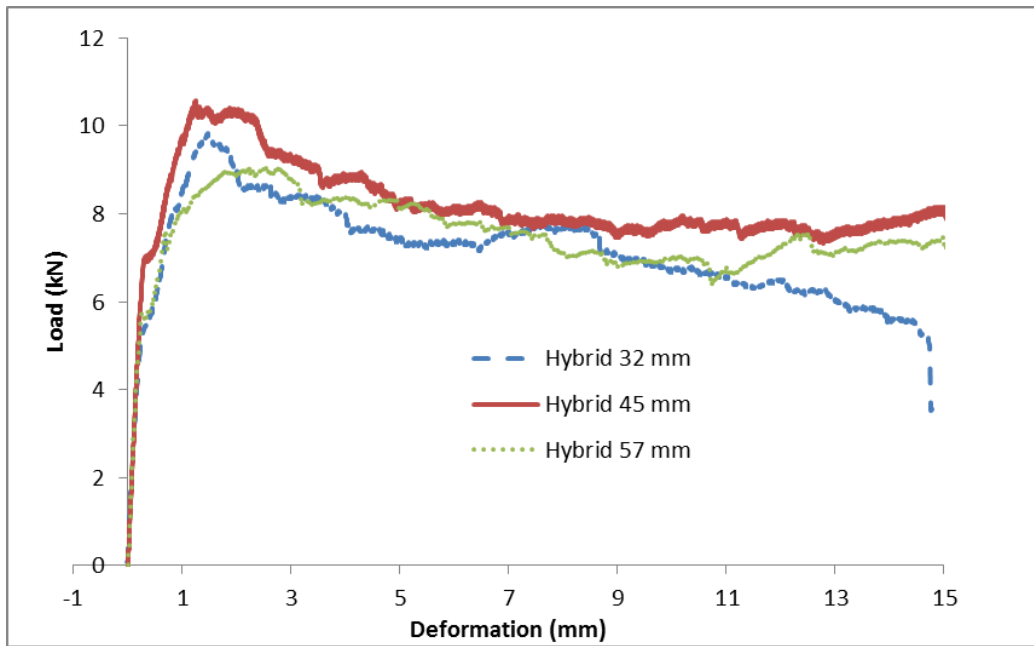


Figure 2.8: Hybrid (2 layer carbon, 1 layer E-glass). Load vs. Deformation plot for the three different edge distances.

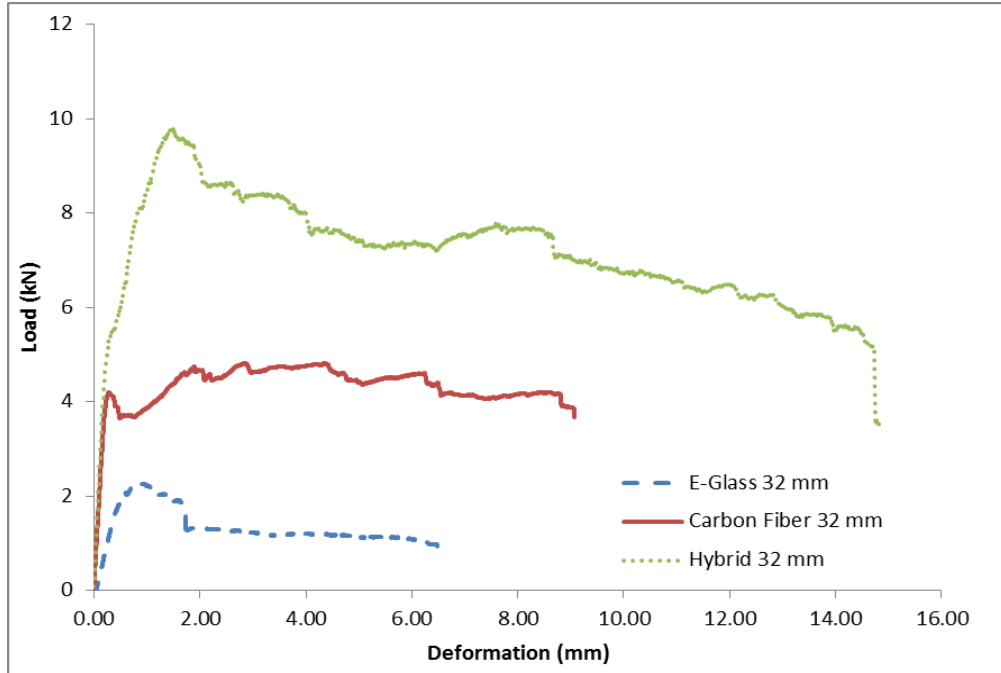


Figure 2.9: Comparison of the three materials tested with same edge distance.

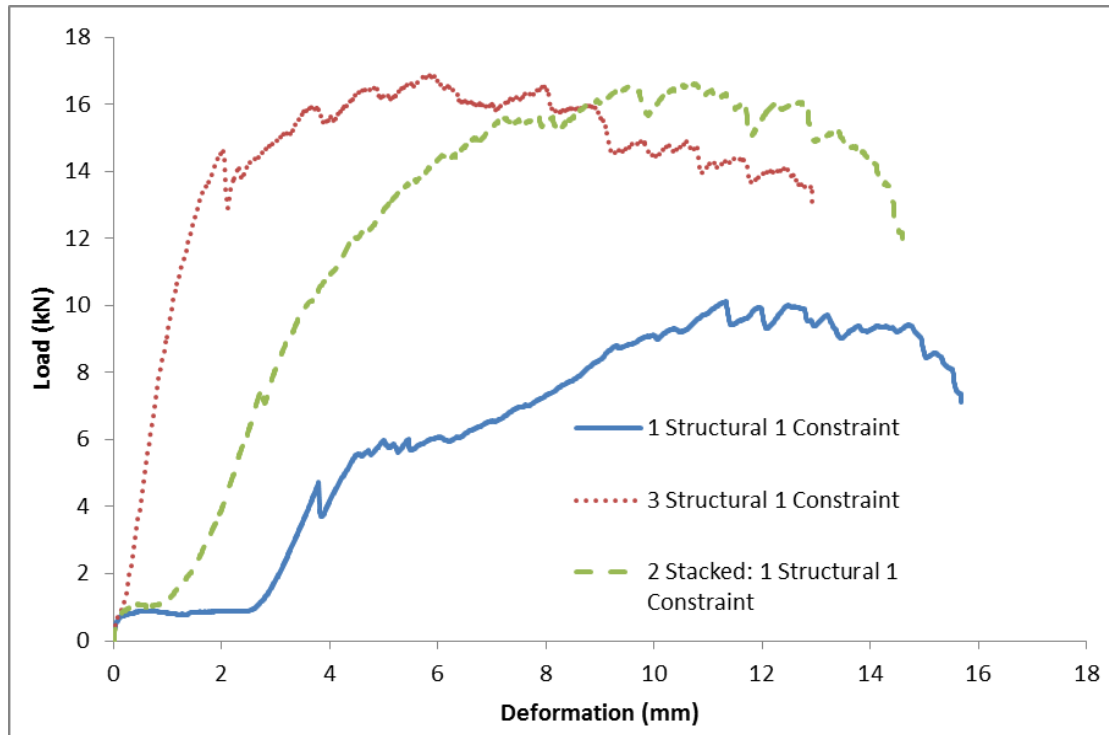


Figure 2.10: Typical Load vs. Deformation plot for three different collar options.

Single fastener dowel bearing tests were conducted with the three different likely collar materials and the results are shown in Figure 2.10. The three collar materials tested (3 structural layers, 1 structural layer, and two stacked composite shells) were compared. The two-stacked composite shells had a slightly lower stiffness than the three structural layer coupons due to the reduced thickness and one less layer of structural E-glass fiber. The two-stacked composite shells carried a maximum load close to that of the three structural layers. The final design recommendation for the collar based on ease of manufacturing and the results of the fastener bearing strength tests presented here is the two stacked composite shells made with one layer structural E-glass fiber and one layer constraint E-glass fiber.

The hybrid samples were then tested against a potential E-glass fiber collar material to mimic field conditions. The E-glass fiber collar layup used one layer of diameter constraint E-glass fiber infused to three layers of structural E-glass fiber. The nominal thickness of one layer of structural E-glass fiber is 1 mm (0.05-in). The total nominal thickness of the collar material was 5 mm (0.20-in). This layup was chosen because it is currently used in arch bridges construction and has similar axial and shear strength properties as the two-layer carbon fiber arches. Seven specimens were tested with a single Huck blind fastener connecting hybrid carbon fiber coupons to the E-glass fiber collar coupon, as shown in Figure 2.11.

Attaching the rivets with the pneudraulic rivet gun caused some matrix cracking in the constraint E-glass fiber side of the CFFT coupons; therefore, a washer was placed on the constraint E-glass side of the hybrid coupon to reduce this matrix cracking. This was done for the coupon testing only, since attaching washers

to the inside of the hollow CFFT was difficult and unnecessary because the flow media cushioned the rivet and the matrix did not crack. The thicker, stiffer collar material was initially loaded into the top grips to ensure torsion was not introduced to the system. The hybrid material was then aligned in the bottom grips and the grips closed. The specimens were tested in tension at a rate of 1 mm/min (0.05-in/min) until bearing failure occurred (deformation reached 13 mm (0.5-in) or 1.5 bolt diameters) and the test was ended. It can be seen in Figure 2.9 that the two-layer carbon specimen maintained its peak load past half a bolt diameter of deformation, therefore the test was continued until the load decreased below 80% of the peak load, or one and a half bolt diameters of deformation was reached. The average peak failure load as shown in Table 2.3 was 9kN (2024 lb) with a COV of 6.2%. Ultimately, however, the three layer structural E-glass fiber layup used in these tests was not chosen for the splice collar design due to manufacturability, which necessitated additional single fastener testing.

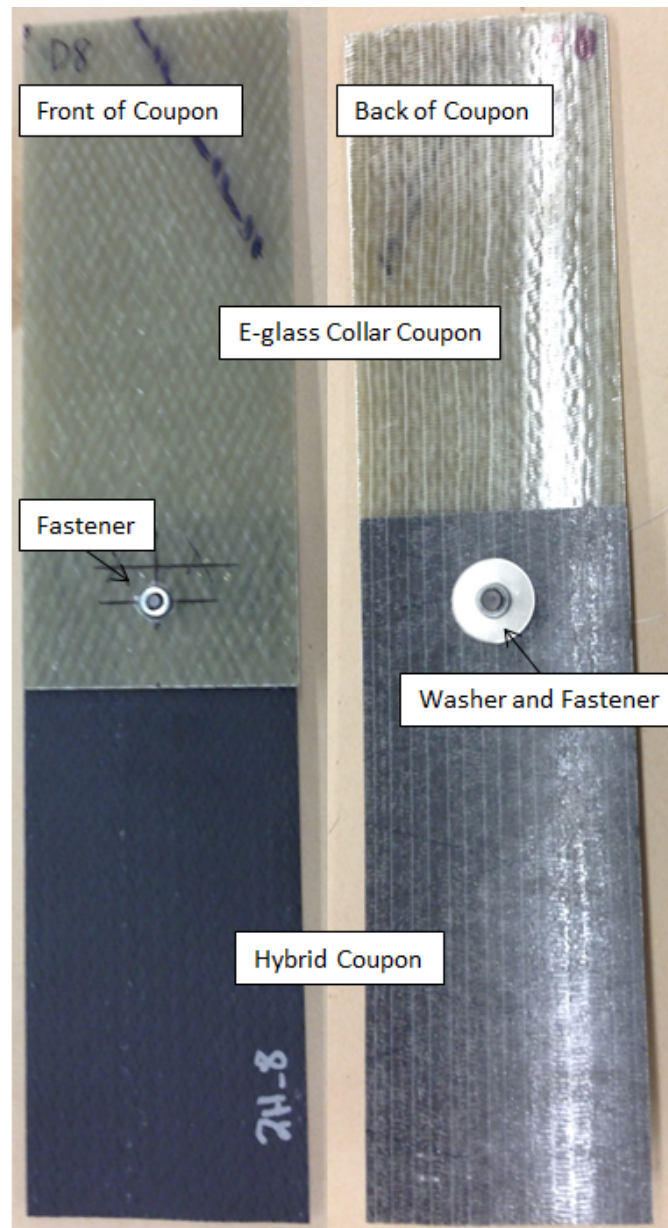


Figure 2.11: Hybrid specimen attached to E-glass fiber collar material.

### 2.3.2. Single Fastener Lap Shear Testing of Braided Collar Material

The bearing strength of the collar material was determined by testing the three different structural E-glass fiber layer configurations. The coupons maintained the same dimensions, 254 mm (10-in) long by 102 mm (4-in) wide, but varied in number of structural E-glass fiber layers. Three collar material layups were

considered: one layer of E-glass fiber diameter constraint and one layer structural E-glass fiber with a nominal thickness of 3 mm (0.1-in), one layer of E-glass diameter constraint and three layers of structural E-glass fiber with nominal thickness of 5 mm (0.2-in), and two un-bonded stacked composite shells each having one layer constraint E-glass fiber and one layer structural E-glass fiber with a nominal thickness of 5 mm (0.2-in). The stacked composite shells were used to determine the effects of combining stacked shells of collar material and its effect on the maximum bearing strength.

The coupons were tested against a steel backing plate and connected using a 8 mm (5/16-in) bolt as a dowel and a 10 mm (3/8-in) hole diameter. The steel backing plate was placed in the top grips, the specimen was lined up with the hole and bottom grips, the bolt was hand tightened to the coupon with a large group of washers and the matching nut, and the lower grips tightened on the collar specimen, Figure 2.12. The coupon was tested in tension at a rate of 1 mm/min (0.05-in/min) until bearing failure occurred, or 13 mm (0.5-in) deformation was reached. All three material layups were tested in the same way to obtain dowel-bearing strength of the individual layers of collar. The two stacked composite shell coupons had similar stiffness (matching slopes in the load deformation curve) to the three layer infused coupons, and was determined to be a good candidate for use as a collar material. More details on its fabrication and use for the collar are given in Chapter 4.



Figure 2.12: Two un-bonded stacked composite shells for the collar in the bearing test setup.

The last group of single fastener tests consisted of two stacked composite shells, one layer constraint E-glass fiber and one layer structural E-glass fiber layup attached to the hybrid CFFT coupon using a Huck fastener. The composite shell coupons were stacked with the structural E-glass fiber layer facing up and Pliogrip 7779 urethane adhesive was used to adhesively bond the two coupons together at the end of the specimen where it would be placed in the grips along a length of 51 mm (2-in). This was done to ensure the two-stacked composite shells did not experience uneven loading or move relative to each other. A washer was placed on the front of the specimen (E-glass fiber collar side) to mimic the actual conditions of the manufactured splice. The washer was not placed on the backside, as in prior testing, to reduce matrix cracking in the hybrid material, since this would better reflect as-built conditions in a splice. The specimens had initial curvature due to

unsymmetrical layup of both composite shells. This caused some initial cracking when the specimens were closed in the grips Figure 2.13. The coupons were tested in tension until a combination of fastener pull through and bearing failure occurred. The average peak load of the sample set was 6.62 kN (1489 lb), Table 2.3, which is less than the average load observed when the hybrid material was tested with a steel backing plate.

The original fastener specimens were tested with a washer placed on the back or E-glass fiber side of the coupon to reduce resin matrix cracking. In actual field manufacturing conditions, placing a washer inside of the tube was unnecessary because of the flow media. The flow media is used inside of the tubes during manufacturing and matrix cracking was not observed on the E-glass fiber side of the specimen, the flow media helped absorb the impact from riveting. Although washers were not needed on the inside of the tube, another problem occurred during the collar riveting process. The carbon and E-glass fiber tubes are less stiff than the more common materials like steel. The tubes also have a circular cross section, not flat. This caused rivet pull through or an uneven or angled rivet connection. A picture of the rivet with a washer and the rivet without in the same collar material can be seen in Figure 2.13. To mitigate this, a washer was placed on the outside of the collar, which reduced the angle of the rivet. Further, longer rivets, 37 mm (1.445-in) unclamped, were purchased to avoid the rivet pull through failure.

When the single fasteners were installed to mimic an actual splice, the washer was placed on the structural E-glass side of the collar (in real conditions the outside of the tube) as seen in Figure 2.14 instead of the E-glass fiber side of the hybrid

coupon (in field conditions the inside of the tube). This change in placement caused a reduction in capacity because the connection experienced a combined failure of fastener pull through and bearing. The washer increased the capacity when it was on the inside of the tube because it stopped the rivet from tearing through. Failure of the fastener with the washer on the outside of the tube was observed at lower deformations and a lower peak load. The actual condition with the washer on the collar structural E-glass side specimen failure can be seen in Figure 2.15. Six specimens were tested with the same material layup, but the washer was placed on the E-glass fiber side of the hybrid coupon and the test confirmed the washer placement increased the connection capacity. The specimens had an average ultimate load of 9.29 kN (2111 lb) with a COV of 5%. This value is more consistent with the previous single fastener tests conducted. A summary of the single fastener results comparing the two collar materials and washer placement is shown in Table 2.3.



Figure 2.13: Comparison of rivet. Left - Rivet using washer  
Right - Rivet without a washer.

Table 2.3: Summary of Single Fastener Hybrid Coupons Tested with Different Collar Materials

Coupon	Edge Distance mm(in)	Average Thickness mm(in) [COV]	Washer Placement	Average Maximum Load kN(lb)	Average Bearing Strength MPa(ksi)	E-glass Collar Material
Hybrid	32 (1.25)	3 (0.0934) [2.09]	Constraint (inside of tube)	9.0 (2024)	419(60.8)	3 layer structural
Hybrid	32 (1.25)	3 (0.0976) [3.53]	Structural (outside of collar)	6.7 (1521)	289(42.0)	2 stacked shells (unbonded)
Hybrid	32 (1.25)	3 (0.1154) [2.93]	Constraint (inside of tube)	9.3 (2111)	445(64.6)	2 stacked shells (unbonded)



Figure 2.14: Two stacked collar layers tested against the hybrid composite.



Figure 2.15: Failure of actual layup used in connection. Left- Collar layers peeling up, Right- Bearing failure of hybrid composite.

### 2.3.3. Multi Fastener Lap Shear Tests

In addition to the previously detailed single fastener testing, lap shear tests were conducted on specimens with two and three fasteners in the direction of load. The same coupon dimensions were used, 102 mm (4-in) wide by 254 mm (10-in) long, and 10 mm (3/8-in) holes were drilled into both the 3 mm (0.1-in) thick carbon-E-glass fiber hybrid coupon and the 5 mm (0.2-in) thick E-glass fiber collar coupon consisting of three layers structural E-glass fiber and one constraint layer of E-glass fiber. The center to center spacing used was twice the minimum specified in the Final Pre-standard of four times the fastener diameter 64 mm (2.5-in) (ASCE 2010). The coupons, Figure 2.16, were tested in a lap shear configuration for tension loading similar to the single fastener testing.

One face of the coupons was spray painted with a speckle pattern to allow use of Aramis digital image correlation system to measure surface strains as shown in Figure 2.17. The full-field strain distribution recorded by Aramis is shown in

Figure 2.18, with an average strain of 0.13% at maximum load. When two fasteners in a row were tested, the coupons carried an average maximum load of 15.3 k N (3438 lb), with a COV of 6.0%. Figure 2.18 also shows that the area around the fastener was not clearly recorded and because of the washer we are not able to see if the strain was equal around each fastener and assess load sharing between fasteners. If equal load sharing is occurring between fasteners, each fastener is carrying around 7.7 kN (1700 lb). If unequal load sharing is occurring between fasteners, and the single fastener tests represent the fastener closest to the edge, the first fastener is carrying about 8.9 kN (2000 lb) and the second fastener carries 6.3 kN (1400 lb).

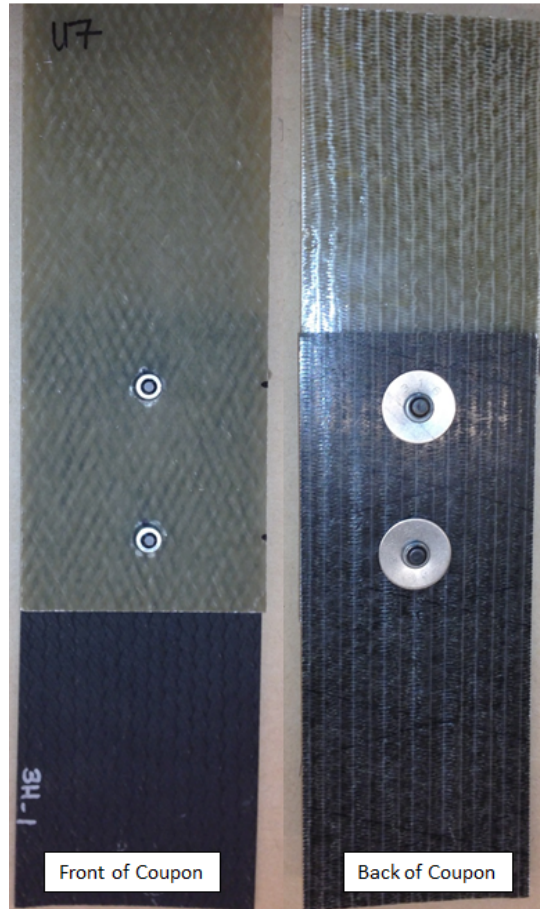


Figure 2.16: Two-fastener specimen.

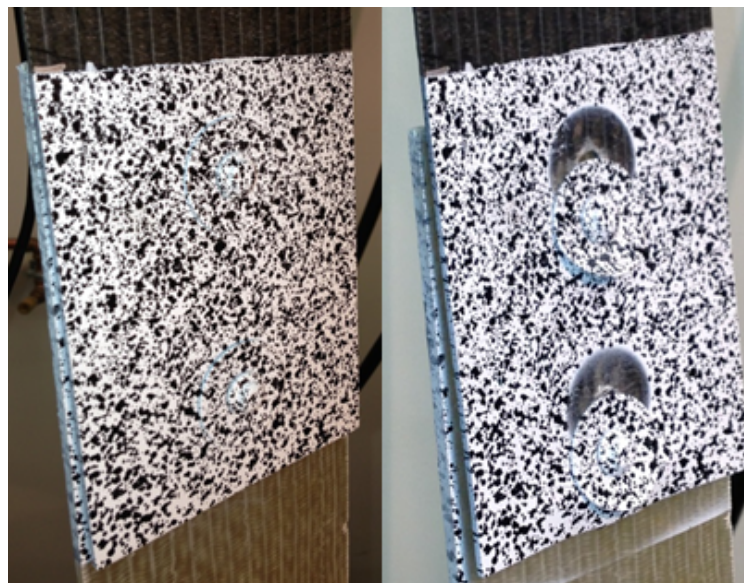


Figure 2.17: 2 Fastener specimen. Left- Specimen speckle pattern for digital image correlation. Right- Typical bearing failure of 2-fastener coupon.

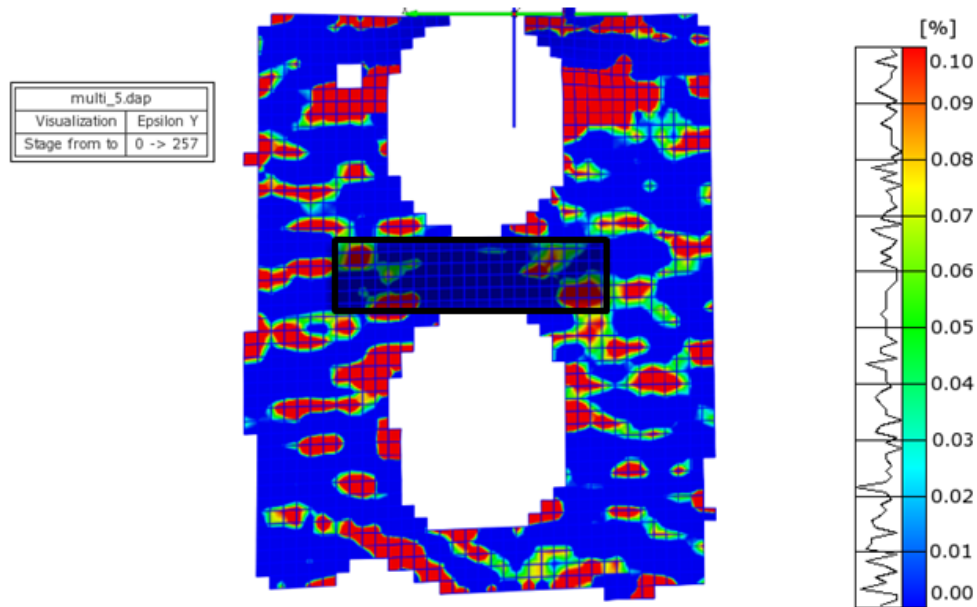


Figure 2.18: Strain distribution field for multi\_5 two-fastener specimen.  
Average strain computed from shaded area.

The test configuration for three fasteners was the same as the single- and two-fastener configuration. The coupon dimensions were 102 mm (4-in) wide by 254 mm (10-in) long. The edge distance of the first fastener was 32 mm (1.25-in) and the fastener spacing between the three fasteners was 64 mm (2.5-in). The coupons, shown in Figure 2.19, were tested in a tension lap shear configuration and the bearing strength determined. Aramis digital image correlation system was used to measure surface strains with the three-fastener configuration. The full-field strain distribution, Figure 2.20, was used to determine the strain and if load sharing occurred between fasteners. The average strain recorded by Aramis was 0.13% at maximum load, similar to the two-fastener specimen. The average maximum load of the specimens was 25.6 kN (5675 lb), with a COV of 5.9%. If equal load sharing occurred in the fasteners then one fastener in the three-fastener configuration

carries 8.45 kN (1900 lb). It could also be said that if the first fastener carries 8.9 kN (2000 lb), as discussed in single fastener testing, then the other two each carry 8 kN (1800 lb). This correlates better with the data collected during the single fastener testing using the three structural layer collar, but does not explain the two fasteners in a row giving 10% lower individual fastener results than predicted from single fastener testing.

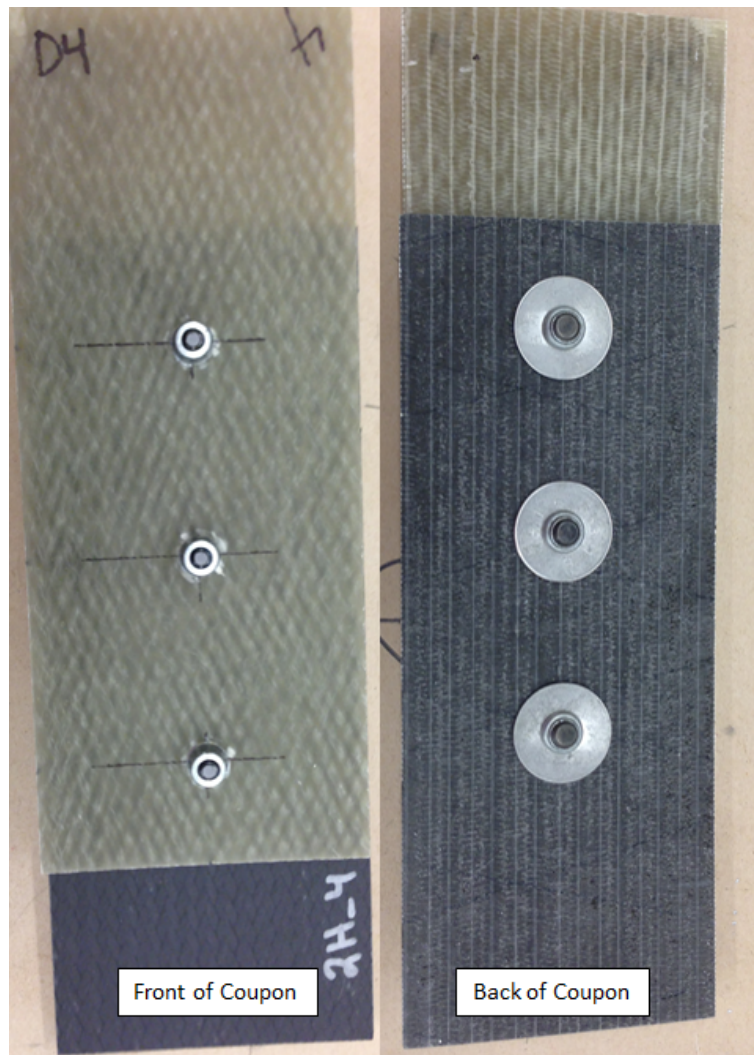


Figure 2.19: Three-fastener specimen.

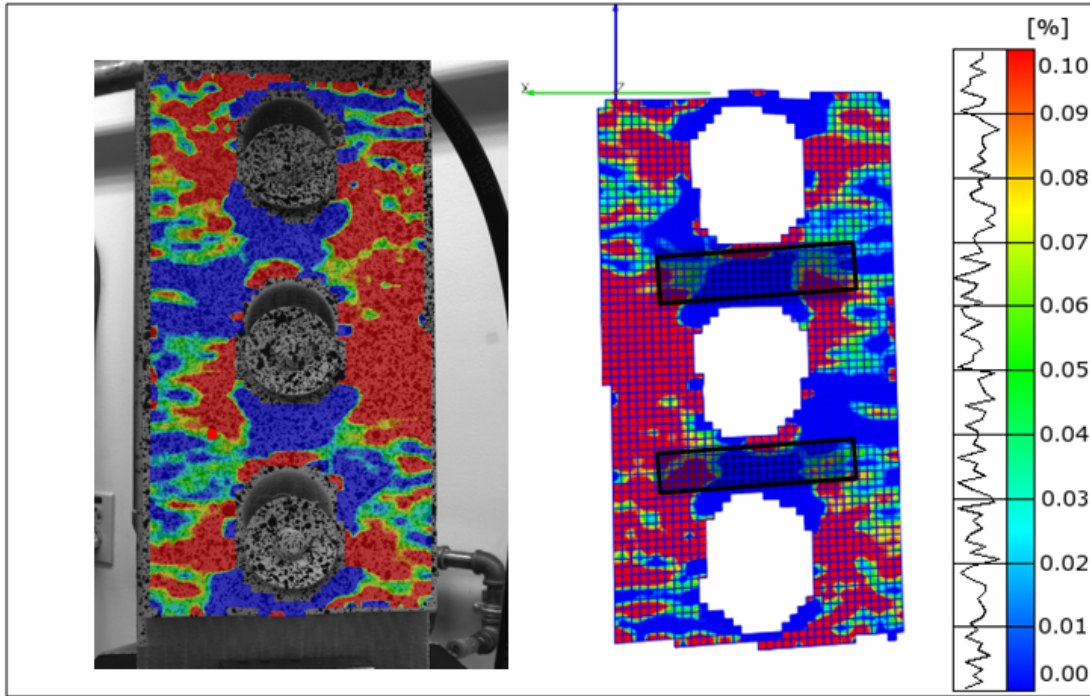


Figure 2.20: Three-fastener strain field for multi\_9 specimen  
 Left- strain field on specimen Right- 3D image transformed in Aramis.

Table 2.4: Multi-fastener Test Summary

Coupon	Laminate Layup	Fasteners Tested	Average Width mm(in) [COV]	Average Thickness mm(in) [COV]	Bearing Strength MPa(ksi)	Average Maximum Load kN(lb)	Failure Mode
Hybrid	2 Layer C 1 Layer G	2	101.3 (3.9903) [0.09]	2.291 (0.0902) [11.9]	348 (50.4)	15.3 (3438)	Bearing
Hybrid	2 Layer C 1 Layer G	3	101.4 (3.9942) [0.05]	2.482 (0.0977) [2.1]	378 (54.8)	25.2 (5675)	Bearing

The load-deformation plot for a the typical responses of each coupon with one, two, and three fasteners can be seen in Figure 2.21. The summary for multi-fastener testing is shown in Table 2.4. It can be observed by the plot that the increase in maximum bearing strength from one fastener to two fasteners was about

40%, while the increase in maximum bearing strength from two fasteners to three fasteners was about 60%. Preliminary calculations of bearing strength indicated that 2 or 3 fasteners per row would be sufficient to design a reasonably sized collar. The bearing strength per fastener is listed in Table 2.4, for 2 fasteners the maximum bearing strength reached 358 MPa (50.4 ksi) and 3 fasteners reached 378 MPa (54.7 ksi). A single fastener reached 419 MPa (60.8 ksi). The design recommendation is that the collar be attached to the CFFT with nine rows of two Huck fasteners spaced at 32 mm from the end (centerline of splice) and 64 mm spacing between fasteners. Although one circumferential group of nine fasteners was calculated to be sufficient for the collar design, two fasteners in a row were chosen to be conservative and ensure an adequate splice. Details on the design of the splice are given in Chapter 4.

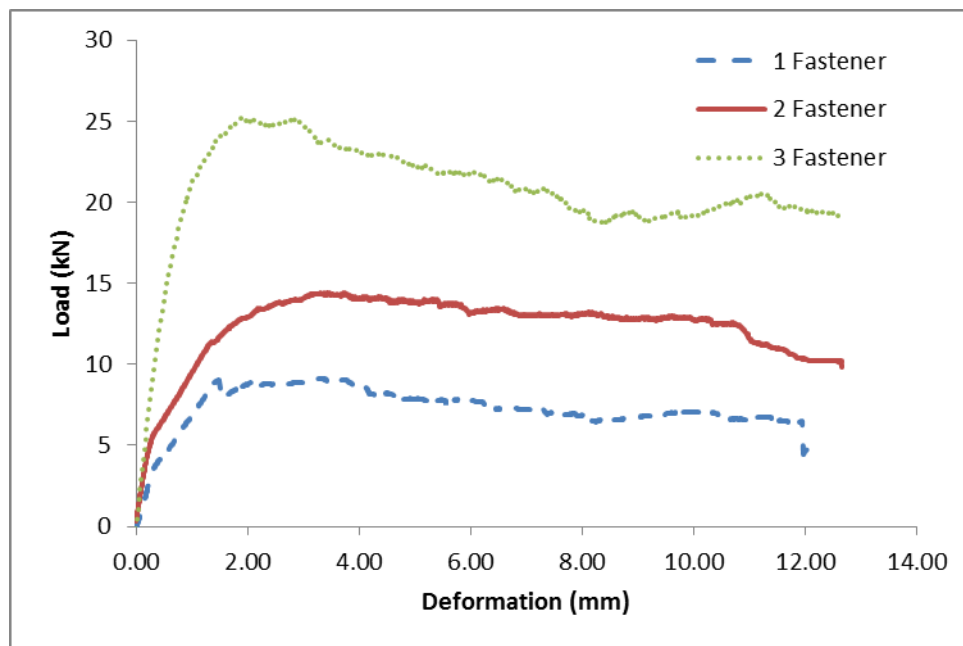


Figure 2.21: Typical Load vs. Deformation for varying number of fasteners.

## 2.4 Fastener Testing Summary & Conclusion

The experimental data collected from single fastener tests allowed us to characterize the bearing strength of the hybrid material and verify the edge distance based on recommendations from the LRFD Final Pre-standard for Pultruded Sections. The single fastener specimens failed in bearing and a combination of bearing and fastener pull through in some cases. It was observed when comparing the individual material layers in bearing versus the hybrid layup response that the combination does not just increase the strength by adding the two material strengths, but improves the addition of bearing strength by 27%. Meaning the maximum bearing load of the hybrid materials is 27% higher than the sum of the bearing load of the E-glass fiber and carbon fiber material. It was found that the minimum edge distance of four times the bolt diameter suggested by LRFD Final Pre-standard for Pultruded Sections is acceptable because the hybrid material was ductile, each fastener test yielded similar peak strength results, and increased edge distance did not substantially increase overall strength and deformation.

Testing two and three fasteners in a row using the hybrid material connected to the collar-like material allowed design recommendations to be made for the external reinforcing connection based on the experimental capacity. The fasteners failed in bearing similar to the single fastener tests. Fastener pull-through was not observed in the sample sets. The amount of load sharing could not be determined between fasteners. Further mechanical fastener testing should be conducted if the fastener, fastener size, or material is changed in the connection. The results presented in this chapter were used to design the splice detailed in Chapter 4.

## **CHAPTER 3 PULLOUT STRENGTH TESTS OF CARBON FIBER COMPOSITE CABLE (CFCC) FOR SPLICING CFFT**

### **3.1 Introduction**

The pullout strength tests considered two different test parameters, rebar material type and embedment length into concrete. Tests were performed to determine the feasibility of different reinforcing materials and required development lengths. The tests were conducted using a modified version of ASTM C900. ASTM C900 determines the pullout force required to pull a metal insert from hardened concrete. The metal insert is either cast-in-place or installed into hardened concrete and uses a jack system against a bearing ring to either determine the ultimate strength or verify the required strength has been attained. The insert is pulled in tension perpendicular to the concrete until rupture occurs or required load is reached. The pullout test conducted used cast-in-place rebar instead of a metal insert. Two different FRP reinforcing materials were tested to assess the viability of an all FRP splice. Steel reinforcing was tested as a baseline material having well-known behavior and properties. This chapter discusses the CFCC reinforcing material only, E-glass fiber rebar and steel rebar test discussion and results can be found in Appendix A.

### **3.2 Testing Materials and Specimen Fabrication**

Four CFFT specimens were tested. The rebar material used for the test, Figure 3.1, was a 17 mm (0.677-in) 1 x 7 strand Carbon Fiber Composite Cable (CFCC). The diameter bar was chosen based on interaction diagrams created for the

CFCC material and design further discussed in section 3.4. The material properties provided by Tokyo Rope, Inc., give an effective cross-sectional area of  $151 \text{ mm}^2$  ( $0.234 \text{ in}^2$ ), a tensile elastic modulus of  $155 \text{ kN/mm}^2$  ( $22400 \text{ ksi}$ ), and an ultimate tensile strength of  $2.69 \text{ kN/mm}^2$  ( $390 \text{ ksi}$ ). The rebar was tested in a  $381 \text{ mm}$  ( $15\text{-in}$ ) diameter CFFT, by embedding two colinear bars in the tube (one on each end) with a  $610 \text{ mm}$  ( $24\text{-in}$ ) gap between them at the centerline of the tube. The CFFT tubes included a spiral of the same material. In addition to facilitating fabrication of the rebar cage, the spiral is required in the splice to carry internal shear. The CFCC spiral was a  $8 \text{ mm}$  ( $0.295\text{-in}$ ) bar with a  $353 \text{ mm}$  ( $13.9\text{-in}$ ) diameter and  $127 \text{ mm}$  ( $5\text{-in}$ ) pitch.

The specimens were manufactured using existing FRP tubes. The FRP tubes were cut to various lengths depending on the embedment length of rebar to be tested. The CFCC spiral was then placed in the tube using a spacer from the tube's edge to ensure correct clear cover for the rebar. The rebar spiral ran the entire length of the CFFT tube. Each specified embedment length of rebar was attached to the spiral. The specimens were placed vertically for concrete filling, Figure 3.2; the specimen layout was symmetric for each end of the tube. The tubes were filled with a self-consolidating concrete (SCC) that includes an admixture that compensates for shrinkage and expands at the dosage used. The SCC design strength was  $27.6 \text{ MPa}$  ( $6000 \text{ psi}$ ). The concrete cured for 90 days prior to testing. Concrete cylinders were tested in accordance with ASTM C39. Six  $152 \text{ mm}$  ( $6\text{-in}$ ) diameter concrete specimens were tested. The average concrete compressive strength at the time of pullout testing was  $59.8 \text{ MPa}$  ( $8680 \text{ psi}$ ).

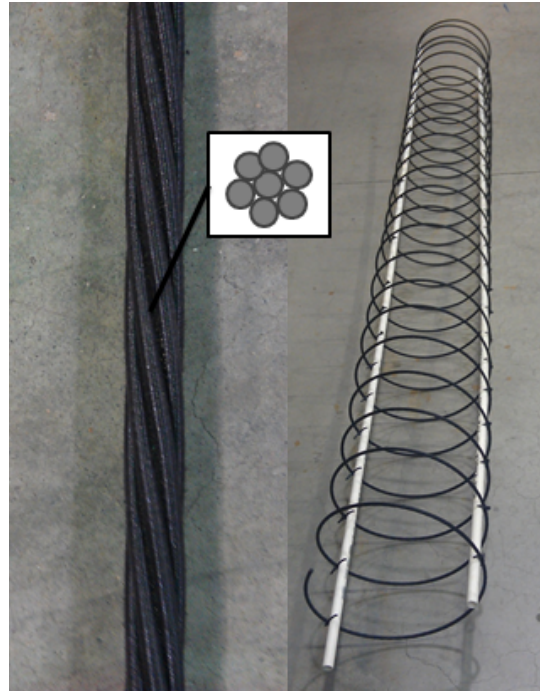


Figure 3.1: 1x7 CFCC strands, Left – 17 mm (0.677-in) CFCC used in pullout test, Right – 8 mm (0.295-in) CFCC spiral.

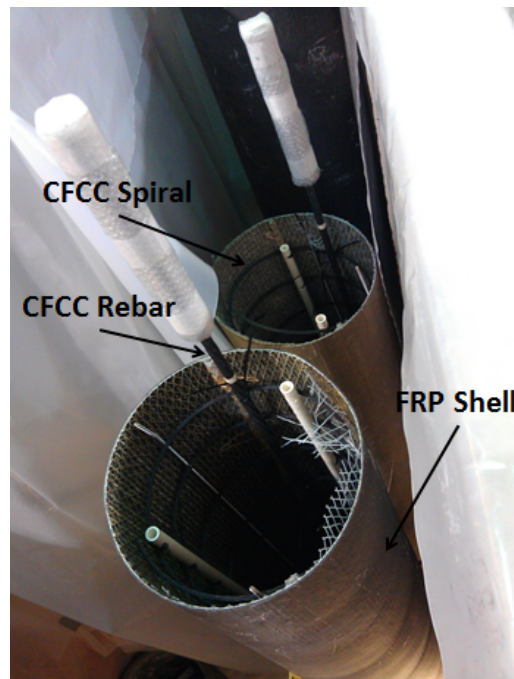


Figure 3.2: Pullout specimen before filling with concrete.

### 3.3 Test Configuration

The specimens were tested horizontally in tension using a 1300 kN (300 kip) load actuator (AEWC 939 load cell), Figure 3.3. The rebar at one end of the specimen was attached to the actuator, and the rebar at the other end was attached to a fixed reaction block. The specimens used a grouted threaded coupler that was pre-attached by Tokyo Rope, Inc., the CFCC manufacturer. The coupler was attached to the actuator and the fixed end section using steel plates with holes in the center for the threaded portion to fit through and a nut on the back of the plates. The test rate for initial pullout failure of the test specimens was 1.27 mm/min (0.05 in/min).

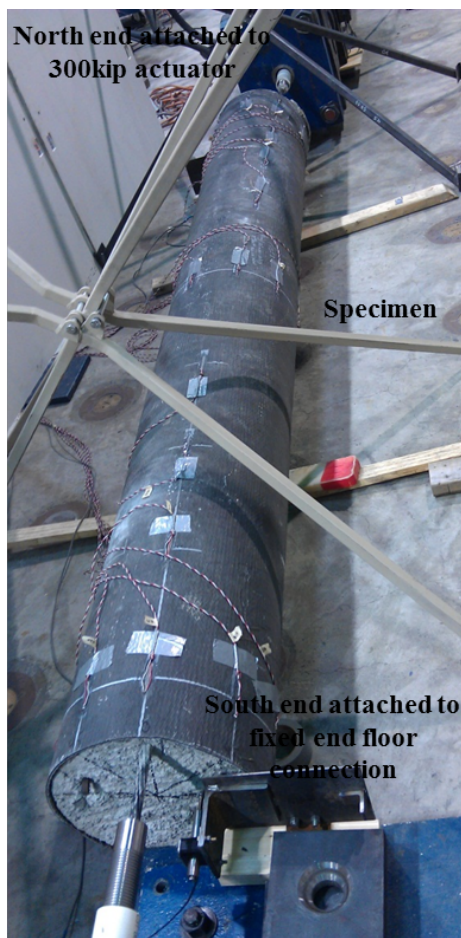


Figure 3.3: Pullout test setup.

The instrumentation for the test included 21- 51 mm (2-in) long N2A350 ohm strain gauges, two  $\pm$  13 mm (0.5-in) LVDTs, and two 51 mm (2-in) gauge length extensometers. As shown in Figure 3.4 the strain gauges were placed on the CFFT both longitudinally along the rebar centerline and circumferentially around the CFFT to assess transfer of stress to the FRP shell. An LVDT was placed at the north and south ends of the specimen. The extensometers were placed on each exposed rebar end extending from the concrete.

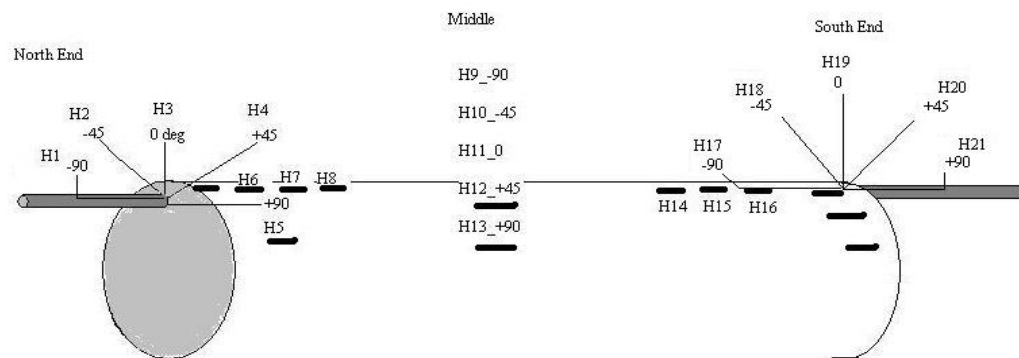


Figure 3.4: Strain gauge layout for pullout test.

### 3.4 Estimation of Embedment Lengths Used in Test Program

In an actual bridge, the arches have both moment and axial forces acting at the splice location caused by permanent and live loads. The ultimate factored design moment used to calculate bar stresses was 46.3 kN-m (410 in-kip) along with a factored ultimate design axial compression of 243 kN (54.6 kips). These values were provided by AIT, and are based on a typical, as-built composite arch bridge. The diameter of the bar was chosen based on interaction diagrams created specifically for CFCC using the AASHTO LRFD Guide Specifications for the design of concrete-

filled FRP tubes for flexural and axial members, section 2.9 *Design for Axial Compression*. The interaction diagram created for a 17 mm (0.677-in) CFCC rebar and associated calculations are provided in Appendix B. Three points on the diagram were calculated, nominal axial resistance, nominal moment resistance, and the balance point. The factored design axial and moment values provided by AIT fell within the interaction diagram when the splice was reinforced with 17 mm (0.677-in) rebars.

The embedment length, as seen in Figure 3.5, is the distance the rebar must be embedded in the concrete to develop a certain tension force. This value is calculated using an equation that depends on the concrete compressive strength, the tensile strength the bar needs to develop, and the bar diameter. The work performed by Domenico (1995) indicates that shorter flexural bond lengths of CFCC pre-stressing strands may be acceptable (Domenico 1995). It was found by Domenico (1995) that the bond strength between the CFCC and concrete was around five times that that of steel pre-stressing strands. Further research into the topic by Mahmoud (1997) indicates that the flexural bond length needed for CFCC is about 25% of what is predicted by ACI. Four CFCC specimens were tested. Equation 3.1 shows the recommended equation used to determine the development length of an FRP rebar embedded in concrete, ACI 440 equation 11-6, This equation was modified to account for the change in the relationship between area and diameter in the equation because the actual area of the helical cable is smaller than a solid circular cross-section for the same diameter. The modified equation is shown in Equation 3.2.

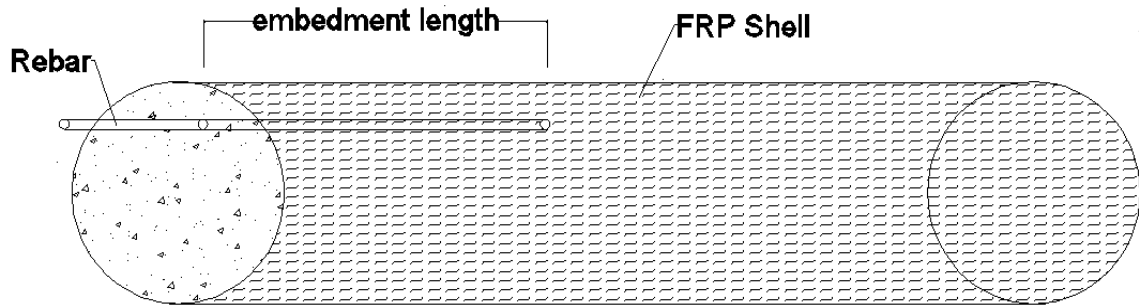


Figure 3.5: Example of embedment length in CFFT.

$$l_d = \frac{\alpha \frac{f_{fr}}{0.083\sqrt{f_c'}} - 340}{13.6 + \frac{C}{d_b}} d_b \quad \text{Equation 3.1}$$

$$l_d = \frac{f_{fr} - \pi 0.85 \frac{d_b^2}{A_b} \sqrt{f_c'}}{\frac{\pi d_b}{A_b} (3.4 + 0.25 \frac{C}{d_b}) f_c'} \quad \text{Equation 3.2}$$

Where:

$A_b$  = bar area mm<sup>2</sup> (in<sup>2</sup>)

$d_b$  = bar diameter mm (in)

$C$  = minimum (spacing, cover dimension) mm (in)

$f_c'$  = concrete compressive strength MPa (psi)

$f_{fr}$  = the required bar stress in MPa (psi)

$l_d$  = development length of reinforcing bar in mm (in)

$\alpha$  = bar location modification factor assumed to be 1.0

The modification required shorter development lengths to reach the design stresses than the original equation used for the E-glass fiber bars. The stress to be developed

was found to be 992 MPa (144 ksi) and was determined using strain compatibility for a 300 mm (11.8-in) diameter cross-section with 6 CFCC bars evenly spaced around the circumference. The lengths tested included a lower bound, slightly larger than the minimum  $20d_b$  provided by ACI440 381 mm (15-in), the value given to us by Equation 2 of 1067 mm (42-in), and two additional values of 914 mm (36-in), and 1219 mm (48-in). Development length tested and calculated capacities based on the ACI equations are summarized in Table 3.1 for the CFCC. The pullout capacities, or forces required to pull the bar from concrete, were determined using Equation 3.3, a modified version of ACI440 equation 11-3. The actual conditions were plugged into the modified equation, values chosen for embedment length, the actual conditions for concrete compressive strength and clear cover, than multiplied by the cross-sectional area to get the force capacity.

$$f_f = \sqrt{f_c} \left( \frac{16l_e}{d_b} + \frac{1.2l_e C}{d_b^2} + 400 \right) \quad \text{Equation 3.3}$$

Table 3.1: CFCC pullout test matrix

TEST	Embedment Length	Bar length needed	CFFT length	ACI Predicted Capacity
1	38.1cm(15in)	2.13m(7ft)	0.914m(3ft)	76 kN(17.2 kip)
2	91.4cm(36in)	2.13m(7ft)	2.74m(9ft)	128 kN(29 kip)
3	107cm(42in)	2.13m(7ft)	3.05m(10ft)	144 kN(32.4 kip)
4	122cm(48in)	2.13m(7ft)	3.35m(11ft)	159 kN(35.8 kip)

### 3.5 Carbon Fiber Composite Cable (CFCC) Pullout Tests

Four CFCC specimens were tested. The shortest specimen length was 0.965 m (38-in) and the CFCC was embedded 381 mm (15-in) into the concrete. The estimated 381 mm (15-in) embedment length capacity was 76 kN (17.2 kip), and the bar pulled out of the concrete at 122.8 kN (27.6 kip). The 381 mm (15-in) embedment length was slightly larger than the minimum value of  $20d_b$ , where  $d_b$  is the bar diameter, suggested by ACI 440, and was used to determine a lower bound for embedment length of CFCC.

The 2.7m (9 ft.) specimen had CFCC embedded 914 mm (36-in) into the concrete and had an estimated embedment length capacity of 128 kN (29 kip). The specimen was loaded to 50% of its estimated capacity, 53.4 kN (12.2 kip), and unloaded to remove extensometers. The specimen was then tested to an initial failure of 264 kN (59.4 kip). The initial failure mode was bar pullout from the concrete. The initial bar pullout was 25 mm (1-in). The rate of testing was then increased to 51 mm/min (2-in/min) and the specimen retested to a maximum load of 226 kN (50.9 kip), at which point the bar steadily pulled out from the concrete. The pullout failure progression can be seen in Figure 3.6.

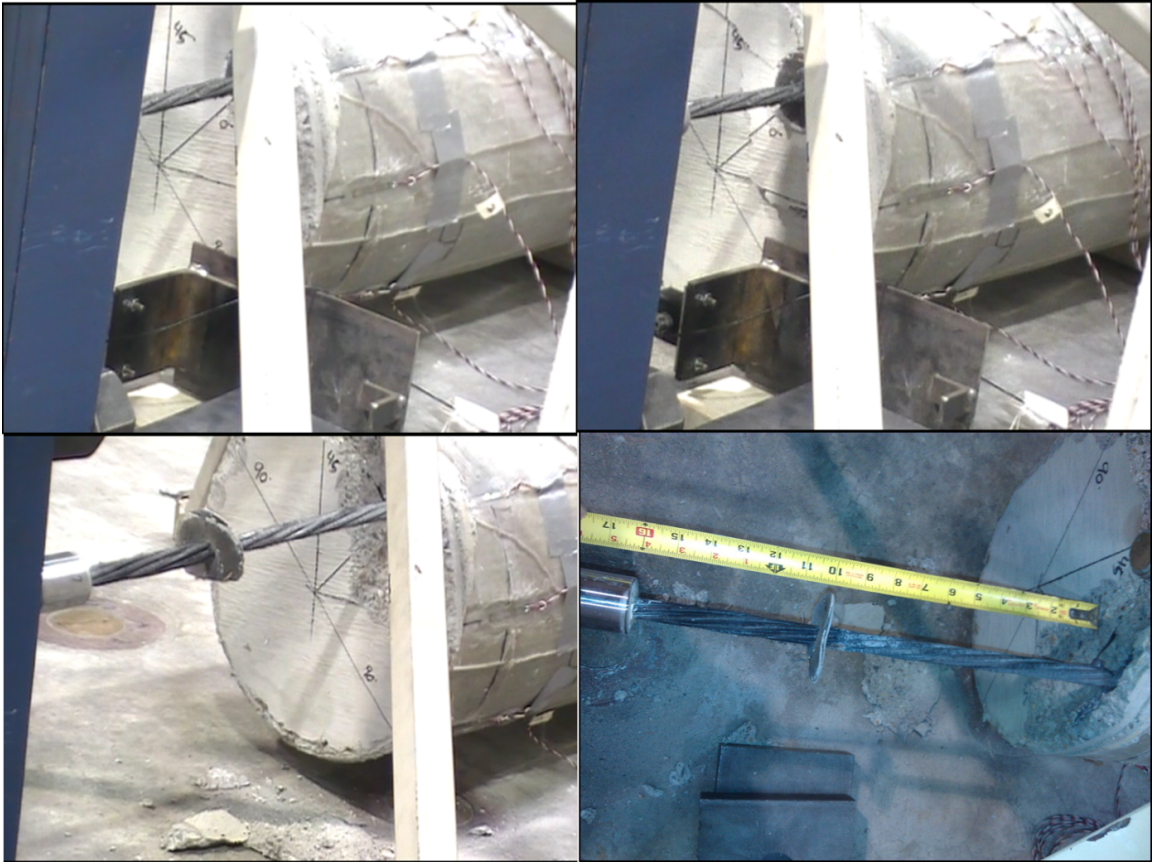


Figure 3.6: CFCC 36-in embedment length specimen. Top left- Specimen at beginning of test, Top right- Specimen being pulled from concrete at initial failure, some concrete cracking observed, Bottom left- Continued pullout after initial failure capacity reached, Bottom right- Final bar pullout.

The next specimen was 3.05 m (10 ft.) in length and had a 1067 mm (42-in) embedment length in concrete. The estimated capacity of the 1067 mm (42-in) development length determined according to ACI 440 was 144 kN (32.4 kip). The specimen was loaded to 50% capacity, 58.3 kN (13.1 kip), and unloaded to remove extensometers from the bars. The specimen was then tested to the initial failure mode, bar pullout from concrete, 253 kN (56.8 kip). The load rate was then increased to 39.4 mm/min (1.55-in/min) and the specimen retested to a load of 145 kN (32.5 kip), and the bar steadily pulled from concrete.

The longest specimen was 3.35 m (11 ft.) in length and had a 1219 mm (48-in) embedment length in concrete. The estimated capacity for the specimen was 159 kN (35.8 kip). The specimen was loaded to 50% capacity 62.3 kN (14 kip) and the extensometers were removed. It was then loaded to 235 kN (52.9 kip) and the steel plate fixtures showed yield and the specimen was unloaded. The plate fixtures were changed and the specimen was retested. It reached 282 kN (63.3 kip) before initial failure mode of bar pullout occurred. The specimen load rate was changed to 50.8 mm/min (2-in/min), and the specimen retested to a load of 238 kN (53.6 kip), and the bar steadily pulled from concrete. A load-deformation curve for all four specimens to initial failure can be seen in Figure 3.7. The 1219 mm (48-in) specimen curve is linear until failure. This is because the specimen was tested twice.

Table 3.1 shows a summary of the four tests comparing the ACI 440 predicted values with the experimental values. The failure load refers to the maximum load experienced by the specimen where initial (25.4mm) pullout of CFCC occurred. The strain data recorded from the gauges in each test had the highest strain readings on the shell down the line of the bar.

Referring back to Figure 3.4, these were gauges H6, H7, H8, H11, H14, H15, and H16. Located at the end of the bar, H8 and H14 recorded the largest strain. The maximum strain recorded, 0.46%, occurred in 914 mm (36-in) embedment length test. This could be caused by the higher load the gauges read to or because the specimen was shorter than the other two. A summary of the strains through the four specimens is shown in

Table 3.3. It should be noted that due to the shorter length of the 381 mm (15-in) embedment length specimen, only four gauges were used down the bar line (2 on either bar). The LVDTs read a horizontal movement of the specimen of 15 mm (0.6-in) before initial failure this value was common for all four of the CFCC tests.

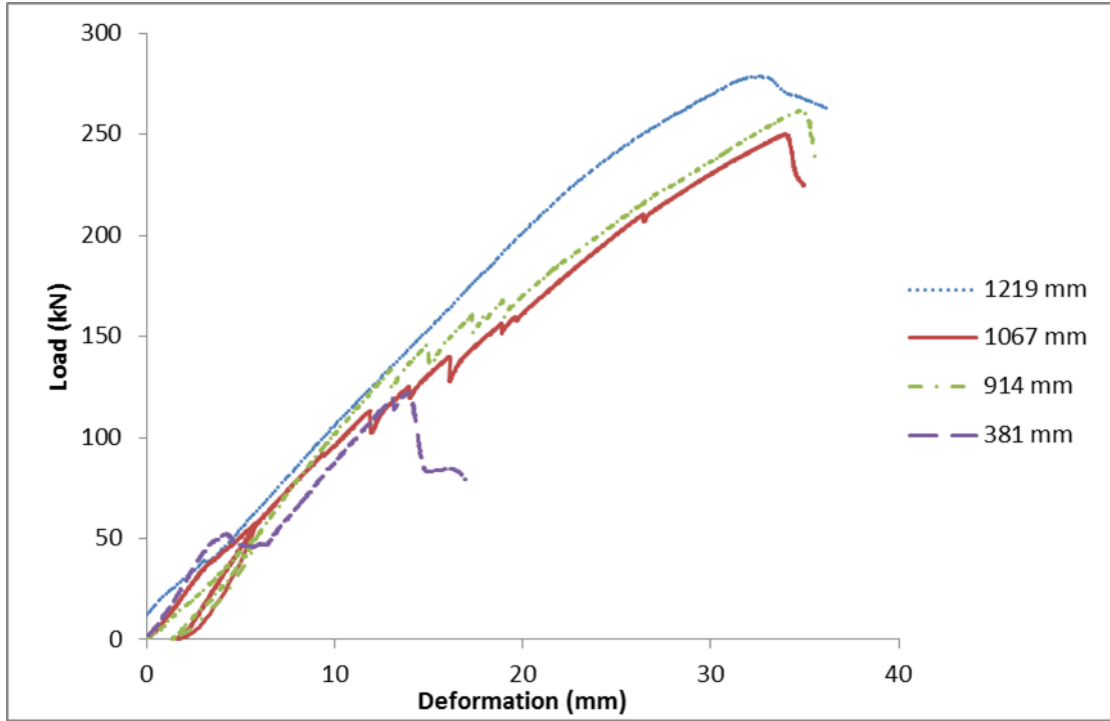


Figure 3.7: CFCC load vs. deformation comparison for the four development lengths.

Table 3.2: Summary of CFCC Pullout Test

Test	Development Length Tested mm(in)	Maximum Load kN(kip)	Failure Mode
1	381 (15)	122.8(27.6)	Bar pullout from concrete
2	914 (36)	264(59.4)	Bar pullout from concrete
3	1067 (42)	253(56.8)	Bar pullout from concrete
4	1219 (48)	282(63.3)	Bar pullout from concrete

Table 3.3: % Strain in gauges down the bar line of CFCC specimens

Specimen mm(in)	Load kN(kip)	H6 (%)	H7 (%)	H8 (%)	H11 (%)	H14 (%)	H15 (%)	H16 (%)
1. 381(15)	124(27.9)	0.08	-	0.09	-	0.01	-	-
2. 914(36)	264(59.4)	0.00	0.30	0.46	0.36	0.38	0.21	0.00
3. 1067(42)	253(56.9)	0.05	0.25	0.25	0.27	0.30	0.13	0.04
4. 1219(48)	234(52.7)	0.10	0.20	0.27	0.23	0.27	0.20	0.20

### 3.6 CFCC Embedment Length Results and Conclusions

The higher-than-expected experimental capacities reached by all four CFCC specimens confirms that the embedment lengths needed to reach the capacity required for this design are shorter than what was predicted based on the ACI 440 equations modified to account for the true ratio of bar perimeter to area.

Table 3.4 summarizes critical results for the CFCC tests and compares the ACI predicted capacity to the observed experimental capacity. The modified ACI 440 equation does not account for the larger perimeter or surface area of the cable, and

based on the larger maximum load values reached experimentally the equation remains conservative. The pullout failures were observed at almost double the predicted capacity. Based on these values, the highest stress in the bar reached during the 1219 mm(48-in) test was  $1.87 \text{ kN/mm}^2$  (270.5 ksi) which is 70% of the ultimate tensile strength of  $2.69 \text{ kN/mm}^2$  (390 ksi) reported by Tokyo Rope, Inc. The bars did not develop the full tensile capacity. As noted in the ACI 440 commentary, the equations provided by ACI 440 have only been significantly validated in the literature for E-glass fiber bars. This study attempted to extend this validation to carbon fiber composite cables used as rebar, and account for the embedment of the rebar in confined concrete. The 0.965 m (38-in) CFCC specimen was manufactured and tested after the three CFCC specimens with longer embedment lengths exhibited higher-than-expected capacities to give a lower bound of the CFCC bar pullout capacity for design of splices in the arches.

Table 3.4: CFCC Test Summary

Rebar Material	Development Length Tested mm(in)	ACI Predicted Capacity kN(kip)	Maximum Load kN(kip)	Failure Mode
CFCC	381(15)	76(17.2)	122.8(27.6)	Bar pullout from concrete
CFCC	914(36)	128(29)	264(59.4)	Bar pullout from concrete
CFCC	1067(42)	144(32.4)	253(56.8)	Bar pullout from concrete
CFCC	1219(48)	159(35.8)	282(63.3)	Bar pullout from concrete

To create an all FRP splice, the carbon fiber composite cable appears to be a viable option with regard to performance and ease of construction. The CFCC specimens exhibited the expected failure mode of pullout from concrete and failed at almost double the expected capacity in all four cases. The CFCC pullout tests created an upper and lower bound for using the CFCC as rebar embedded in concrete. The CFCC's lightweight and flexibility allow easy handling and manufacturability. However, while the CFCC performed well, it could not be procured in time to make beam specimens with spliced connections. Therefore, steel rebar was chosen for the splice tests that are detailed in the following chapter. If the steel splice performs well, this implies that CFCC could be substituted for steel in future applications provide appropriate embedment lengths are used; the results reported here can provide guidance as to the required embedment lengths and what future testing might be required.

## **CHAPTER 4 MANUFACTURING OF BEAMS AND ARCHES AND SPLICE DESIGN FOR CONSTRUCTION LOADS**

### **4.1 Introduction**

The splice was designed with an external reinforcing collar for the construction load case that includes applying the decking and filling the arches with wet concrete. Design values provided by AIT for a current arch geometry were used to create a reasonable external splice. The collar materials were selected to maintain similar strength properties to the carbon fiber CFFT. The external splice design was based on the experimental values collected during the fastener tests, beams were

manufactured using a typical carbon-glass layup, and the collar strength was tested by loading a hollow tube in three point offset bending. After the hollow beam specimens were tested, spliced arches were manufactured to ensure the proposed splice design is feasible.

#### **4.2 Design of External Reinforcing Collar**

Construction and filling loads were used to design the external reinforcing at the splice location. A RISA model, Figure 4.1, was used to determine the shear and moment at the apex of the arch. The arch dimensions used, 9.75 m (32 ft) span and 4.87 m (16 ft) radius, 305 mm (12-in) cross-sectional diameter, were provided by AIT. A distributed filling load of 1.25 kN (280 lbs) per node was used and determined using the typical concrete unit weight  $22.8 \text{ kN/m}^3$  (145 pcf) and multiplying it by the gross cross-sectional area and element length. A construction point load of 4.45 kN (1000 lbs) was used to account for the presence of workers and additional wet concrete in a funnel or trough that is present during filling. These values were used to calculate the maximum shear and moment at the apex during filling. The design values calculated at the apex were a service moment of 4.88 kN-m (3.6 ft-kips), shear of 2.22 kN (0.5 kips), and axial force of 7.1 kN (1.6 kips). Due to the semi-circular geometry of the arch, this design provided a scenario for the design since the apex bending moment was large.

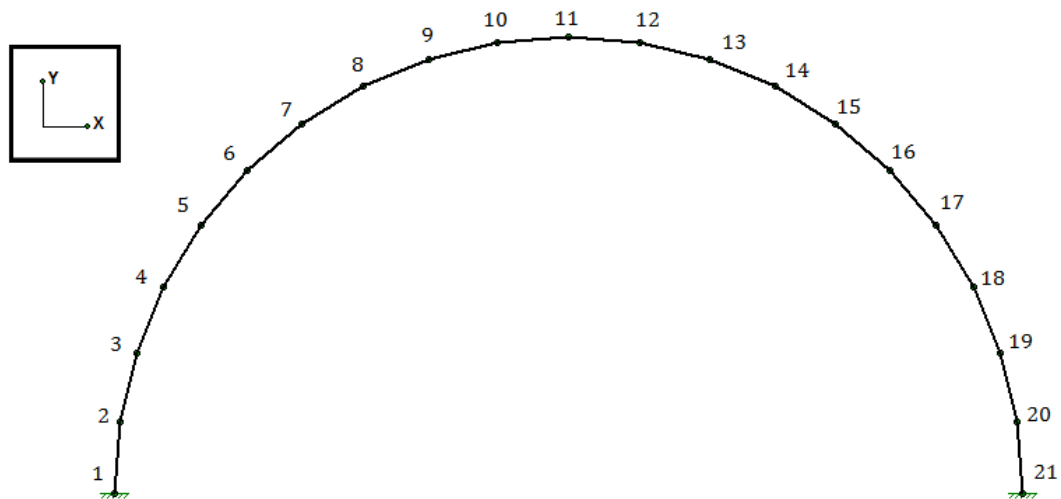


Figure 4.1: RISA Model, 21 Nodes, 20 Elements.

Using the required design moment at the apex, the force per millimeter width was determined by first calculating the moment of inertia of a thin tube with the thickness ignored and using a nominal radius of 150 mm (5.9-in). The force per unit length along the tube circumference required for the connection was calculated to be 69 N/mm (400 lb/in) of width. This was determined by assuming the cross-section is linear-elastic and that the neutral axis for the circle occurs at mid-height. This allows the force per millimeter width to be computed using Equation 4.1. The two fastener experimental capacity found in Chapter 2, 15.3 kN (3438 lb), was then used with a factor of safety of 2 to calculate the required minimum spacing of fasteners around the circumference of the tube, Equation 4.2, where  $F_{\text{bearing}}$  is the fastener ultimate bearing capacity, FS is the factor of safety, and  $f_b$  is the calculated force per millimeter circumference.

Two fasteners had double the minimum capacity required for the splice design, 148 N/mm (850 lb/in), and it was decided to use a two-fastener layout

around the circumference of the collar. The collar design recommends 9 rows of two fasteners around the tube circumference, Figure 4.2. The predicted moment capacity of this splice based on the first fastener bearing failure is 10.5 kN-m (7.7 ft.-kip), which is 114 % greater than the expected service load moment in the 9.75 m span and used as a target structure.

$$f_b = \frac{M_{req'd} \cdot r}{I}$$

Equation 4.1

$$S_{min} = \frac{F_{bearing}}{FS \cdot f_b}$$

Equation 4.2

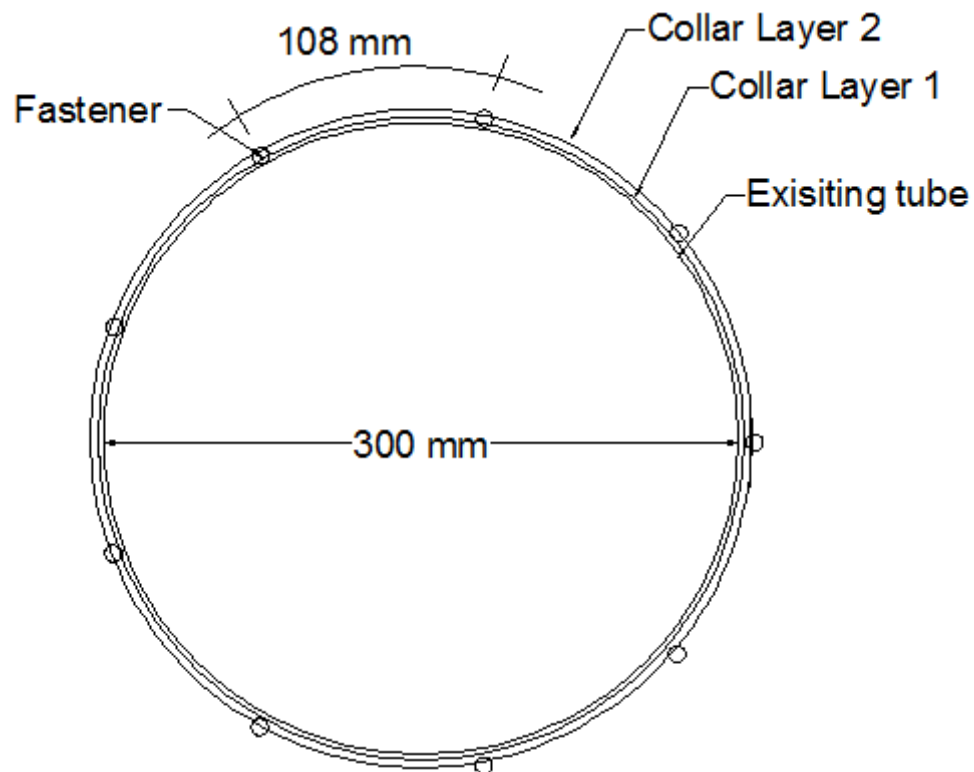


Figure 4.2: Cross-section of fastener spacing around circumference of specimen.

The minimum edge distance of 32 mm (1.25-in) for both the collar and the internal CFFT tubes and 64 mm (2.5-in) fastener spacing should be used. Therefore the collar length should be a minimum of 254 mm (10-in long). As a precaution during

initial connection design a 610 mm (24-in) collar was used. The collar materials used were two stacked, un-bonded, composite shells each having one layer of constraint E-glass fiber and one layer of structural E-glass fiber reinforcement.

#### **4.3 Beam and Collar Manufacturing**

Seven beam specimens were manufactured with an external reinforcing collar. Eight 300 mm (11.8-in) diameter CFFT specimens total were manufactured using two layers of braided structural carbon fiber (UM6448) and one layer constraint E-glass fiber (UM 6447) (according to work instruction WI - M - 21). The specimens were infused with Derakane 610 C vinyl ester resin applying the VARTM process. The cured specimens were cut to 3.66 m (12 ft) long samples, and then cut again at midspan to incorporate the splice. The collars were also 300 mm (11.8-in) diameter and manufactured with the VARTM process using Derakane 610 C vinyl ester resin with one layer of structural E-glass fiber and one layer constraint E-glass fiber. After curing, the collars were cut to 0.61 m (2 ft) lengths, and a slit was made longitudinally down its length to allow the collar to fit over the existing CFFT. The CFFT tube and collar are shown in Figure 4.3.

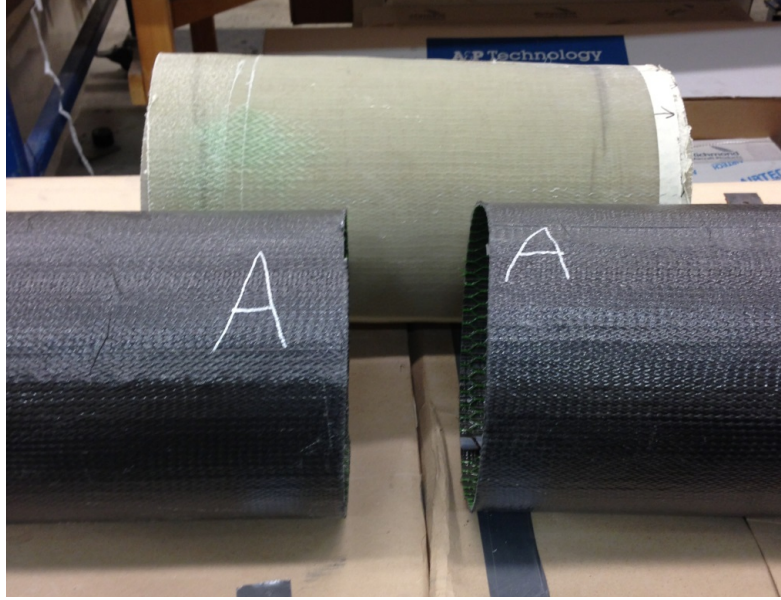


Figure 4.3: Two sections of carbon fiber CFFT and the E-glass fiber collar.

#### 4.4 Installation of the External Collar

The specimens were manufactured in a series of steps which are shown in Figure 4.4. The first collar was placed on one half of the CFFT. The centerline was marked on the collar and this mark was used to position the first beam section. The second collar was put on, and the centerline of the CFFT inside and the collar was marked again. The slit in the collar caused a gap in both of the collars. The gaps were offset and located in the compression zone of the beam where they would have minimal impact. The second half of the CFFT tube was inserted into the collar and the collar was ratchet strapped to the CFFT as tightly as possible maintaining the tubes correct alignment.

The hole placement for drilling was then marked out with nine rows of two fasteners spaced at 32 mm (1.25-in) and 64 mm (2.5-in) from centerline beam as shown earlier in Figure 4.2. Two 10 mm (3/8-in) holes were drilled at designated locations to attach the splice to one side. The collar was attached to one side with

two 8 mm (5/16-in) Huck BOM-R10-14 rivets on opposing sides of the cross-section. For the specimens including rebar, which were ultimately filled with concrete and tested as described later in Chapter 5, the side without the collar attached was removed and the rebar was inserted into the CFFT. The connection was then reassembled, ratcheted tightly, and the rest of the 36 total holes were drilled and rivets attached. The rivets were attached in a star pattern to ensure the collar contacted the tubes as evenly as possible around the circumference. A completed beam specimen is shown at the bottom of Figure 4.4. Three specimens had the collars attached completely without the rebar cage and were used in fill load testing. One CFFT specimen did not incorporate a splice to compare the full strength of a CFFT beam to the splice strength observed. A summary of the specimens manufactured is shown in

Table 4.1.

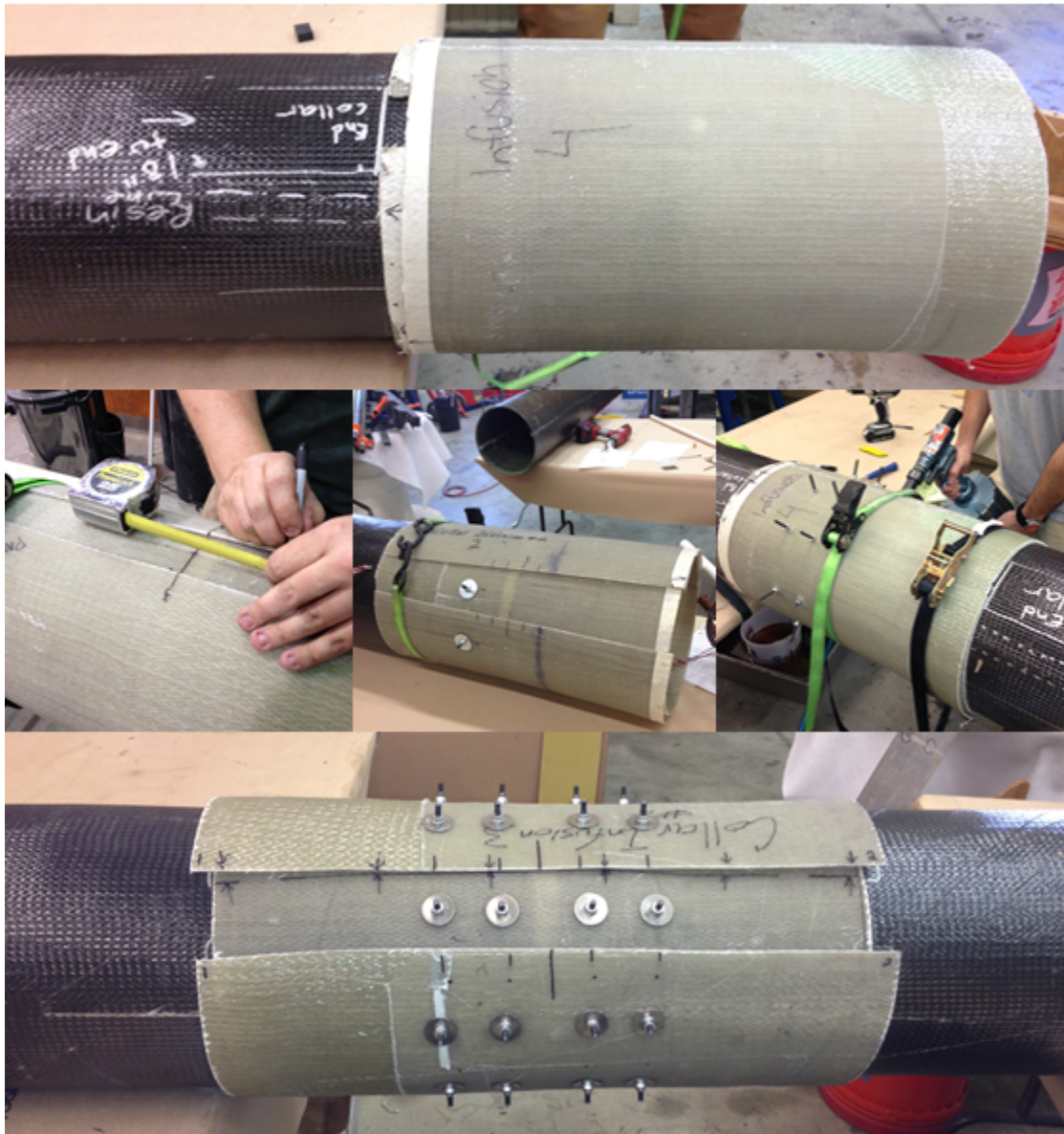


Figure 4.4: Beam manufacturing sequence. Top: Collar placed on half the beam, Middle: Left- Marking out the fastener placement, Middle- Collar attached to one side, Right- Attaching the rest of the rivets, Bottom: Fully attached collar with rivets.

Table 4.1: Summary of Manufactured Beam Specimens

Specimen Name	Test Used	Rebar Cage Inside?	Comments
Tube A	Hollow (fill) test	No	Tested to failure, could not be used for filled beam test
Tube B	Filled beam test	Yes	-
Tube C	Filled beam test	Yes	-
Tube D	Filled beam test	Yes	-
Tube E	Filled beam test	Yes	-
Tube F	Hollow (fill) test/Filled beam test	No/Yes	Tested to filling load, rebar cage put in after for filled test
Tube G	Hollow (fill) test/Filled beam test	No/Yes	Tested to filling load, rebar cage put in after for filled test
Control	Filled beam test	No	-

#### 4.5 Fill Load Testing (Hollow Beam Testing)

Hollow beam specimens were tested to mimic the construction loads the arches would experience when being filled with concrete. The specimens were connected with mechanical fasteners only and tested. Internal reinforcing was not used. The specimens were subjected to a three point offset bend test using the MTS winch system. The offset bend test ensured that the proper shear and moment would occur at the splice location to mimic filling of an arch. Three specimens were tested with a span of 3.05 m (10 ft), and the load applied using the winch and 203 mm (8-in) wide strap located 0.85 m (2.8 ft) from the south end.

The statics to determine the beam test setup are shown in Figure 4.5, where  $P$  is the applied load,  $a$  is the distance from south support, and  $L$  is the beam span. The distance from the south support,  $a$ , was calculated using Equation 4.3. Using the given values and calculated  $a$  value, the fill-load to get the correct shear at midspan

was calculated to be 8 kN (1800 lb) using Equation 4.4. The moment at the splice was then checked with Equation 4.5, and although lower than required, 3.4 kN-m (2.5 ft-kip) the design moment of 4.9 kN-m (3.6 ft-kip) was observed by inducing the factor of safety described below.

$$a = L - \frac{M_{req'd}}{V_{req'd}} \quad \text{Equation 4.3}$$

$$P_V = \frac{V \cdot L}{a} \quad \text{Equation 4.4}$$

$$M = \frac{P_M \cdot (L - a) \cdot a}{L} \quad \text{Equation 4.5}$$

All three were tested to a fill-load of 12 kN (2600 lb) which induces the target shear of 8 kN (1800lb) multiplied by a factor of safety of 1.4. Increasing the target shear by 40% allowed the target moment to be reached in the splice. The test setup is shown in Figure 4.6. The instrumentation used in the test included two string pots to measure deflection. One string pot was located at the application of the load and one was located at the centerline of the beam span. The three specimens were tested in load control. Tube A was tested to failure, Tube F and Tube G were proof-load tested to the fill-load capacity.

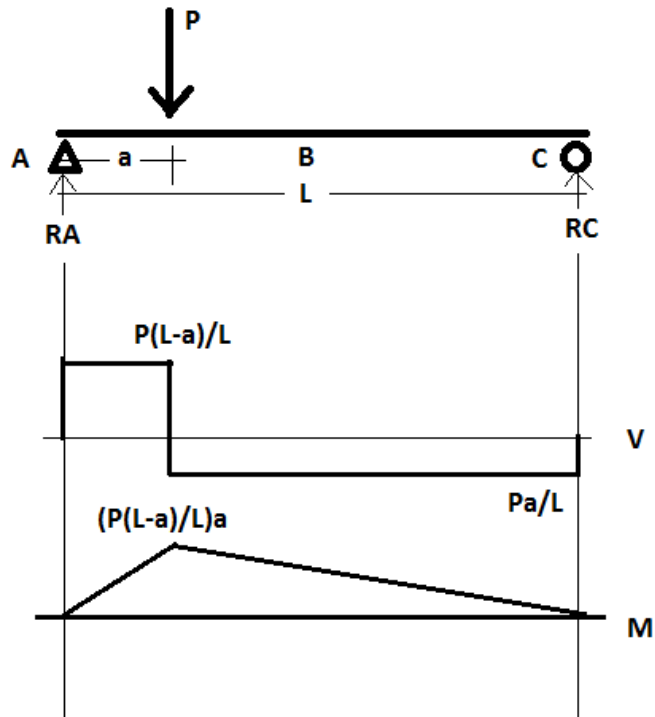


Figure 4.5: Shear and moment diagrams to determine fill test conditions.



Figure 4.6: Hollow beam offset three-point bend setup.

Tube A was tested first and buckling failure occurred in the CFFT specimen. Since this test was to run until failure occurred, a 25 mm (1-in) gap was maintained at the splice between the two CFFT halves to prevent any additional capacity and stiffness that might be provided by the two CFFT halves bearing against each other. The specimen was the worst case scenario and should provide a lower bound for the collar strength because it was the first specimen manufactured and some of the rivets pulled through or were angled into the material, as discussed in Chapter 2. The specimen was tested in load control and preloaded to 0.89 kN (200 lb). The specimen was loaded with a load rate 0.44 kN/min (100lb/min) until the maximum capacity of the load cell was reached 13.3 kN (3000 lb). The load cell was switched with a larger capacity load cell and the test repeated. Buckling failure of the CFFT was observed at the location of load application. The failure load was 18.7 kN (4200 lb) and is shown on the load-deflection plot, Figure 4.7. Bearing failure of the rivets through the collar was not observed; the buckling failure is shown in Figure 4.8. The failure load of 18.7 kN (4.2 kip) was 1.6 times greater than the calculated load at first bearing failure in the rivets due to moment and 2.3 times the load required to produce the service load shear of 8 kN (1.8 kip) expected during filling.

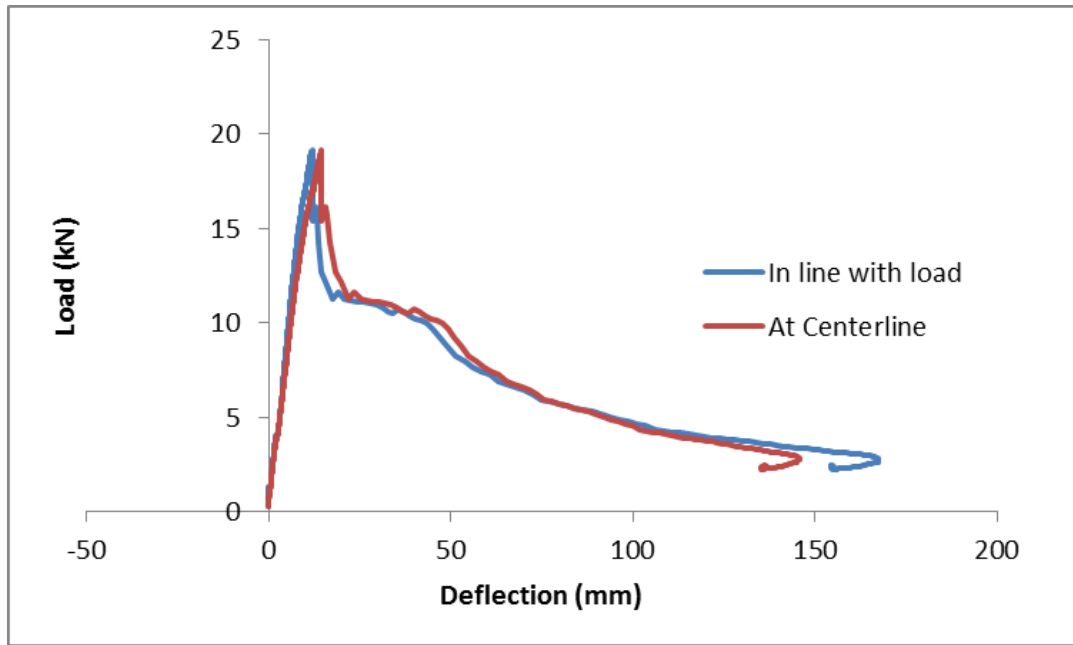


Figure 4.7: Load-deflection plot for Tube A tested to failure.



Figure 4.8: Buckling failure at location of load application.

Tube G and Tube F were tested to 11.5 kN (2600 lb), 1.4 times the expected equivalent filling load of 8.0 kN (1800 lb). The typical load-deflection plot can be seen in Figure 4.9. From the load-deflection plot it can be observed that no permanent deformations occurred at midspan as it returned to its original deformation after unloading. The string pot located at the application of load was stuck and stopped recording when the beam was unloading. The preload was to ensure that the collar would be able to maintain the construction load during concrete filling. The summary of hollow beam testing is shown in Table 4.2 where the maximum moments and shears induced in the splice and at location of load application are listed.

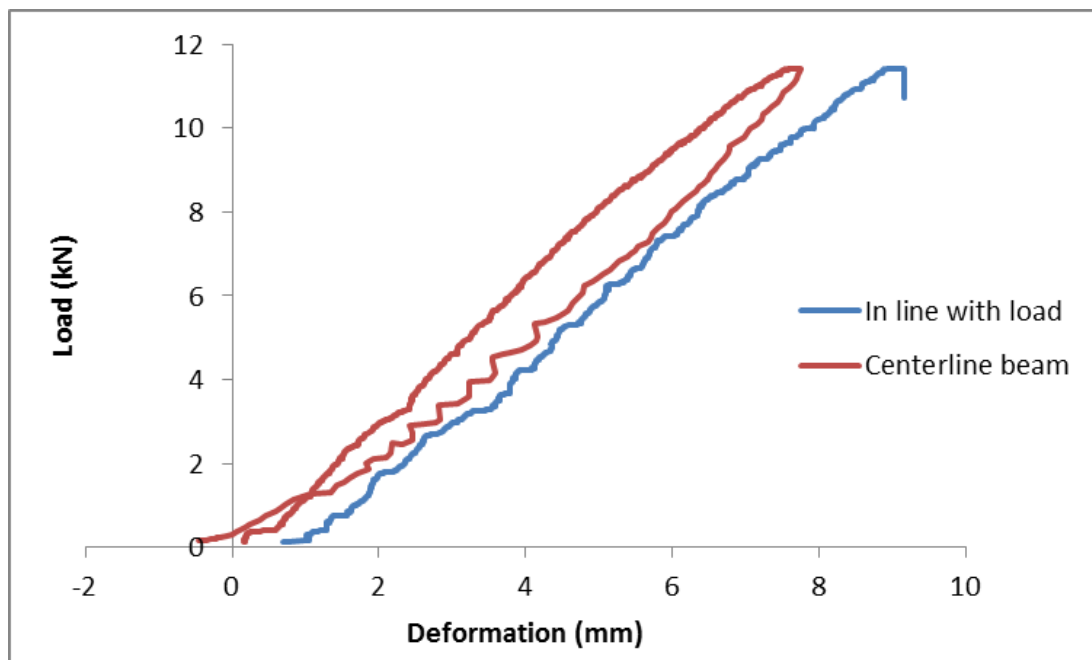


Figure 4.9: Load-deflection plot for Tube G.

After the specimens were tested to mimic filling load conditions, six specimens with rebar cages for internal reinforcing for the complete connection

were filled with concrete. One specimen without a splice was filled with concrete to be used as a control beam and compare to the results of the splice.

Table 4.2: Summary of Hollow Beam Tests

Specimen	Ultimate Load kN (lb)	Induced Shear (V) at Splice kN (lb)	Induced Shear at Load app. ( $V_{max}$ ) kN (lb)	Induced Moment (M) at Splice kN-m (ft-lb)	Induced Moment at Load app. ( $M_{max}$ ) kN-m (ft-lb)
Tube A	18.7 (4200)	5.2 (1176)	13.5 (3024)	8.0 (5900)	11.5 (8500)
Tube F	11.4 (2597)	3.2 (728)	8.3 (1870)	4.9 (3600)	7.1 (5240)
Tube G	11.4 (2597)	3.2 (728)	8.3 (1870)	4.9 (3600)	7.1 (5240)

#### 4.6 Arch Manufacturing

Arches were manufactured using two layers of structural carbon fiber and one layer constraint E-glass fiber. Like the beams discussed in section 4.3, arches were infused using Derakane 610 C vinyl ester resin applying the VARTM process. Two 3.96 m (13 ft) radius and 6.71 m (22 ft) span arches were manufactured to maintain the same conditions as previously tested by Bannon (2009), allowing results to be comparable. After cure, the arches were cut in two at midspan. Using the same formwork as the arches, collars were infused with one layer structural E-glass fiber and one layer constraint E-glass fiber. This ensured the collar would have the same radius as the arch. After infusion, the collars were cut to 0.61 m (2 ft) lengths. In the arch shape, the longitudinal slit on the collar was placed to make sure to allow the gap to occur in the compression zone of the arch, about 30 degrees from the top of the arch cross-section in both directions.

The same arch formwork was used in spliced arch manufacturing. This allowed for the arch splice to maintain the same radius as the two spliced arch halves. After the arch was cut at its apex and the two arch halves placed back on the formwork, the collar was set on one half of the arch and the center line of the collar was marked at roughly 0.31 m (1 ft). The spliced arch manufacturing sequence is shown in Figure 4.10. The other half of the arch was then inserted into the collar. The collar was tightly ratcheted to the existing CFFT, maintaining proper arch shape and gap location for the collar.

Nine locations around the circumference were marked out on the collar at the centerline of the arch spacing around the circumference of 113 mm (4-7/16-in). The locations for fastener placement were then marked out at 32 mm (1.25-in) and a 64 mm (2.5-in) spacing on both sides of the arch centerline. Two 10 mm (3/8-in) holes were drilled at designated locations to attach the collar to one side. The collar was attached to one side with two 8 mm (5/16-in) Huck BOM-R10-14 rivets on opposing sides of the cross-section. The unattached side of the arch was removed and a 1.2 m (4 ft) rebar cage was inserted 0.61 m (2 ft) into one side of the arch. The other CFFT side of the arch was carefully replaced over the rebar cage and underneath the collar. The collar was re-tightened down with the ratchet strap to the CFFT, and the arch was shape was checked. The rest of the 36 total holes were drilled into the collar and CFFT and the rivets were attached. The completed arch is shown in Figure 4.11. The arches were manufactured in a manner as close as possible to how the beams were manufactured, in an attempt to mimic the same

steps done previously. The only major difference for the arch manufacturing was the formwork must be included for manufacturing to maintain the proper arch radius.



Figure 4.10: Arch manufacturing sequence, Top: Left – Arch with collar on, Right- Collar ratcheted down to CFFT sides, Middle: Left- Rivets being used to attach one side of the collar, Right- Rebar and second side of arch being put together, Bottom: Complete collar.



Figure 4.11: Completed unfilled, spliced arches.

#### **4.7 Summary of Results and Recommendations**

The collar design tested in the hollow beam test, nine rows of two fasteners on both sides of the arch splice, proved effective for the goal of carrying the construction filling loads. The proposed design carried the 1.6 and 2 times the service load moment and shear expected during field filling of a typical 305 mm (12-in) diameter arch, respectively. This splice was then used to manufacture two spliced arches. The next step in the process, as discussed in Chapter 5, is testing concrete-filled beams and arches with internal reinforcing at the splice to ensure that they can carry all long-term dead loads and live loads.

## **CHAPTER 5**

### **SPLICE DESIGN AND FULL-SCALE VALIDATION FOR LONG TERM LOAD CASE**

#### **5.1 Introduction**

In addition to the concrete filling and construction loads described in Chapter 4, the splice must carry all long-term dead loads due to backfill, paving, railings and other items, as well as, live load. The splice incorporated a rebar cage designed to carry internal shears and moments due to long-term dead and live loads for the lifetime of the bridge. The internal splice was tested in CFFT beam tests. The beam test results were then used to determine if the splice was feasible for arches used in bridge construction. Although the CFCC reinforcing performed well in the development length tests detailed in Chapter 3, long CFCC lead time constraints led to a steel reinforcing cage being chosen for the splice design. The CFCC reinforcing may be tested later in filled beams to assess the feasibility of an all FRP splice.

#### **5.2 Splice Design for Long-Term and Live Loads**

The splice was designed using ACI 318 Chapter 10 Flexure and Axial Loads for short columns. The factored ultimate moment of 46.3 kN-m (34.2 ft.-kip), factored design axial load of 552 kN (124 kip), and factored shear of 39 kN (8.8 kip) were provided by AIT and used with the interaction diagrams to determine the area of steel required for the splice at the apex of the arch. Six #6 (19 mm) bars were chosen for the internal reinforcement of the splice, and a cross-section is shown in Figure 5.1. This area of steel gives a nominal moment capacity of 164 kN-m (121 ft.-kip) and nominal axial capacity of 2200 kN (494 kip). Six #4 bars and six #5 bars have adequate nominal capacities to carry the ultimate moment and axial load. Six

#4's can carry 80 kN-m (59 ft.-kip) of moment and 1930 kN (434 kip) of axial load. Six #5's can carry 119 kN-m (88 ft.-kip) of moment and 2048 kN (460 kip) of axial. A conservative design was chosen for the splice to ensure success. The factored nominal moment and axial capacity of the #6 bars was determined using a  $\phi$  factor of 0.75 based on ACI 318 Section 9.3.2.2 Compression controlled sections with spiral reinforcing. The factored moment capacity was calculated as 123 kN-m (90 ft.-kip) and factored axial capacity was 1647 kN (370 kip). The cross-section details the internal rebar cage, the CFFT shell, external reinforcing collar, and rivets. ACI 318 Chapter 12 Development and splices of reinforcement, simplified equations from section 12.2.2 were used to determine the required development length for the #6 bars. Calculations for the development length, found in Appendix B, gave a required embedment length of 589 mm (23.2-in). The development length is the length of rebar embedment in concrete required to develop the yield stress of the bar. A 610 mm (24-in) embedment length was utilized, and the lap splice modifier of 1.3 was not used for this design. It should also be noted that a single embedment test of a #4 (13 mm diameter) steel rebar was conducted as described in Appendix A which demonstrated the adequacy of the ACI equations for predicting development length. For the spliced connection this means the internal rebar will be embedded 610 mm (24-in) into both sides of CFFT.

The internal reinforcing for the splice also required a steel spiral to carry shear forces and hold the bars in the proper locations equidistant around the circumference of the tube. Per AIT, the factored shear due to long-term load and live load was 39 kN (8.8 kip). ACI 318 Chapter 11 Shear and Torsion was used to design

the shear reinforcing. A #4 (12.7 mm) bar was chosen for the spiral reinforcing. This size rebar was chosen so a larger pitch could be used and concrete could flow between the rebar. The rebar spiral had a 254 mm (10-in) diameter and 127 mm (5-in) pitch. The total length of the complete design for internal reinforcing was 1.22 m (4 ft.). The combined nominal shear capacity of the of the spiral and concrete core was calculated to be 187 kN (42 kip), the factored shear capacity, 140 kN (31 kip), was calculated using a  $\phi=0.75$  for shear and torsion provided by ACI 318 Section 9.3.2.3. The chosen internal reinforcing provides a structurally conservative solution. The larger spiral size was used to permit a larger pitch to allow for better flow of concrete during manufacturing. The internal reinforcing design is shown in Figure 5.2. After the splice design was completed, the rebar was tied and incorporated in the manufacturing process of the beams described in Chapter 4. Six specimens contained steel rebar at the splice location and were filled with concrete.

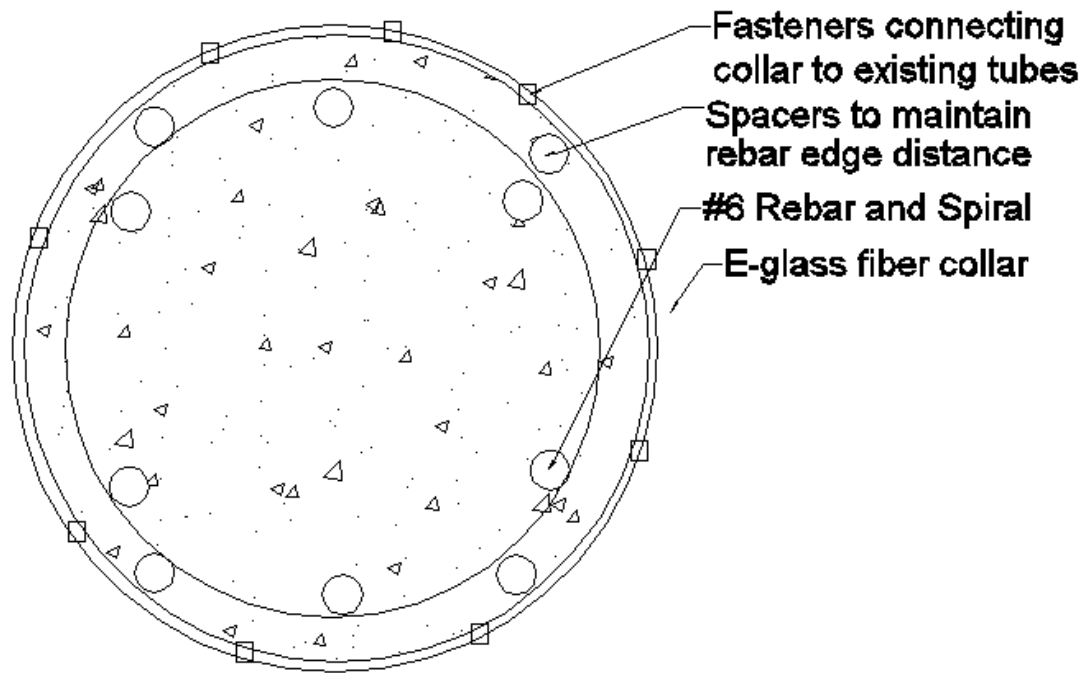


Figure 5.1: Cross-section of the connection

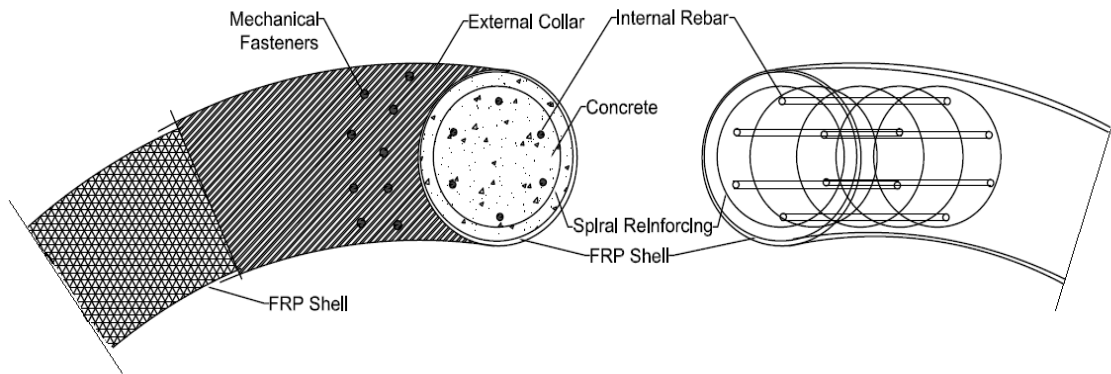


Figure 5.2: Elevation view of the complete splice design

### 5.3 Spliced Beam Tests (Concrete Filled)

Seven total beam specimens were filled with SCC and tested in an offset three-point bend test setup. The offset loading caused a shear and moment at the location of the splice. The shear and moment diagrams corresponding to this loading are shown in Figure 5.3, where  $a$  is the distance from the south end equal to

1.52 m (5 ft.),  $P$  is the applied load,  $L$  is the span length equal to 3.2 ft. (10.5 ft.), and  $B$  is the location of the splice (mid-span). This loading would cause the maximum shear and moment to occur as close to splice location as possible and was as close to the centerline span as possible while still causing a shear and moment. The predicted load to reach the nominal capacity of the splice was calculated as 150.6 kN (33.9 kip). This would cause a shear at the splice location of 66.3 kN (14.9 kip) greater than the ultimate shear, but less than the nominal, and moment of 105.7 kN-m (78 ft.-kip) greater than the ultimate moment, but less than the nominal. It should be noted that the maximum shear and moment does not occur at the location of the splice, but at the location of load application. The maximum nominal capacity for shear was calculated to be 187 kN (18.9 kip) and moment was calculated to be 164 kN-m (86.9 ft.-kip). Similar calculations used to determine the location of the load application can be found in Chapter 4.

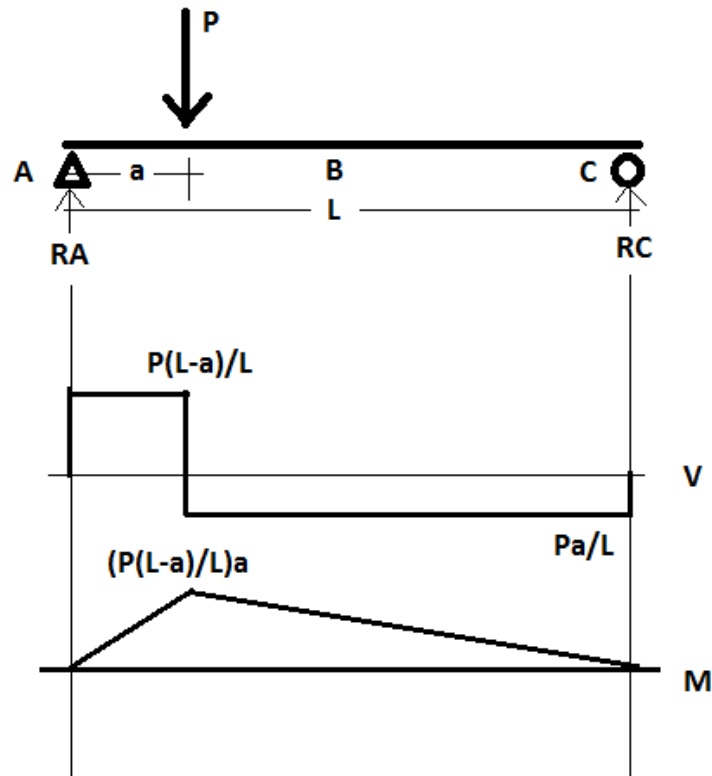


Figure 5.3: Shear and moment diagram for the filled beam test.

A picture of the offset three-point bend test is shown in Figure 5.4. Specimens were tested using a 1300 kN (300 kip) actuator (AS 939) and frame. The South end is the left side of the figure, support A. The instrumentation for the test included 15 - 51 mm (2-in) long N2A350 ohm strain gauges on the CFFT shell and three (1/8-in) CEA-06-125UN-350 ohm strain gauges on the tension rebar. The rebar at the very bottom of the splice shown previously in Figure 5.2: Elevation view of the complete splice design, two  $\pm 13$  mm (0.5-in) LVDTs, and one 305 mm (12-in) string pot located at mid span. The strain gauges were placed on the extreme compression fiber, neutral axis, and extreme tension fiber of the cross section, shown in Figure 5.5. The 15 strain gauges were placed on the shell at the beam ends 305 mm (1 ft.) from the end of span, the end of the rebar 610 mm (2 ft.) from

centerline span, and mid span (on the collar), shown in Figure 5.6. The gauges placed on the steel reinforcing inside the tube, were placed on the longitudinal tension rebar as shown in Figure 5.7. They were placed at the centerline splice connection and beam to determine when the steel rebar yielded during the test. Individual rebars were tested for yield strength comparison described later in the chapter.



Figure 5.4: Offset three-point beam test setup.

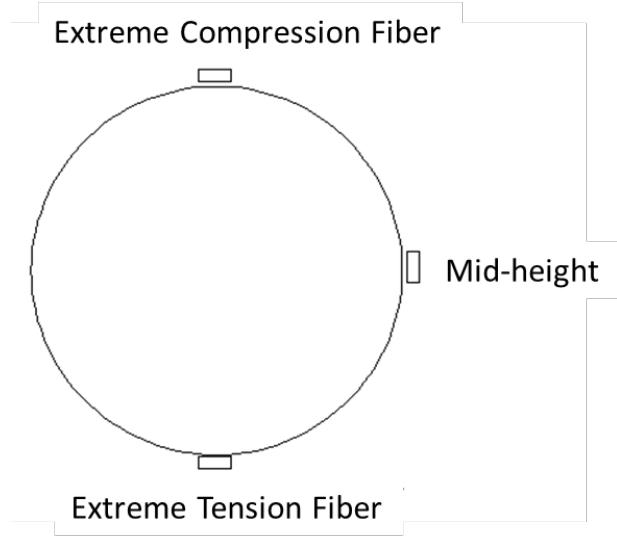


Figure 5.5: Location of the strain gauges on the beam cross-section.

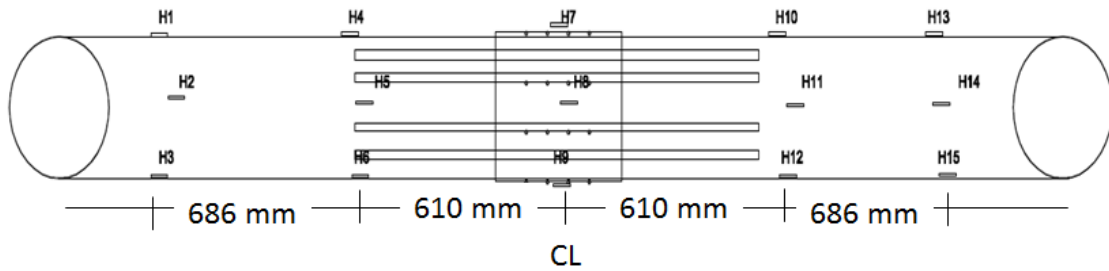


Figure 5.6: Strain gauge placement on the length of the beam specimen.

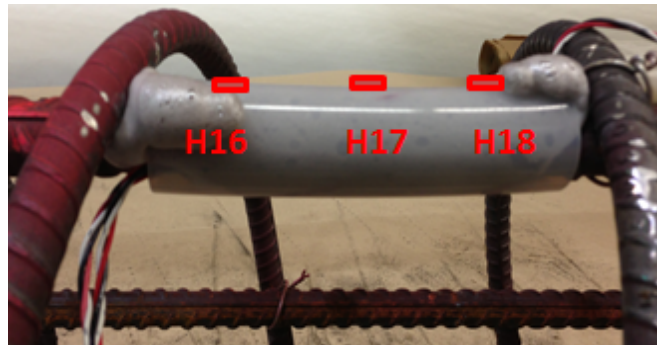


Figure 5.7: Gauge placement on outside edge of tension rebar, protected for concrete fill.

Four spliced beam specimens were tested with the collar fully intact. Two beams were tested with the collar cut circumferentially at the splice centerline to assess the contribution of the riveted collar to the ultimate strength. A picture of an intact collar and cut collar is shown in Figure 5.8. One control specimen with no splice and a continuous CFFT shell was also tested to provide baseline data. The specimens were tested at a load rate of 10.2 mm/min (0.4-in/min). A summary of the beam specimens tested is shown in Table 5.1. Tube F and Tube G, as discussed in Chapter 4, were preloaded to 11.6 kN (2600 lb) before concrete filling to check their capacity under concrete fill loads. The SCC design strength was 27.6 MPa (6000 psi). The concrete cured for 60 days prior to testing. Concrete cylinders were tested in accordance with ASTM C39. Three 152 mm (6-in) diameter concrete specimens were tested 28 days after the pour and at the time of the beam testing. The average 28-day concrete compressive strength was 55.8 MPa (8101 psi). Three 152 mm (6-in) diameter concrete specimens were tested for the 60-day strength. The average concrete compressive strength was 37.3 MPa (5413 psi) after 60 days. However, this 60-day strength was likely not a good representation of the actual compressive strength because the cylinders were tested improperly and without pads, so the data for time of testing is not considered further.



Figure 5.8: Top – Tube E with collar intact, Bottom – Tube D with collar cut circumferentially.

Table 5.1: Summary of Beam Specimens Tested

<b>Specimen Name</b>	<b>Pre-load kN (lb)</b>	<b>Collar attached? (Y/N)</b>
Tube A	19.4 (4350) Failure observed	-
Tube B	-	No
Tube C	-	Yes
Tube D	-	No
Tube E	-	Yes
Tube F	11.6 (2600)	Yes
Tube G	11.6 (2600)	Yes
Control	-	-

A control specimen was tested to generate baseline results. The control was a straight CFFT beam with a 3.05 m (10 ft.) long span and no splice. The load-deformation plot for the control beam is shown in Figure 5.9. The maximum deflection reached for the specimen before failure was 76 mm (2.99-in) at the load application, 93 mm (3.7-in) at mid-span. Bending failure of the FRP occurred at 180.8 kN (40.6 kip) and is shown in Figure 5.10. The moment induced at the mid-span due to the failure load was 126 kN-m (93 ft.-kip). The maximum moment at the location of load application was 141 kN-m (104 ft.-kip). This value was slightly lower than the average experimental moment value for beam tests conducted by Bannon (2009), of 152 kN-m (112 ft.-kip). The moment-strain relationships for all the gauges described above are shown in Figure 5.11, Figure 5.12, Figure 5.13, Figure 5.14, and Figure 5.15. The moment value is calculated at the gauge location. The gauges are grouped based on location on the beam span. From the data you can see that the typical CFFT beam specimen strain response. The greatest strains, 0.8% read on the tension gauges, were recorded by the gauges closest to the application

of load and experienced the greatest amount of deflections, H6, H9, and H12. The greatest compression strain observed was 0.4%. A noticeable change or jump in the graph can be seen in the figures at 20 kN-m (198 kip-in). It is likely that the concrete cracked at this point and the value is consistent with experimental results found by Bannon (2009) where there was a jump in the moment-strain plot at 22.6 kN-m (16.7 ft.-kip) due to concrete cracking. Bannon (2009) observed a maximum compression strain of 0.4%, a maximum tensile strain of 1.0%, and a maximum displacement of 114 mm (4.5-in).

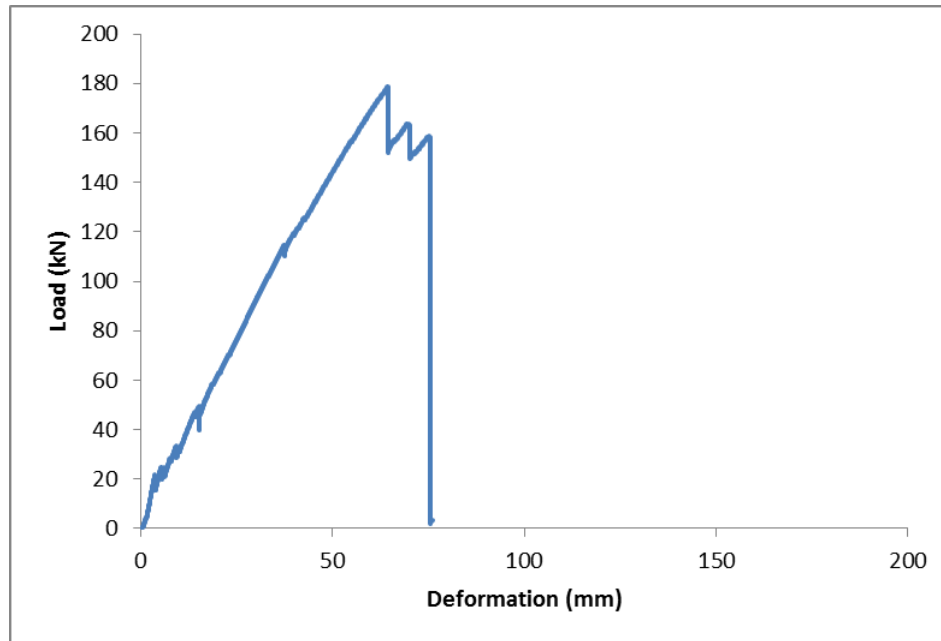


Figure 5.9: Load-deformation plot for the control specimen.



Figure 5.10: Control beam specimen before and after test, Top- Untested beam, Bottom- FRP tension failure of the specimen due to bending.

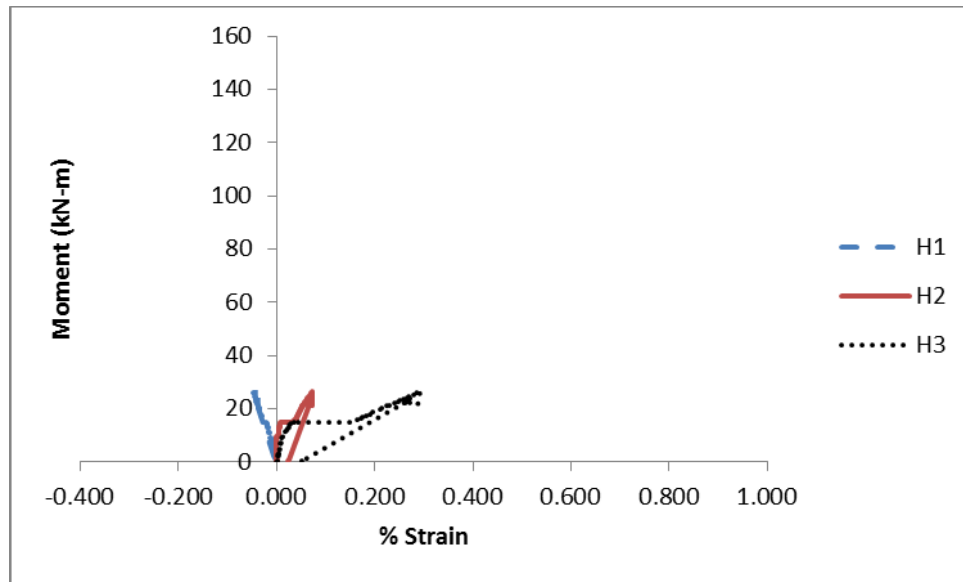


Figure 5.11: Moment-% strain plot for the Control specimen North End gauges.

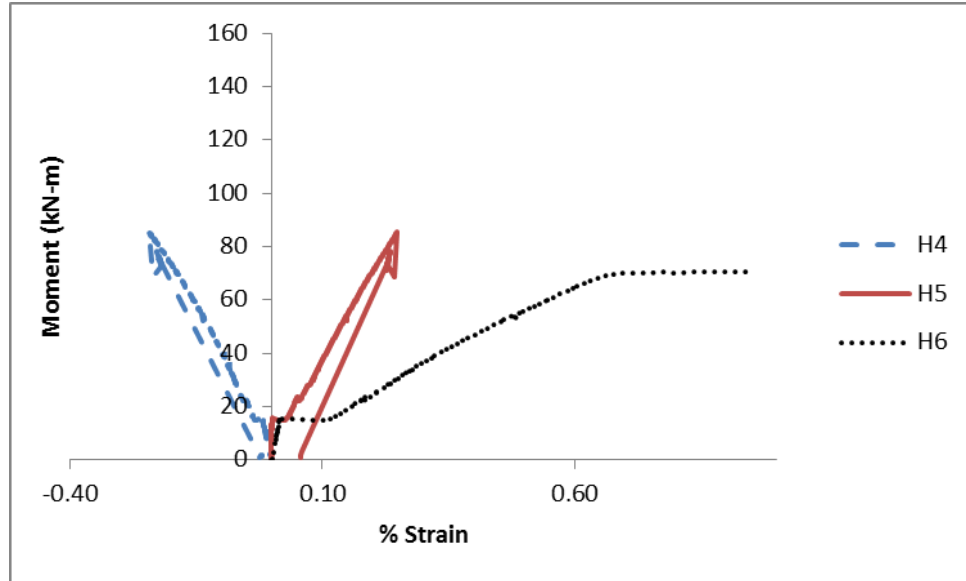


Figure 5.12: Moment-% strain plot for the Control specimen North Rebar End gauges.

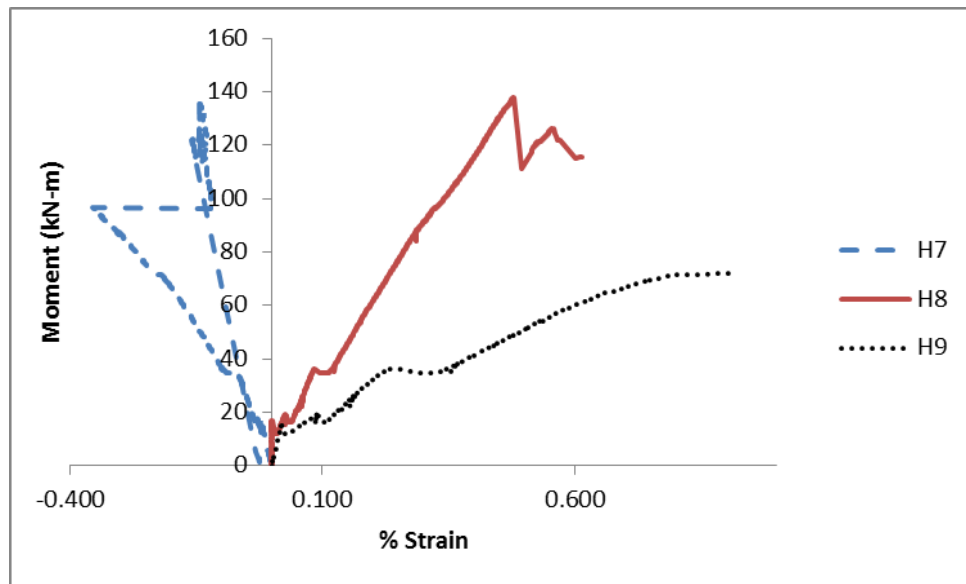


Figure 5.13: Moment-% strain plot for the Control specimen Mid-span gauges.

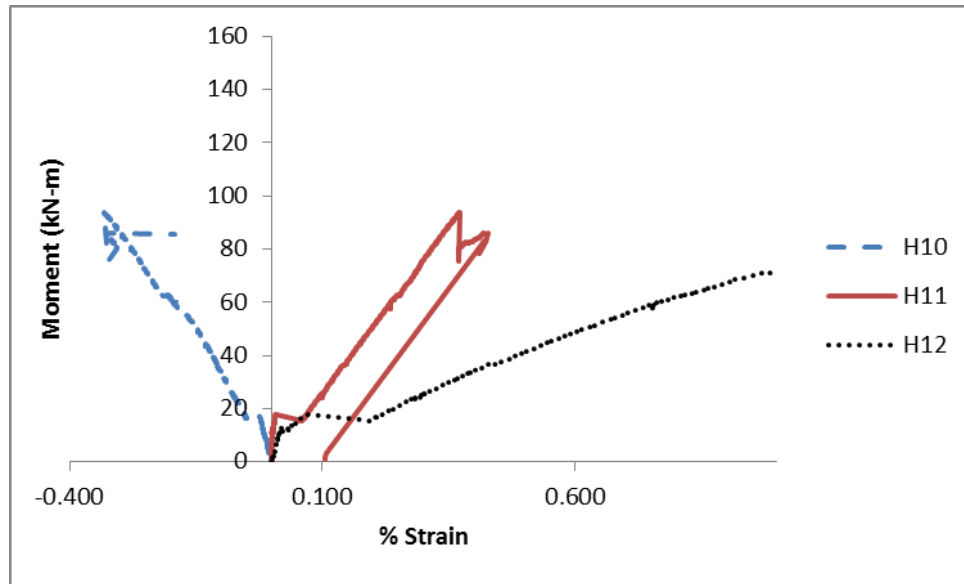


Figure 5.14: Moment-% strain plot for the Control specimen South Rebar End gauges.

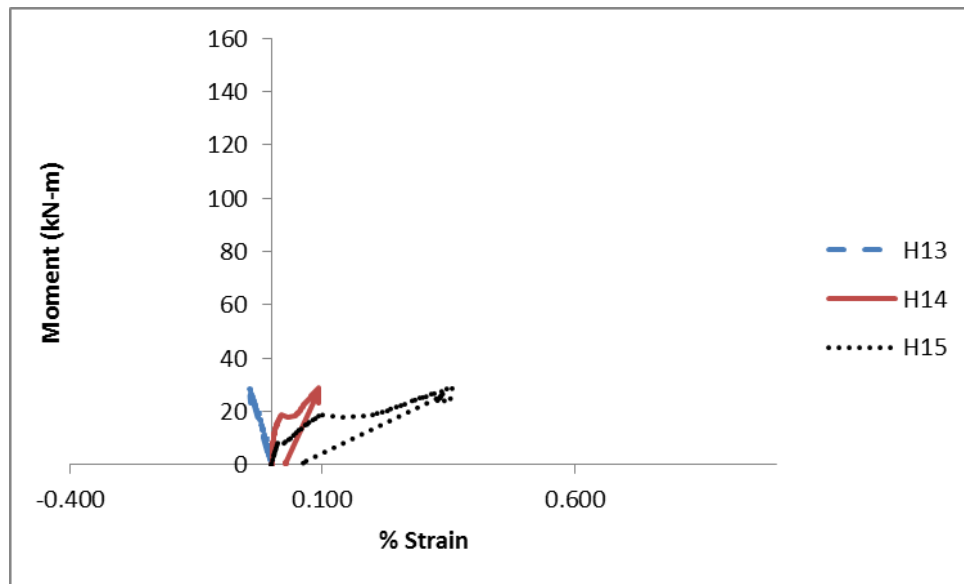


Figure 5.15: Moment-% strain plot for the Control specimen South End gauges.

Four specimens, Tube C, Tube E, Tube F, and Tube G, were tested with the collar intact. Failure occurred when the two sides of CFFT separated and exposed the rebar cage. Bearing and pullout failure of the rivets could be observed in the collar. The load-deformation plot for all four tests is shown in Figure 5.16. From the plot, a more ductile behavior is observed than for the control specimen. The

specimens sustained a peak load for an estimated 150 mm (5.9-in) before failure occurred at the splice location. Average deformation at failure was 208 mm (8.2-in), COV of 8.2%. The average maximum load for the four specimens was 187 kN (42.6 kip), COV of 1.9%. The peak load reached by the sample set was 194 kN (43.7 kip). This load induced a moment in the splice of 132 kN-m (97.6 ft.-kip), and shear of 83 kN (19 kip). These values were greater than the ultimate moment of 46.3 kN-m (34.2 ft.-kip) and shear of 39 kN (8.8 kip) and greater than the nominal design moment, 123 kN-m (90 ft.-kip), and shear, 77 kN (17.4 kip). The failed Tube F is shown in Figure 5.17, and the failure underneath the collar is shown for Tube G in Figure 5.18. Tube F and Tube G tested to the similar ultimate load cases to Tube C and Tube E, but failed at a lower deformations. The ultimate deformation for Tube F and Tube G was about 13% lower than Tube E and Tube C. This could have occurred because the collar system in both sustained permanent deformation that was not initially noticeable because it was in the CFFT not the collar.

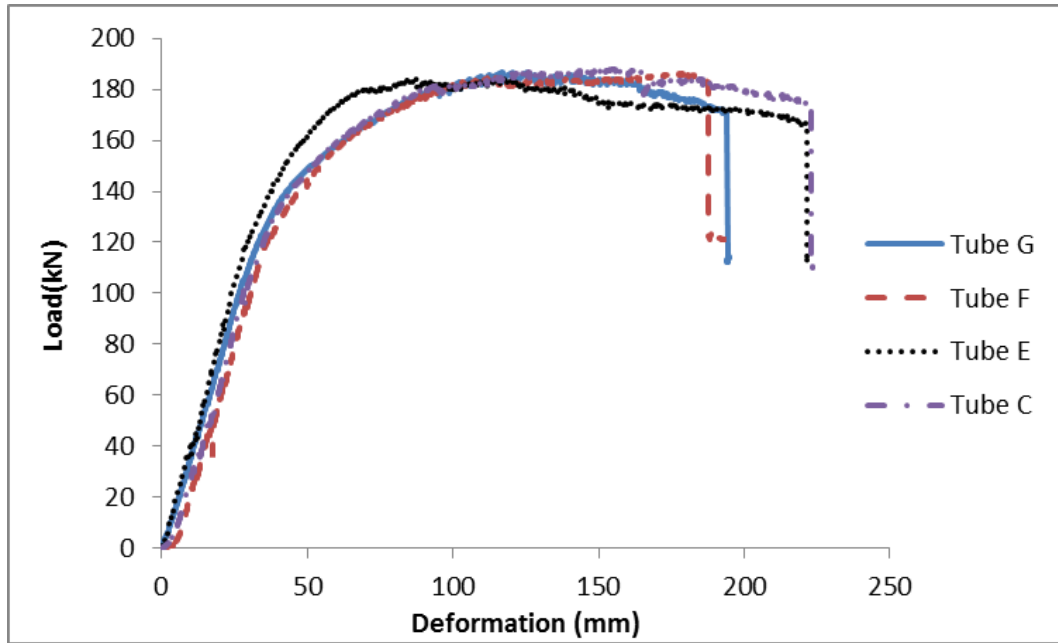


Figure 5.16: Load- deformation plot for beam specimens with the collar intact.



Figure 5.17: Failed Tube F.

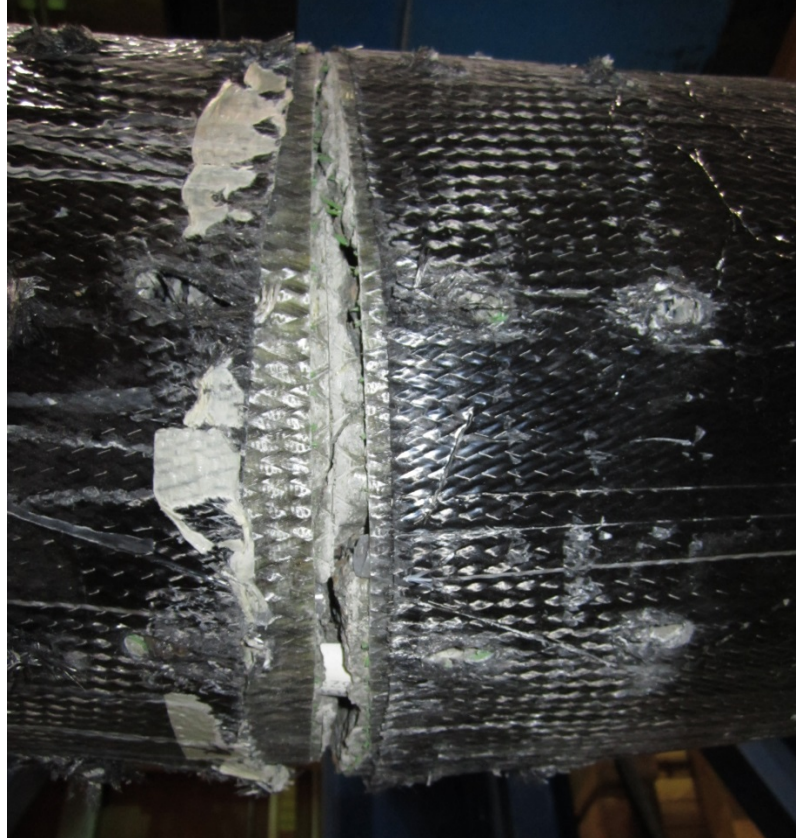


Figure 5.18: Failed Tube G with collar removed, bearing failure of rivets through the CFFT and concrete section separated at centerline.

The moment-strain relationship was recorded for the three of the four beam specimens tested with the collar intact. Tube E plots, shown in Figure 5.19, Figure 5.20, Figure 5.21, Figure 5.22, and Figure 5.23, as with the control beam, show the largest strains occurred on the extreme tension fibers and closest to the location of load application. The plots for Tube F and Tube C are located in Appendix C. In the beam it is where the rebar cage ends and recorded by gauges H6 and H12. The gauges recording strain on the collar did not read correctly. The gauges H7, H8 and H9, Figure 5.21, gathered a noisy amount of compression strain and tension strain throughout the tests this was consistent for all data gathered by the collared beam

tests. The strain data for Tube G was not correctly recorded and could not be included.

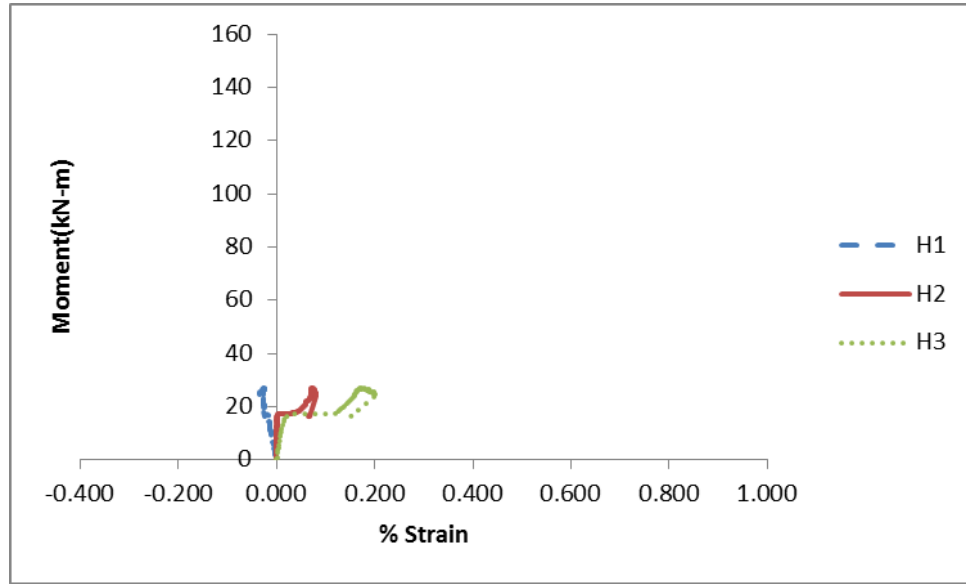


Figure 5.19: Moment-% strain for Tube E North End.

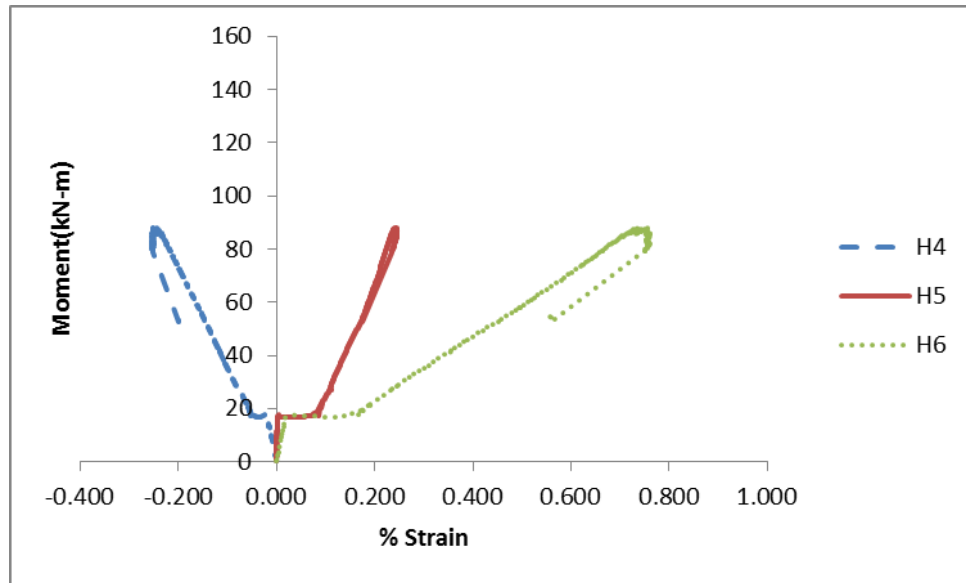


Figure 5.20: Moment- % strain for Tube E North Rebar End.

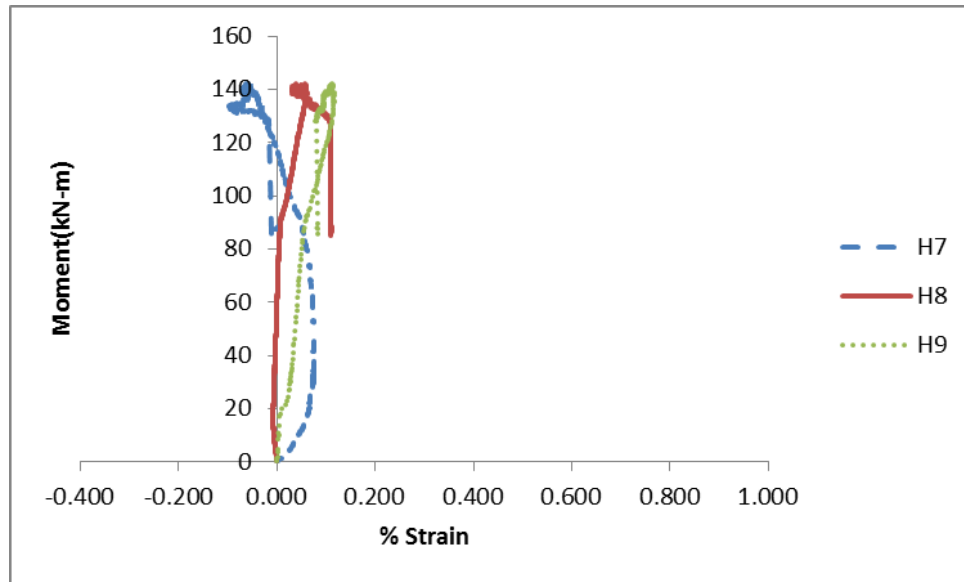


Figure 5.21: Moment-%Strain for Tube E Mid-span on collar.

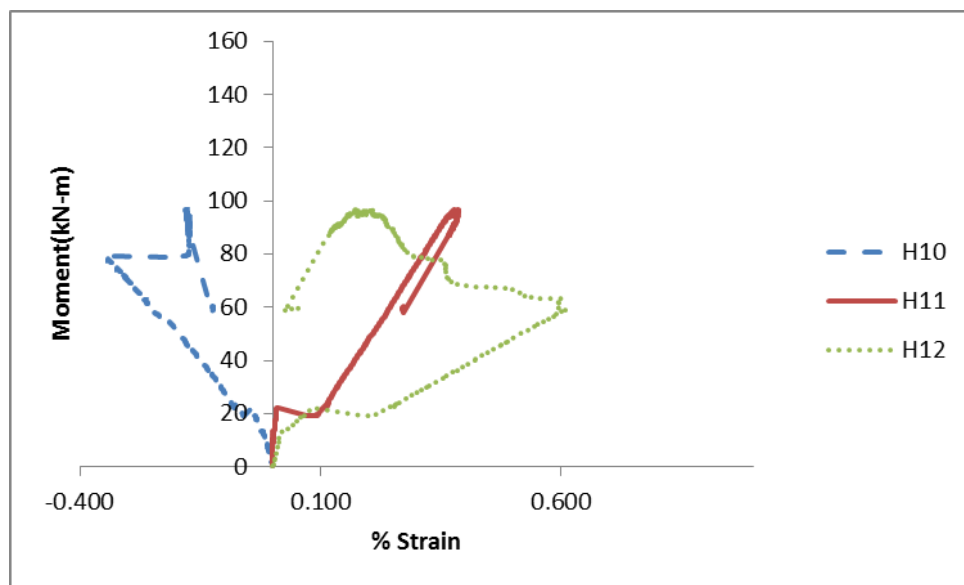


Figure 5.22: Moment-%Strain for Tube E South Rebar End.

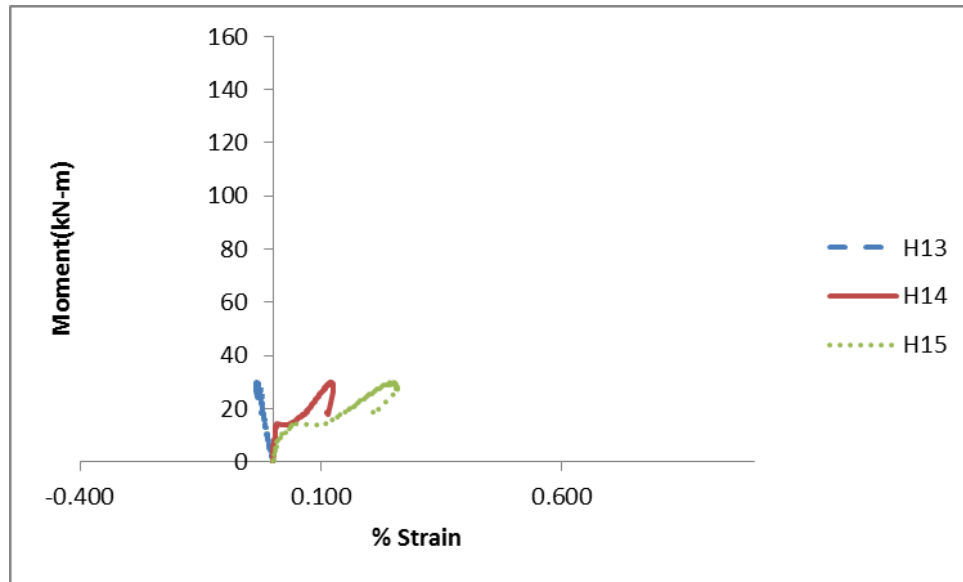


Figure 5.23: Moment-%Strain Tube E South End.

Three strain gauges were placed on the steel rebar during the beam tests. The moment versus percent strain were compared with single straight rebar tests to compare the yield of the bars. The load versus deformation plot is shown in Figure 5.24. The average yield load was 123 kN (27.7 kip). During the beam tests, the average yield load was lower, around 85 kN (19 kip). The average moment corresponding to the yield of the reinforcing was 65 kN-m (48 ft.-kip). Although the load at which the steel yielded was lower during the beam tests than the straight bar testing, the steel yield strains were typical. The bars yielded around 0.0021.

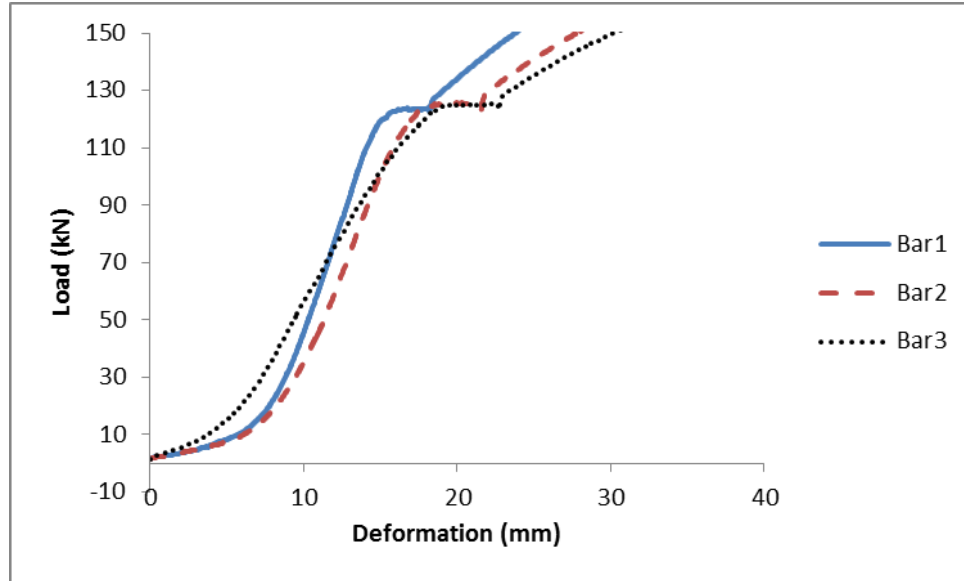


Figure 5.24: Load-deformation plot for #6 rebar tested in tension.

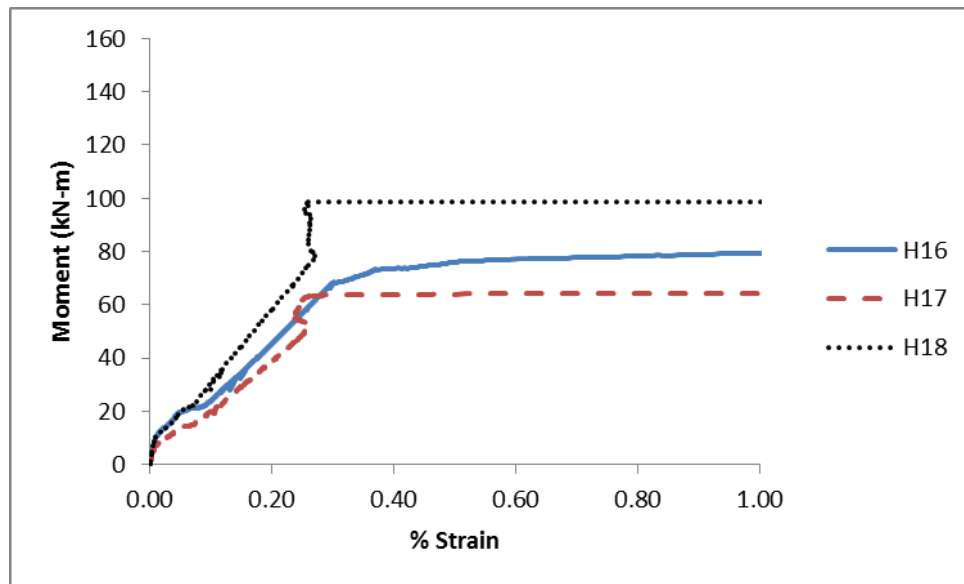


Figure 5.25: Moment-% Strain for tension rebar in Tube E.

Two specimens were tested with the collar cut circumferentially to determine the reduction in capacity. Tube B and Tube D were tested in this manner. A bending failure occurred with separation of the two sides of the CFFC with a concrete crack at the splice location. The average failure load for the specimens was 153.8 kN (34.9 kip). From the load-deformation plot for the two specimens shown

in Figure 5.26, it is observed that the maximum deflection recorded for Tube D was 135 mm (5.31-in) and for Tube B was 190 mm (7.49-in). Tube B is an anomaly and had a more ductile response because the collar had not been cut completely through, which was evident after the test was completed and some of the collar fibers were still intact as shown in Figure 5.27. The value of 135 mm (5.31-in) is the more likely representative of response without the collar attached based on a comparison to the control specimen deformation. The moment-strain responses for Tube D, are plotted in Figure 5.28, Figure 5.29, Figure 5.30, and Figure 5.31. From these plots it is observed that the maximum strain occurred in the extreme tension gauges H6 and H12 similar to the previous tests of the control beam and collar attached. Both plots have similar strain responses with an average maximum moment of 108.7 kN-m (80.2 ft.-kip). There were no gauges at centerline span or on the collar for this test. The plotted response for Tube D shows a linear response because the specimen was retested after a problem with the support was noticed and fixed after the first test.

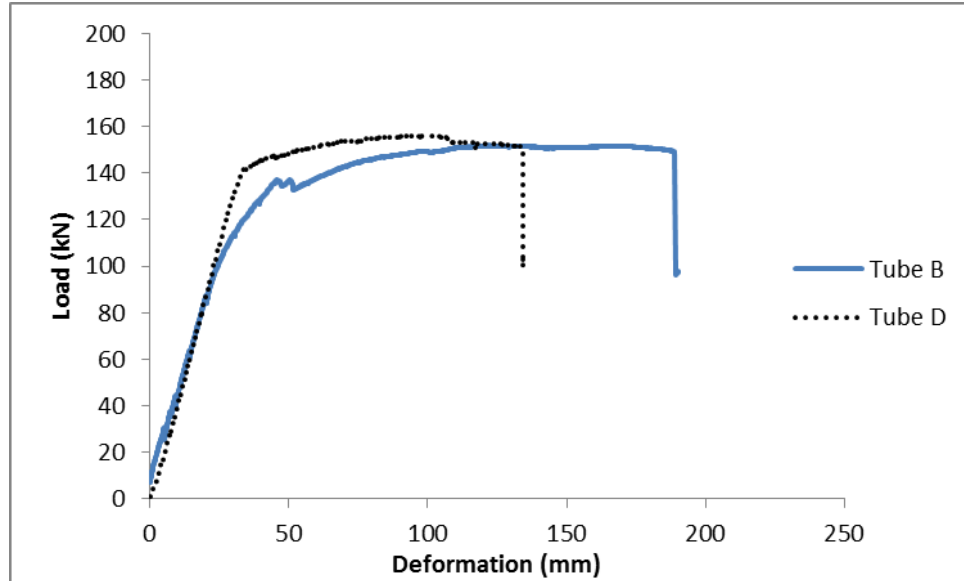


Figure 5.26: Load-deformation of beams with cut collar.

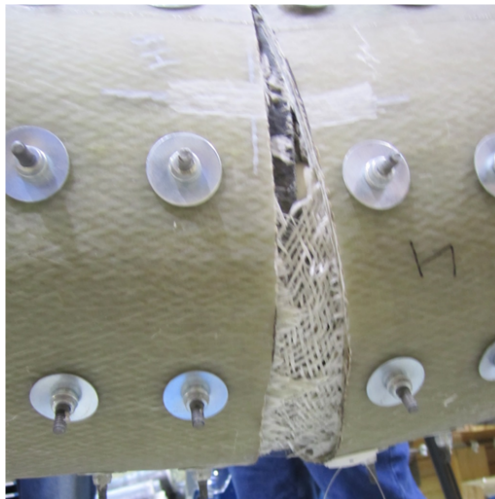


Figure 5.27: Tube B cut collar section with some collar still attached after failure.

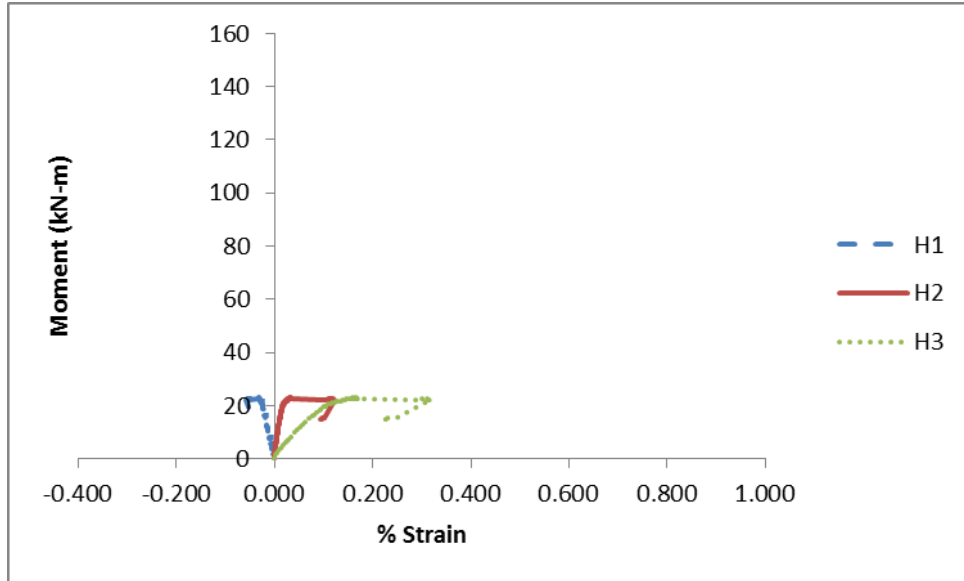


Figure 5.28: Moment- % Strain for Tube D North End.

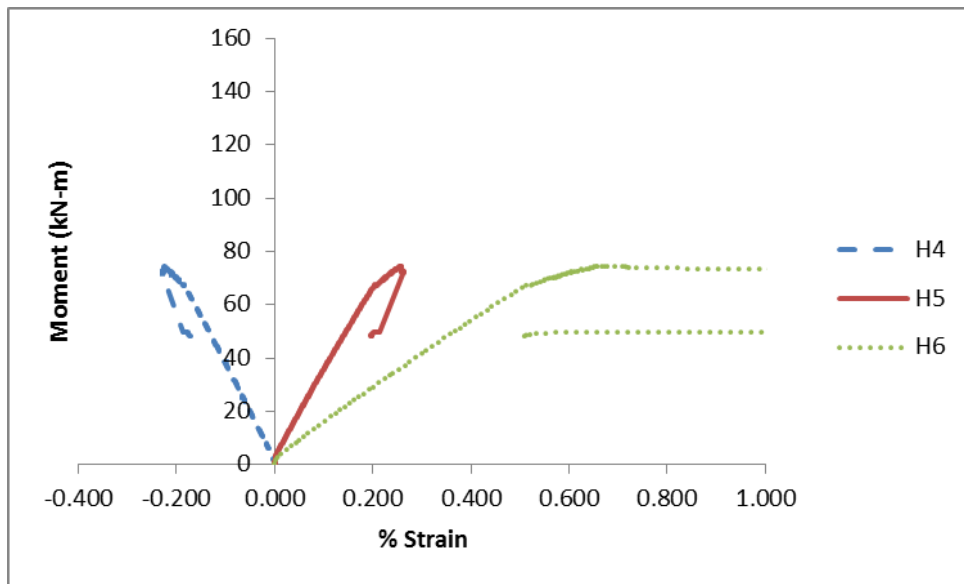


Figure 5.29: Moment-% Strain for Tube D North Rebar end.

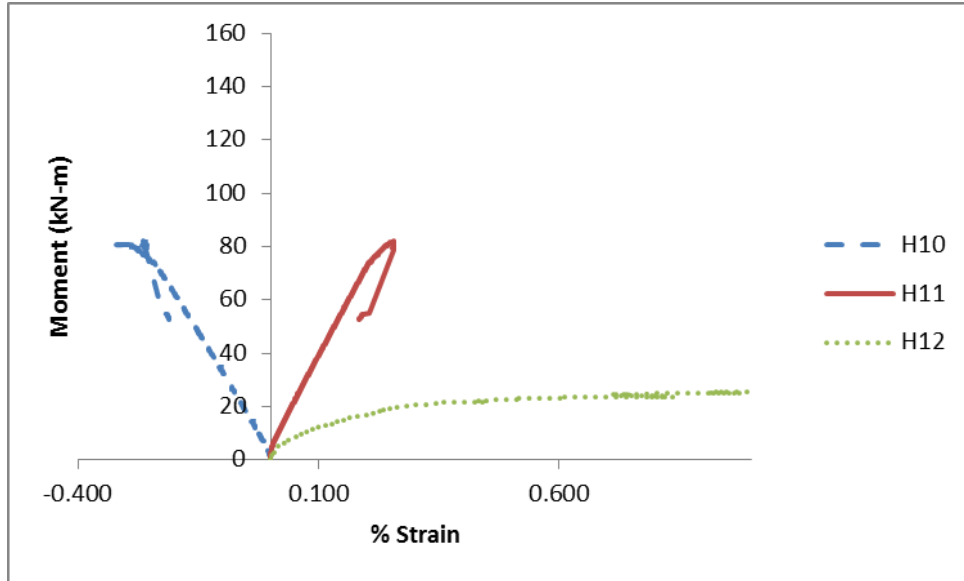


Figure 5.30: Moment-%Strain Tube D South Rebar End.

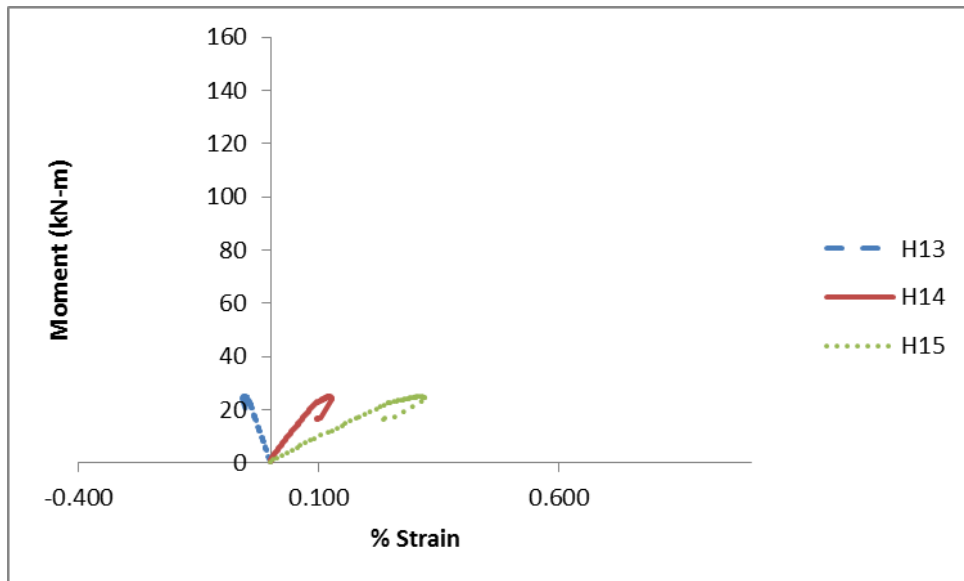


Figure 5.31: Moment-%Strain Tube D South End.

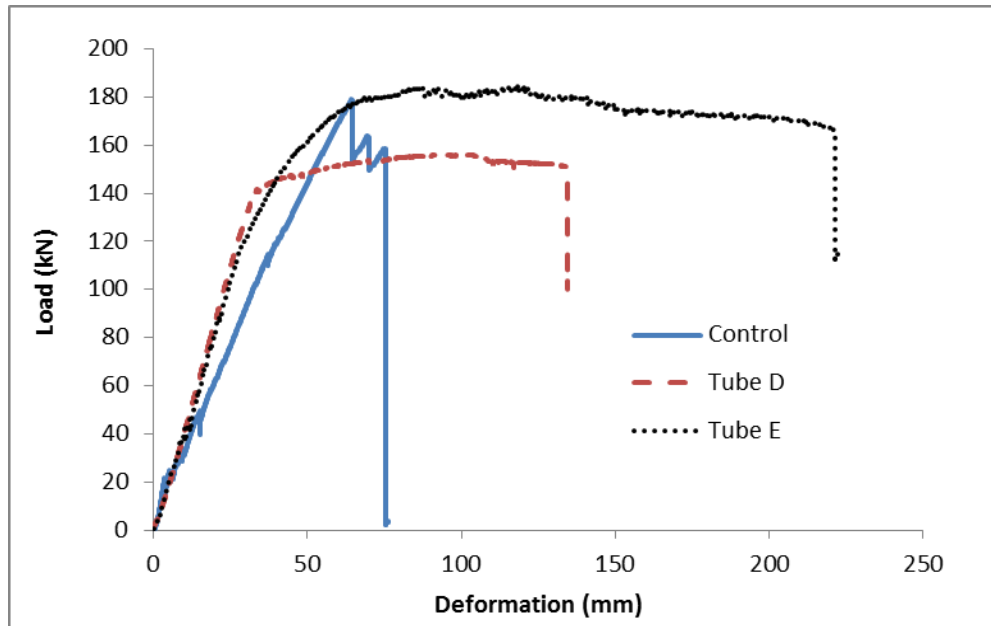


Figure 5.32: Load-deformation comparison of three specimen types tested. Tube D- no collar, Tube E- with collar.

The typical load-deformation plot comparing the three beam specimen types is shown in Figure 5.32. The ductility of the full splice with collar still attached allows for 2.5 times the deformation of the control specimen. The specimen benefitted most using both the collar and the internal reinforcing combined. The specimens with the collar cut had about 85% of the ultimate strength observed by the complete spliced specimen. However, these specimens carried a peak load of 153.8 kN (34.9 kip), which induced at mid-span a moment at the splice of 108 kN-m (80 ft.-kip) and shear at the splice of 68 kN (15 kip). The maximum values for moment and shear occurred at the location of load application were 122 kN-m (990 ft.-kip) of moment and 87 kN-m (19 kip) of shear. The moment is the same as the factored nominal moment capacity determined, and the shear is 8.8 kN (2 kip) greater than the nominal shear capacity for the splice. These values are still greater than the required strength for the splice.

#### **5.4 Summary of Beam Test Results and Recommendations**

The beam tests experimentally validated the ability of the splice to carry long-term dead and live loads, and indicate this splice will be adequate for a typical arch. A summary of the results from the beam tests is shown in Table 5.2. As discussed previously, the complete collar and internal rebar connection working together maintain the best results in replicating a typical carbon CFFT beam.

Table 5.2: Summary of the CFFT beam test

<b>Specimen</b>	<b>Pre-load kN(lb)</b>	<b>Peak Load kN(lb)</b>	<b>Deformation mm (in)</b>	<b>Failure Mode/Comments</b>
Control	-	180.8 (40652)	76 (2.99)	Bending failure of FRP
Tube A	19.4 (4350)	-	167 (6.59)	Shell buckling failure
Tube B*	-	153.4 (34486)	190 (7.49)	Bending failure/concrete separation at splice location
Tube C	-	194.5 (43714)	224 (8.80)	Bending failure/concrete separation at splice location
Tube D*	-	157.7 (35459)	135 (5.31)	Bending failure/concrete separation at splice location
Tube E	-	186.3 (41887)	222 (8.74)	Bending failure/concrete separation at splice location
Tube F	11.6 (2600)	188.1 (42277)	192. (7.56)	Bending failure/concrete separation at splice location
Tube G	11.6 (2600)	188.9 (42466)	195 (7.67)	Bending failure/concrete separation at splice location
* collar cut circumferentially				

## **CHAPTER 6**

### **SPLICED ARCH TEST VERIFICATION**

#### **6.1 Introduction**

For this validation, the arch geometry as manufactured and tested by Bannon (2009) was used so as to have a 'control' set and to compare spliced to intact arch performance. The arches were spliced at the crown with collar and internal reinforcing cage as described in Chapter 4. The arches were manufactured as they would be in the field. For field manufacturing, it is recommended to use the formwork used for infusion to maintain the proper arch radius during splice installation.

#### **6.2 Arch Filling**

Two spliced arches were filled at the crown from the side, or middle of the circular cross-section using a pipe section and trough setup as shown in Figure 6.1. The arches were first set in 0.61 m x 0.61 m x 1.2 m (2 ft. x 2 ft. x 4 ft.) concrete footings. A typical arch is filled with concrete at the apex through a 76 mm (3-in hole). The spliced arches were filled from the side with 41.4 MPa (6000 psi) self-consolidating concrete using two holes as close to the collar as possible, each connected to a trough. It should be noted that the holes for fill were drilled lower than specified, below mid cross-section LVDTs were used during filling at the shoulders and apex to record deflections due to filling loads. Substantial voids were discovered after filling in the arch shoulders. This is likely due to concrete hardening prior to final arch filling.

Additional 25 mm (1-in) diameter fill holes were drilled on the shoulder of each arch to fill the arch voids with grout.



Figure 6.1: Arch setup for filling with concrete from the side.

### 6.3 Spliced Arch Testing

After proper concrete curing, the two specimens were tested to failure to determine the ultimate capacity of the spliced arches. The spliced arch test setup was similar to a standard arch as used by Bannon (2009) to allow comparison with his arch test results (Dagher et al. 2012).

The arches had 9-51 mm (2-in.) long strain gauges on the CFFT shell and 3-3mm (1/8-in.) long strain gauges at the tension most rebar in the splice cage. The gauges were placed similar to the beam tests setup (i.e. at each location, one in the compression face, one near the neutral axis, and a third one at the tension face). Additionally, a total of 5-26-in. string pots were used to estimate arch vertical deflection, including two at the foundation to estimate base rotation. Figure 6.2 below shows the instrumentation test setup

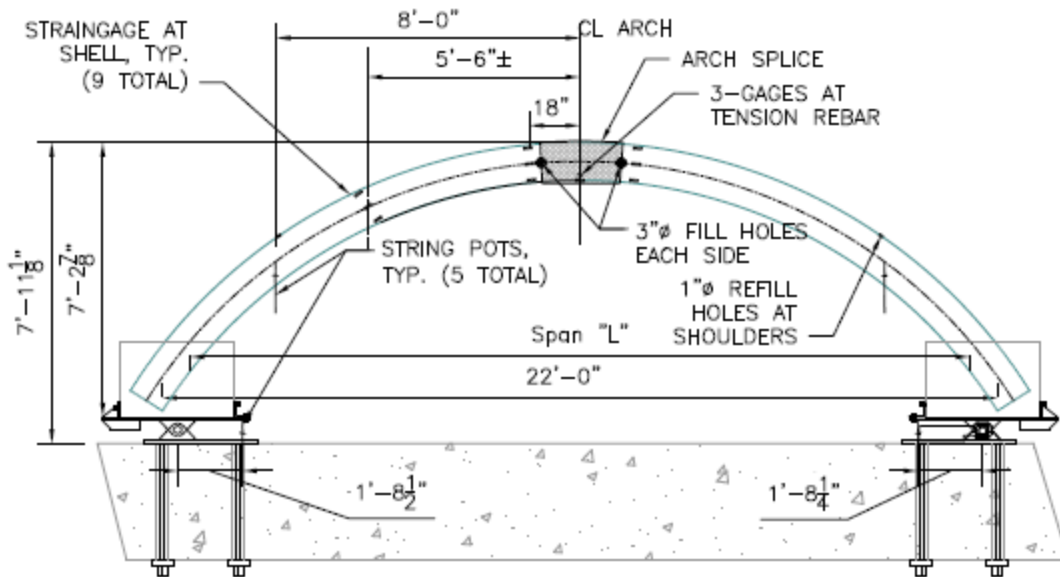


Figure 6.2: Arch Instrumentation setup (looking East).

As for the beam tests in Section 5, the arch test was setup to compare the overall collar effect on the splice. Arch #1 test represented the arch with the collar intact, and Arch#2 test represented the arch with the cut collar at centerline.

During testing, Arch #1 was unloaded and reloaded due to data acquisition error. Only instrumentation data from the re-loading is available, at which point the concrete had already cracked, so no cracked strains were recorded. Based on Figure 6.3, however, one can say that this re-loading did not affect the load displacement relationship for Arch #1.

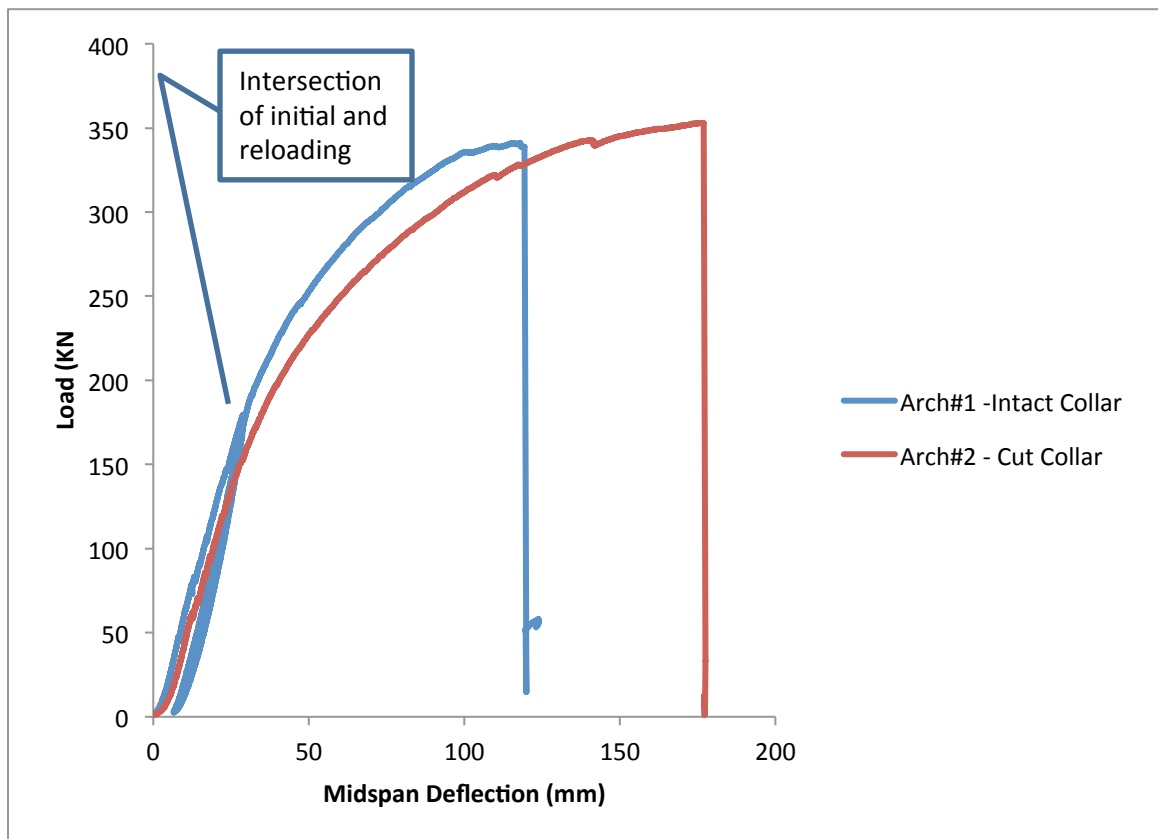


Figure 6.3: Actuator Load-Displacement relationship for each arch.

Arch #1 failed at the North shoulder at the location of the 1" diameter hole (See Figure 6.4) due to shell tension rupture. Arch #2, had slightly higher load capacity, and also failed at same shoulder location.



Figure 6.4: Arch#1 Failure Mechanism.

Note that the crown displacement was expected to be more for Arch #1 with the collar intact than for Arch#2 with the cut collar as occurred in the beam's test (refer to Figure 5.32); However, this was not the case for these tests, and one can infer that Arch #1 failed prematurely, the main reasons being:

- a) Loading was not symmetric since the arch base rotations occurred in the same directions instead of opposite to each other( see Figure 6.7), and the arch shifted North at failure.
- b) Failure initiated exactly at the fill hole location where stress concentrations are the higher.
- c) As will be discussed later in this section (see Figure 6.11), strains at the shoulder were low and not close to tension failure.

Figure 6.5 shows the cut collar behavior of Arch#2. As it was being loaded, the tension face of the arch at the crown was spreading reaching about 38mm (1.5-in) at failure. This represents the ductile behavior of the arch at the crown as the rebar in the cage yields.

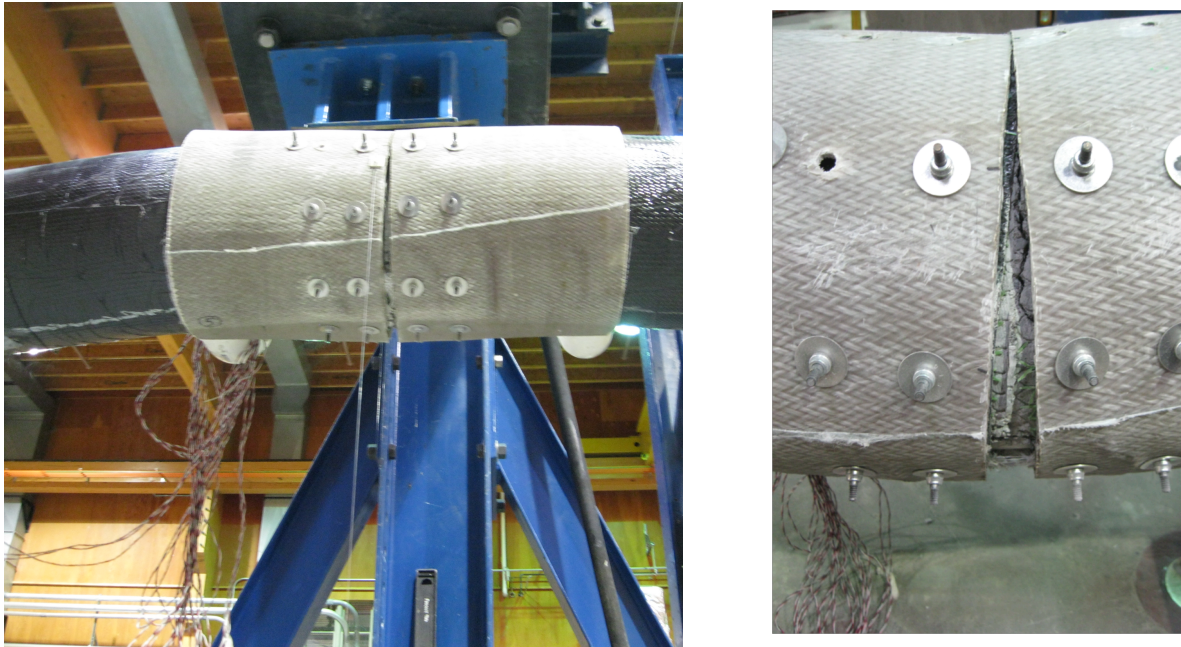


Figure 6.5: Arch#2 Splice behavior at crown with Close-up of Spreading Cut Collar.

The following figures show deformation and base rotation behavior, respectively, for the spliced arches. Note that at the crown (Figure 6.6), Arch#2 deformed vertically 27.5% more than Arch#1 (172 mm versus 100 mm). The reason for the smaller deflection of Arch#1 at the crown is believed to be due to premature failure and will be thus discussed no further. When comparing spliced arch deflections to those un-spliced tests in Bannon's (2009), the spliced arches should be more ductile. Crown maximum deformations on the previous un-spliced arch tests were about 102 mm (4-in), versus a 173mm (6.8-in) deflection for the spliced test with cut

collar in Arch#2. At the shoulder, there was no significant difference on the vertical deformation within the spliced arches tested in this report and the previously un-spliced tested ones.

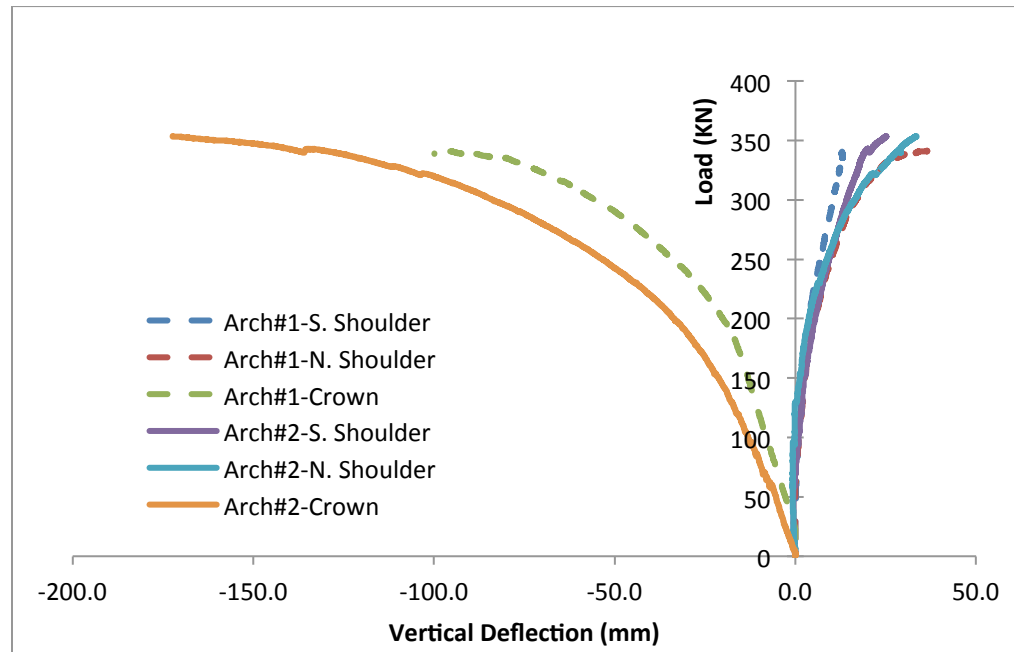


Figure 6.6: Applied Load vs. Vertical Deformation for Spliced Arches.

Figure 6.7 shows rotation behavior of the arches as they are being loaded. One can see the unsymmetrical loading behavior of Arch#1 when looking at the opposing rotations between North and South bases. As discussed, this unsymmetric behavior is likely the cause for this arch failing at lower loads and crown displacements than Arch #2, whose behavior is symmetrical and produced end rotations at failure within 20% of each other (2.8 deg. versus 3.5 deg), averaging 3.2 deg. When comparing this average end rotation to Bannon's (2009), the spliced Arch#2 rotated 75% more than the similar un-spliced arches previously tested (maximum average end rotation estimated at 1.8 deg).

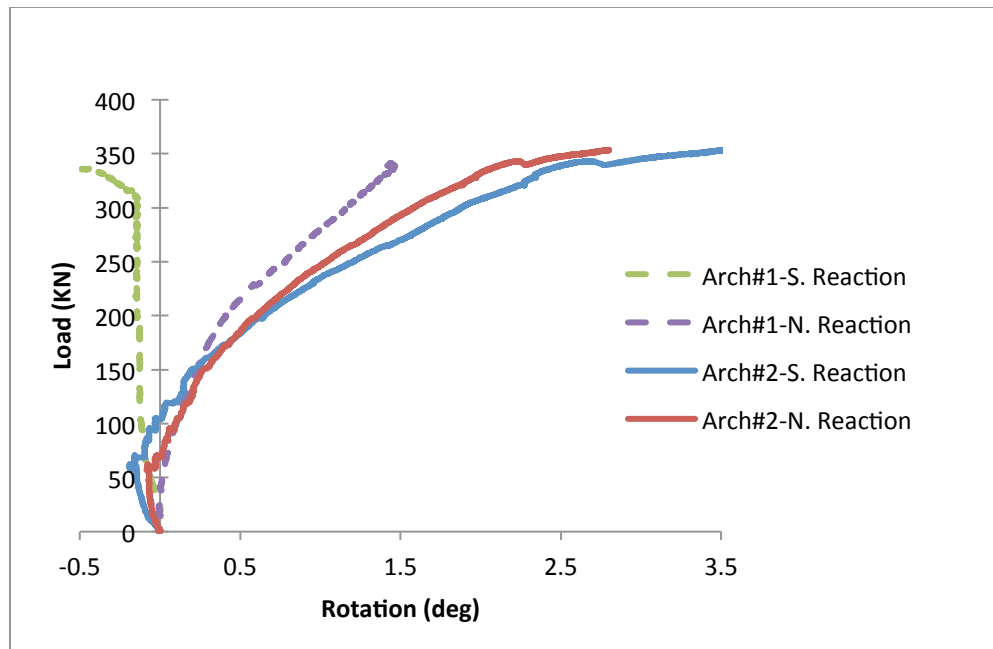


Figure 6.7: Applied Load vs. End Rotation for Spliced Arches.

Strain gage data either side of the splice is shown in Figure 6.8 for the arch with the collar intact (Arch#1), and Figure 6.9 for the cut collar arch (Arch#2). Strains labeled '1' were positioned at the top of the arch (compression face), strains '2' were near the neutral axis face, and Strains 3 at the bottom or tension face near the crown.

From Figure 6.8 one can see that although the compressions stresses were rather uniform likely due to the arch axial load effect during loading, the tension stresses were higher on the North side (where the arch ultimately failed). Note that strains do not capture the concrete cracking strain in Arch#1 since data collection was taken during re-loading of the arch as previously stated.

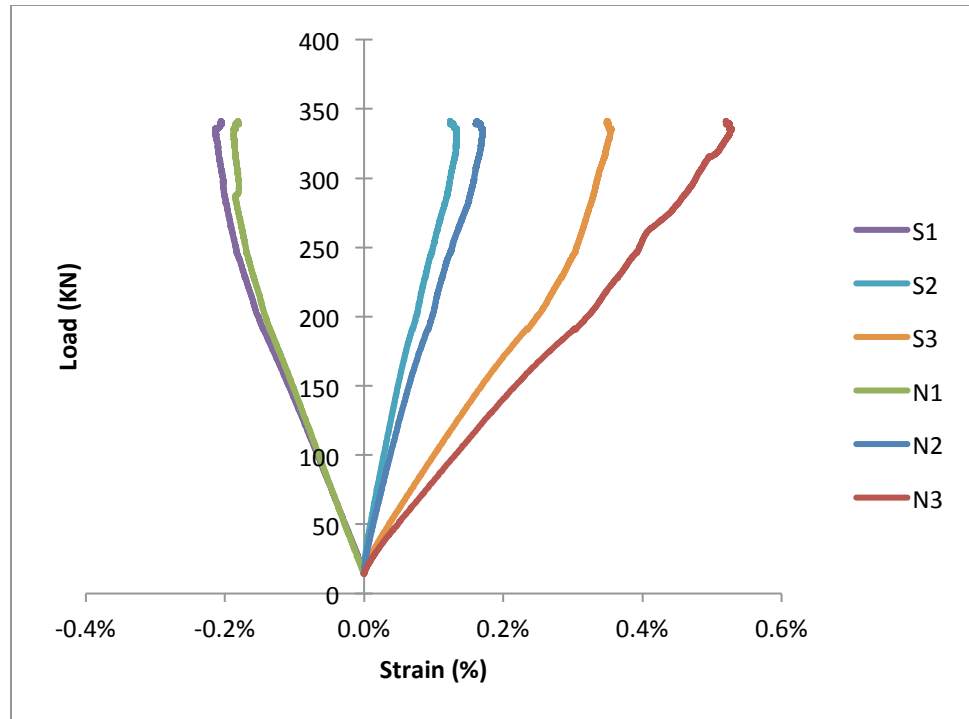


Figure 6.8: Applied Load versus Cross Section Strain North (N) and South (S) of the Splice for Arch#1.

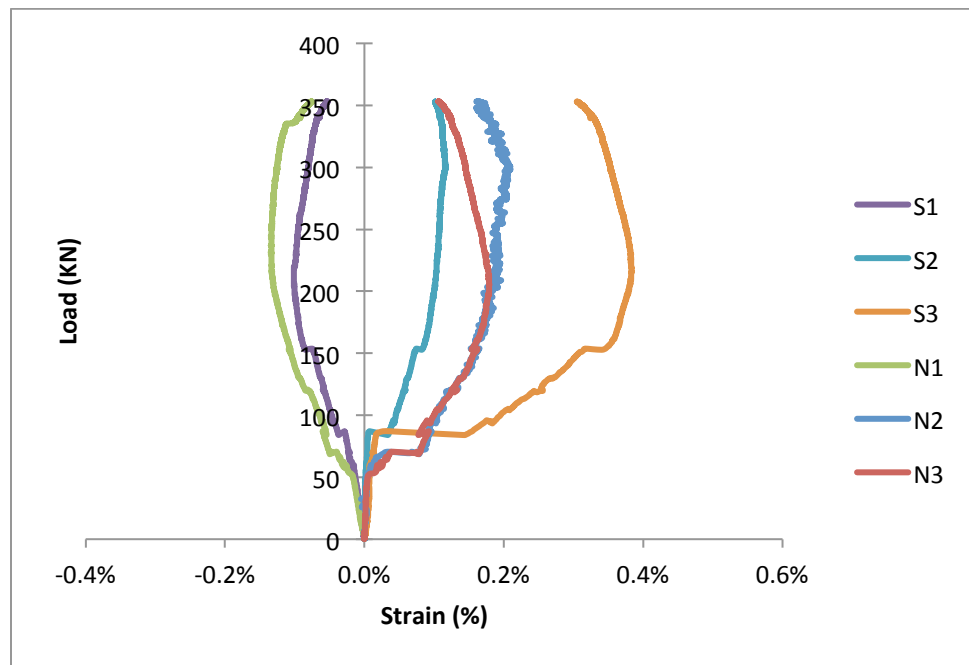


Figure 6.9: Applied Load versus Cross Section Strain North (N) and South (S) of the Splice for Arch#2.

Figure 6.9 captures the load at which the concrete cracks for Arch#2, with cracking initiating about 70 kN (15.7 kips) 18" North of the splice, and about 87 kN (19.6 kips) 457 mm(18-in) South of the splice. This data correlates well with the un-spliced arch data from Bannon (2009), with the load producing concrete cracking in the order of 16 kips (72 kN) to 21 kips (93 kN) depending on the specimen. Note that the strains were more linear for the spliced arch with the collar in place. This is because the intact collar with the rivets provides additional continuity to the FRP shell stresses even during rivet bearing failure.

Although both arches were instrumented at the tension most rebar within the splice, the gages were damaged during test setup for Arch#2 and no data is available. Figure 6.10 shows how the tension rebar started to yield for Arch #1 at about 0.3% strain to about 1.25%, at which point strain hardening occurred. The strain gages failed between 0.5% and 2.4%.

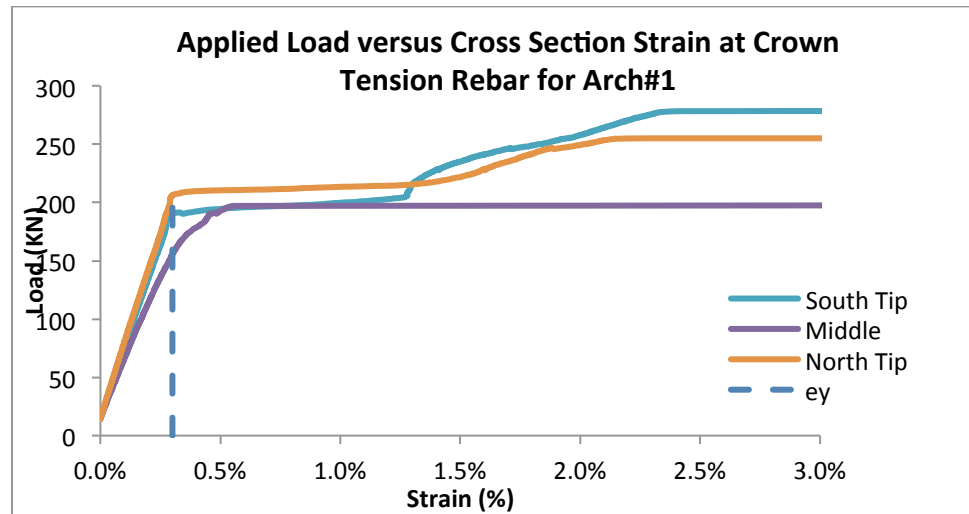


Figure 6.10: Applied Load versus Cross Section Strain at Crown Tension Rebar for Arch#1.

Note that the stresses in the tension rebar were over 4 times higher than those in the tension side of the FRP shell (2.4% versus 0.53% respectively), implying a strain discontinuity due to concrete cracking and debonding from the shell with rebar full tension engagement. Although not measured, this discontinuity (strain gap) is expected to be worst for Arch #2, since it had a larger load capacity, and maximum tension shell strains were smaller than for Arch#1, measured at 0.38%.

Figure 6.11 shows the similarity between the applied load versus strain relationship at the North shoulder and Neutral axis for both arches. Although the tension strain '1' data appears different between specimens, the strain gage for Arch#2 failed at 0.52% and so data beyond 297kN (66.8 kips) is not valid for Arch#1 (Collar Intact) and Arch#2 (with Cut Collar).

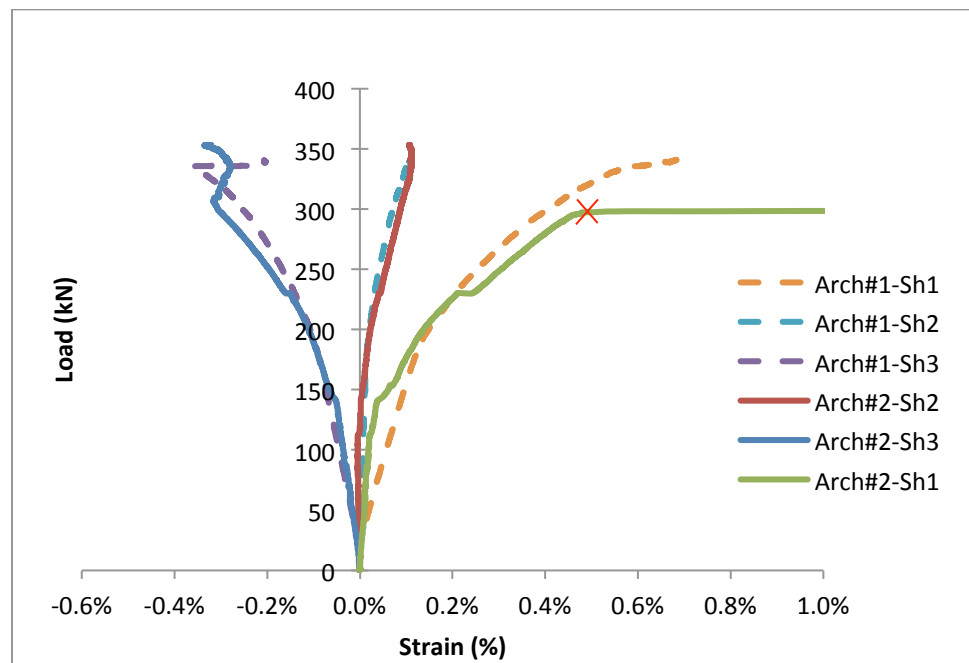


Figure 6.11: Applied Load versus Cross Section Strain at North Shoulder.

Given that the FRP shell ultimate tension strain failure was estimated at 2% (Bannon, 2009), Arch #1 strains were measured at 0.70% near the vicinity of failure, implying a large stress concentration due to 1" fill hole at tension face. Hole stress concentrations based on these measurements are thus likely tripled than if no hole was present.

#### **6.4 Summary of Arch Test Results**

The arch tests experimentally validated the ability of the splice to carry loads that exceed a similar un-spliced arch. A summary of the results from the arch tests as compared to Bannon's (2009) maximum experimental values (here referred to as Control) is shown in Table 5.2. Thus, the splice with internal rebar connection with or without a cut collar is an adequate splice for arches and provides bending strength that exceeds that of an equivalent un-spliced arch. Moreover, it provides additional ductility that might be desirable in some design scenarios. This ductility could not be verified For Arch#1 due to premature failure mainly attributed to non-symmetric arch response during loading, and fill hole location on tension face of CFFT arch shoulder.

Table 6.1: Summary of the CFFT Arch tests

<b>Specimen</b>	<b>Peak Load kN(kip)</b>	<b>Calculated Moment kN-m(kip-in)</b>	<b>Deformation at crown mm (in)</b>	<b>Failure Mode/Comments</b>
Control*	332.3 (74.7)	168.3 (1489)	97 (3.8)	FRP tension rupture at crown
Arch#1- Intact Collar	341.0 (76.7)	172.7 (1529)	100 (3.9)	FRP tension rupture at shoulder- premature failure
Arch#2-Cut Collar	353.1 (79.4)	178.8 (1583)	172 (6.8)	FRP tension rupture at shoulder

\*Based on Bannon's (2009) arch tests with maximum Peak Load (Arch010)

## **CHAPTER 7 CONCLUSIONS AND RECOMMENDATIONS**

### **7.1 Conclusions**

The mechanical fastener bearing strength tests of individual material components used in CFFT construction allowed for characterization of dowel bearing strength of the hybrid material. It was observed when comparing the individual material layers in bearing versus the hybrid layup response that the combination increases bearing strength by 27% more than the sum of the strength of the individual layers. Increasing edge distance beyond the code-recommended minimum value did not substantially increase the maximum bearing strength or the deformation to failure. Bearing failure was observed in all fastener tests. The fastener tests conducted with actual splice condition specimens had combined failure mode of bearing and fastener pull-through. Although ARAMIS digital imaging correlation was used to determine strains over the surface area of the connection for a limited number of specimens, load sharing between fasteners could not be

observed from the strain data. Increasing the number of fasteners did increase the peak load.

The pullout tests determined the ACI equations for development length are conservative for Carbon Fiber Composite Cable (CFCC) since embedment lengths reached over 200% predicted pullout capacity in all four tests. Pullout failures were observed in all four-test specimens. The highest stress in the bar only reached 1.87 kN/mm<sup>2</sup> (270 ksi), 70% of the ultimate tensile strength, 2.69 kN/mm<sup>2</sup> (390 ksi), provided by Tokyo Rope, Inc.

The collar design tested in the hollow beam test, nine rows of two fasteners on both sides of the arch splice, proved effective at carrying the construction filling loads. The proposed design carried the 1.6 and 2 times the service load moment and shear expected during field filling of a typical 305 mm (12-in) diameter arch, respectively. This splice was then used to manufacture six spliced beams and two spliced arches.

The tests of spliced CFFT beams experimentally validated the ability of the internally steel reinforced splice cage (6-#6 with #4 spiral) to carry long-term dead and live loads without contribution from the external collar, although the complete collar and internal rebar connection working together maintain the best results in replicating a typical carbon CFFT beam.

The tests of filled CFFT arches also experimentally validated the ability of the internally steel reinforced splice cage to carry long-term dead and live loads without contribution from the external collar, although it could not validate the expected better performance of the full intact collar splice due to arch premature failure.

Premature failure was attributed to non-symmetric arch response during loading and fill hole location on tension face of CFFT arch shoulder.

## **7.2 Recommendations for use and in draft specifications**

Mechanical fastener testing indicates that the minimum edge distance and spacing recommended by LRFD Final Pre-standard for Pultruded Sections, 32 mm (1.25-in), for edge distance and 64 mm (2.5-in) for spacing should be used for the collar. A minimum of two fasteners in a row should be conservatively used in design. If different fasteners or the arch materials are to be used in a spliced arch, mechanical fastener testing should be conducted again to determine bearing capacity of the new system. Traditional design methods and specifications can be used for an internal steel or glass FRP reinforcing cage.

CFCC's lightweight, flexibility, and durability make it a good candidate for future arch splices and to market an all FRP bridge system. Due to time and material constraints steel rebar was chosen for use in the beam and arch tests. Further beam and development length testing should be conducted using CFCC before implementation to validate and optimize splice designs using CFCC.

After straight beams were manufactured, and hollow beams tested for collar strength, it was recommended to use the splice with a CFFT arch. To maintain the correct arch shape during manufacturing the infusion formwork should be utilized.

The filled beam and arch testing indicates that designing the internally reinforced splice as a beam-column per AASHTO specifications will ensure a structurally adequate connection for long-term dead and live loads.

Fill holes on the arches when voids are encountered should not be located on the tension extreme fiber location for any load scenarios. It is recommended that fill holes are drilled as close to the neutral axis as possible and pressure grout injected to prevent any shell stress concentrations that could result in premature failure.

### **7.3 Future Work**

Additional efforts should focus on manufacturing and testing spliced beam specimens using CFCC reinforcing. Further, refinement of the collar connection to minimize fasteners and permit filling from a hole at the top of the arch should be investigated.

## REFERENCES

- AASHTO (2012). AASHTO LRFD Guide Specifications for Design of Concrete-Filled FRP Tubes for Flexural and Axial Members, AASHTO: 53.
- ACI 318 (2008). Building Code Requirements for Structural Concrete. ACI 318-08. Farmington Hills, MI, American Concrete Institute.
- ACI 440 (2006). Guide for the Design and Construction of Structural Concrete Reinforced with FRP Bars. ACI440.1R-06. Farmington Hills, MI, American Concrete Institute: 44.
- ASCE (2010). Pre-Standard for Load & Resistance Factor Design (LRFD) of Pultruded Fiber Reinforced Polymer(FRP) Structures (FINAL), American Composites Manufacturers Association (ACMA): 215.
- ASTM International. (2010). Standard Test Method for Bearing Strength of Plastics. D953-10. West Conshohocken, PA, ASTM International: 6.
- ASTM International. (2012). Standard Test Method for Compressive Strength of Concrete Cylindrical Concrete Specimens. C39/C39-M-12a. West Conshohocken, PA, ASTM International: 7.
- ASTM International. (2013). Standard Test Method for Pullout Strength of Hardened Concrete. C900-13. West Conshohocken, PA, ASTM International: 10.
- Bannon, D. J. (2009). Characterization of Concrete-Filled Fiber Reinforced Polymer Arch Members. Civil Engineering. Maine, University of Maine. **Master of Science**: 241.
- Berube, K.A., Lopez-Anido, R.A., and Caccese, V., "Integrated Monitoring System for Carbon Composite Strands in the Penobscot-Narrows Cable-Stayed Bridge," Transportation Research Record: Journal of the Transportation Research Board, No. 2050, pp. 177-186, 2008.
- Dagher, H.J., Bannon, D., Davids, W.G., Lopez-Anido, R.A., Nagy, E., and Goslin, K., "Bending Behavior of Concrete-Filled Tubular FRP Arches for Bridge Structures," Construction & Building Materials, (37): 432-439, 2012.
- Domenico, N. G. (1995). Bond Properties of CFCC Pre-stressing Strands in Pre-tensioned Concrete Beams. Civil Engineering. University of Manitoba. **Master of Science**: 171.
- Grace, N. F., T. Enomoto, et al. (2006). "Use of CFRP/CFCC Reinforcement in Pre-stressed Concrete Box-Beam Bridges." ACI Structural Journal: 10.
- Mahmoud, Z. I. (1997). BOND CHARACTERISTICS OF FIBRE REINFORCED POLYMERS PRESTRESSING REINFORCEMENT. Civil Engineering. Egypt, Alexandria University. **Doctor of Philosophy**: 287.
- MaineDOT (2013). Post-Tensioned Carbon Fiber Composite Cable (CFCC), Little Pond Bridge, Route 302, Fryeburg, Maine. Technical Report Augusta, Maine, Maine Department of Transportation: 20

Tokyo Rope, Inc. (2011). CFCC Carbon Fiber Composite Cable. Tokyo, Japan.

Zhu, Z., I. Ahmad, et al. (2006). "Splicing of Precast Concrete-Filled FRP Tubes."  
Journal of Composites for Construction **10**(4): 12.

## **APPENDIX A: PULL OUT TEST FOR STEEL/GFRP**

### **A.1 Pullout test material and embedment lengths**

The rebar material used for the pullout test, include 13 mm (0.5-in) steel rebar, and 25 mm (1-in) E-glass fiber rebar. The steel rebar had an ultimate tensile strength of 413 MPa (60 ksi) and elastic modulus of 200 GPa (29000 ksi). The E-glass fiber rebar had an ultimate tensile strength of 552 MPa (80 ksi) and elastic modulus of 41 GPa (6000 ksi). The steel spiral was a 9.5 mm (3/8-in) bar with a 292 mm (11.5-in) diameter and 76 mm (3-in) pitch, the E-glass spiral was a 10 mm (3/8-in) bar with a 318 mm (12.5-in) diameter and 76 mm (3-in) pitch.

The actuator attachment varied depending on the rebar material. Methods used to grip the rebar specimens varied based on rebar type, and are described later.

The pullout test specimens incorporated two other reinforcing types, steel and E-glass fiber, embedded in concrete with an FRP outer shell. The test setup was similar to Chapter 3. One steel specimen and three E-glass fiber specimens were tested.

Interaction equations describing strength of a member under combined bending and compression per ACI 318 were used to design the splice using steel reinforcement. The steel bar development length was determined using ACI 318 section 12.2.2. It was tested with a 381 mm (15-in) embedment (development) length in concrete.

The three E-glass fiber specimens were tested with different embedment (development) lengths. The required embedment length was calculated as 457 mm per ACI 440 Equation A.1 given below.

$$l_e = \frac{\alpha \frac{f_{fr}}{\sqrt{f'_c}} - 340}{13.6 + \frac{C}{d_b}} d_b \quad \text{Equation A.1}$$

Where:

$d_b$  = bar diameter mm (in)

$C$  = minimum (spacing, cover dimension) mm (in)

$f'_c$  = concrete compressive strength MPa (psi)

$f_{fr}$  = the required bar stress in MPa (psi)

$l_e$  = embedment length of reinforcing bar in mm (in)

$\alpha$  = bar location modification factor assumed to be 1.0

The 457 mm embedment length is the value ACI 440 requires to allow the bar to develop a tensile force of 552 MPa (80 ksi), which corresponds to the factored design moment and axial load given previously. In addition, two longer embedment lengths of 610 mm (24-in) and 914 mm (36-in) were tested. This range of embedment lengths was chosen to permit comparison of measured and predicted capacities.

Table A.1: Summary of the Rebar Development Lengths Tested

TEST	Bar Material and Diameter	Embedment Length	Bar length needed	CFFT length	ACI Predicted Capacity
1	#4 Steel-13mm (0.5in)	38.1cm(15in)	1.52m(5ft)	2.13m(7ft)	50.7kN(11.4kip)
2	#8 E-Glass Fiber-25mm (1in)	91.4cm(36in)	1.52m(5ft)	3.05m(10ft)	239kN(53.7kip)
3	#8 E-Glass Fiber-25mm (1in)	61.0cm(24in)	1.52m(5ft)	3.05m(10ft)	190kN(42.7kip)
4	#8 E-Glass Fiber-25mm (1in)	45.7cm(18in)	1.52m(5ft)	2.44m(8ft)	165kN(37.2kip)

It is important to note that the different reinforcing materials have three different embedment lengths. This is due both to the different development length equation used for steel (ACI 318) as opposed to E-glass, and because of the more severe strength knockdown factors required by ACI 440 for E-glass reinforcement.

## **A.2 Steel Rebar Pullout tests**

The steel specimen was 2.4 m (7 ft.) long with a 13 mm (1/2-in) steel rebar embedded in 381 mm (15-in) in the concrete at each end of the tube. The rebar attached to the actuator and fixed end connection with a steel T-section welded to the rebar, Figure A.1. The specimen was tested to 42.5 kN (9.5 kip), unloaded, and the extensometers were removed to prevent damage to the instrumentation. The calculated capacity of the steel specimen based on its nominal yield strength was 50.7 kN (11.4 kip). The ultimate load reached by the specimen was 81.6 kN (18.3 kip). The failure of the steel specimen occurred at the welded connection where the rebar was attached to the connection plate, Figure A.2. Figure A.3 shows the load vs. deformation response of the steel specimen. The specimen behavior was typical of ductile steel. The curve was linear until slightly larger than expected yield capacity of 50.7 kN (11.4 kip). After yield, strain hardening of the steel occurred and the bar continued to gain strength until rupture. No pullout of the steel bar from the concrete was observed.

The strain gauges, extensometers, and LVDTs all recorded data during the test. The North and South LVDTs read a matching change in horizontal position of the CFFT of 18 mm (0.72-in) independent of the rebar. The extensometer placed on the south rebar, which was also the location of failure, read an overall change in

strain of 0.0037. The instrumentation was removed to before failure to prevent damage. Further analysis reviewing the strain data collected from the extensometer determined that the elastic modulus for the rebar was typical of steel reading 200 GPa (29140 ksi). The strains recorded by the gauges on the shell were very small. The maximum strain was 0.0012 recorded by gauge H3, the gauge placement is shown in Chapter 3.



Figure A.1: Steel T-plate to rebar connection.



Figure A.2: Failure of steel rebar at welded connection.

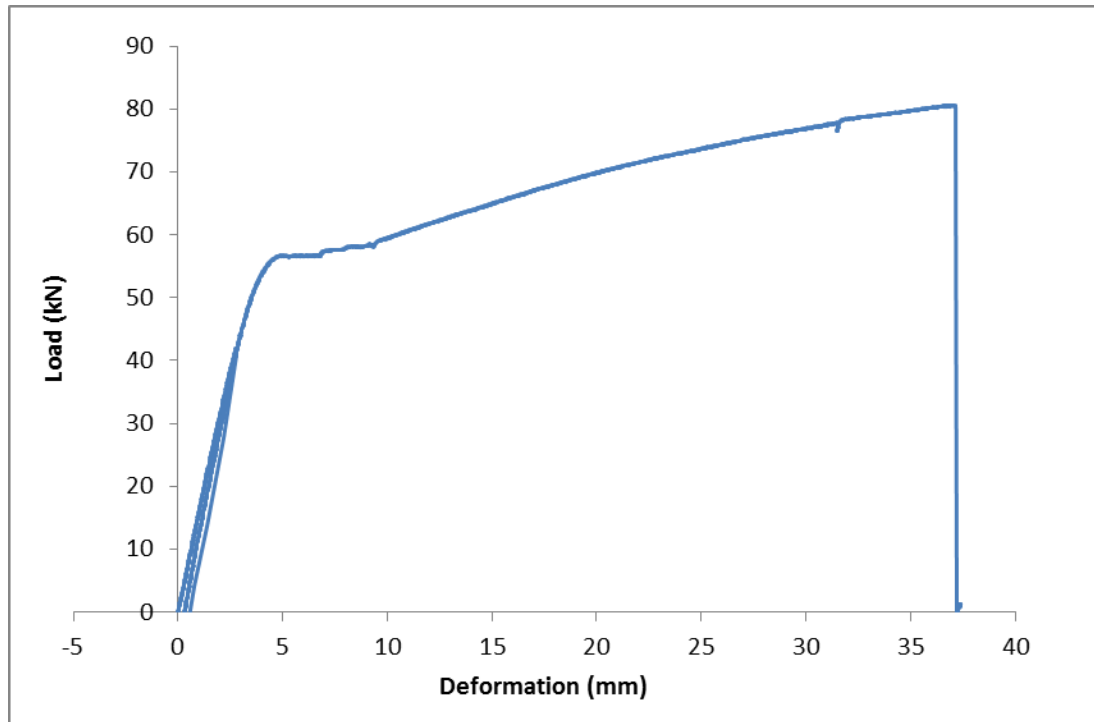


Figure A.3: Load vs. deformation plot for steel rebar pullout test.

### A.3 E-glass Fiber Rebar Pullout Tests

One of the obstacles to testing E-glass fiber rebar is properly gripping the specimen to test it in tension without damaging the bar. Various designs were discussed and two were tested for performance. The first option was a grouted steel pipe section with a welded flange attachment for connecting to the actuator. The grouted coupler was a variation of ASTM D7205. The grout used was Sikadur 30. The design in the standard was modified due to the high load expected during the test, the amount of rebar available for the coupler being less than the ASTM standard called for, and the availability of grout. The bar coupler length required by the standard was 457 mm (18-in) for a No. 8 bar, and the available length was 406 mm (16-in). The grout used in the coupler was an epoxy mortar.

Figure A.4 indicates the failure of mode the grouted coupler. The coupler capacity was initially assessed with a direct tension test on a 3.05 m (10 ft.) bar with couplers on both ends. The coupler failed by pulling from the grout at 221 kN (49.7 kip). The failure occurred below the 245 kN (55 kip) capacity needed to use it for the pullout testing.

The second coupler option considered was a steel mechanical coupler connection that sandwiched the rebar and attached to the actuator with a steel T-section. Figure A.5 shows the final mechanical coupler that was used for pullout testing. The coupler used a garolite liner attached to the inside of the steel with Pliogrip 7779 urethane adhesive to reduce high, localized contact stresses in the E-glass fiber bar produced by the slip critical connection. A 3.05 m (10 ft.) bar was tested with the mechanical connection on both sides and the bar failed in tension at 257 kN (57.8 kip). The mechanical coupler was chosen to be used for testing because it allowed for higher loads and was a more efficient system then the grout method. A summary of the coupler experimental capacities can be reviewed in Table A.2



Figure A.4: Left- Coupler attachment to E-glass bar  
Right- Failure of the bar pullout from grout.



Figure A.5: Mechanical coupler using two steel plates and a garolite and adhesive liner to grip the E-glass fiber rebar.

Table A.2: Summary of E-glass Fiber Coupler Tensions Test

Rebar Material	Development Length Tested mm(in)	Bar Diameter mm(in)	Embedment Material	Capacity Needed for Test kN(kip)	Failure Load kN(kip)	Failure Mode
E-glass fiber	356(14) [both ends]	25(1.0)	Sikadur30 Epoxy Grout	245(55)	221(49.7)	Bar Pulled from grout. No visible bar damage.
E-glass fiber	356(14) [both ends]	25(1.0)	Sikadur30 Epoxy Grout	245(55)	238(53.6)	Failure occurred between sand coating and rebar
E-glass fiber	305(12) [both ends]	25(1.0)	Mechanical Coupler	245(55)	257(57.8)	Bar failed in tension

The smallest E-glass fiber embedment length specimen tested was 2.44 m (8 ft.) long with a 457 mm (18-in) embedment length. One bar in the specimen was inclined at 10 degrees and it caused a failure close to the computed pullout capacity of 164kN(37.2 kip) but due to rupture of the bar instead of pullout. The specimen was loaded to 50% expected capacity, 84.1 kN (18.9 kip), unloaded and the extensometers removed. The failure occurred at 166 kN (37.5 kip) because of the bar shearing. The bar did not pullout from concrete. A picture of the original specimen and the failed rebar can be seen in Figure A.6. The maximum tension strain observed by the shell was 0.001 recorded by gauge H3. The LVDTs read a horizontal movement of the specimen of 18 mm (0.71-in) before failure.

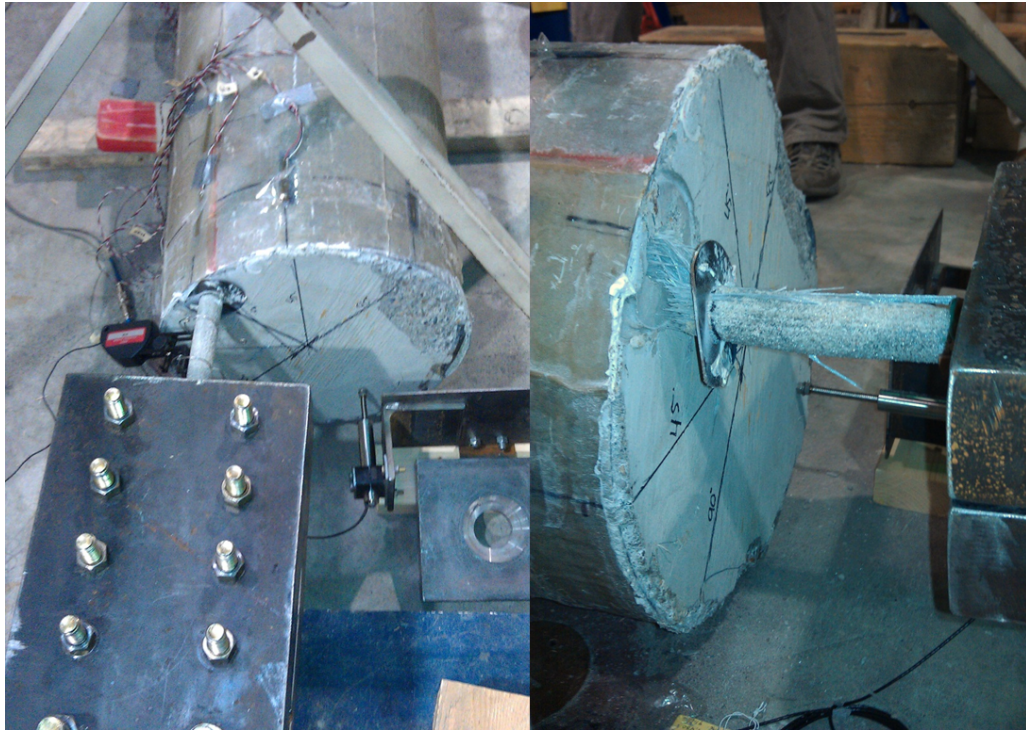
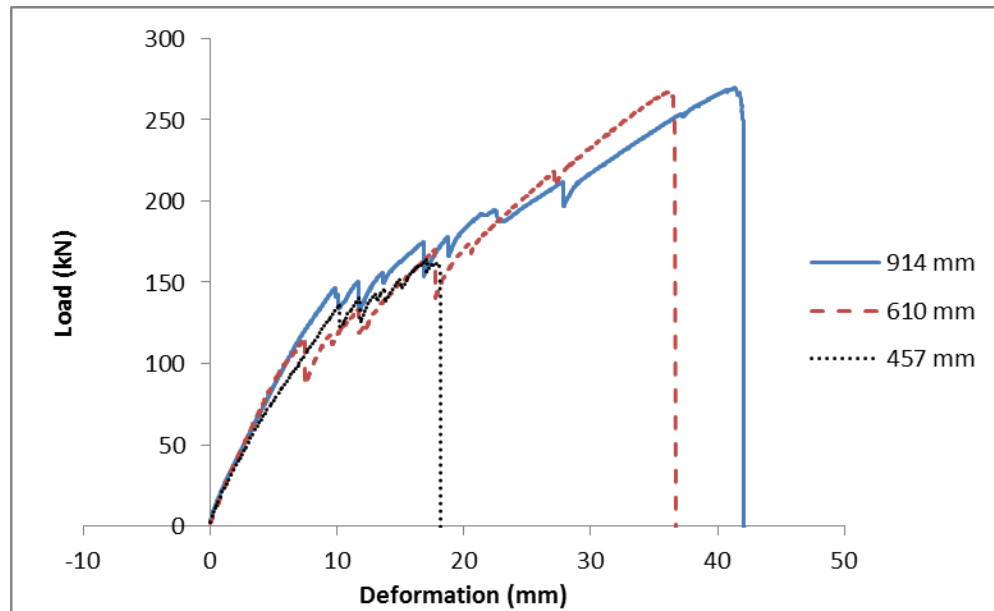


Figure A.6: 457 mm (18-in) E-glass fiber specimen  
Left- Before test Right- Bar combined shear and tension failure.

The next specimen was 3.05 m (10 ft.) long and had a 610 mm (24-in) embedment length. The expected capacity at this development length was 190 kN (42.7 kip). The bar was loaded to 94.3 kN (21.2 kip) and the extensometers were removed. The initial bar failure occurred from pulling out of the mechanical coupler at an ultimate load of 270 kN (60.7 kip). This failure induced a compression wave through the un-failed end of the bar causing the bar to fracture due to compression. There was no pullout of the bar from the concrete. The mechanical coupler was cleaned and reattached, and the specimen was retested. The retested failure occurred at 263 kN (59.1 kip). The failure mode was bar tensile rupture. The bar failure likely occurred at a lower load than the nominal UTS of 552 MPa (80 ksi) because of the initial compression fracture induced from the original test.

The longest E-glass fiber specimen was 3.05 m (10 ft.) long and tested a 914 mm (36-in) embedment length. The estimated capacity for the specified embedment length was 239 kN (53.7 kip). The specimen was loaded to 50% capacity, 116 kN (26.2 kip), unloaded, and the extensometers removed. The bar failed in tension at an ultimate load of 274 kN (61.6 kip) compared to a published ultimate tensile strength of 345.7 kN (77.7 kip). No pullout from concrete was observed. The maximum strain was 0.00018 recorded by gauge H3. The LVDTs read a horizontal movement of the specimen of 17.8 mm (0.7-in) before failure.

A comparison of the load deformation graphs for the three E-glass fiber embedment length specimens can be seen in FigureA.7. The graphs show that specimens tested exhibited similar, nearly linear load-deformation response, and that the 457 mm (18-in) specimen failed at about 50% of the capacity of the other two specimens. This was likely caused because of the misaligned bar.



FigureA.7: Load vs. deformation plot for E-glass bar specimens.

#### **A.4 Results and conclusions**

The steel pullout specimen confirmed the development length equation from ACI is adequate at the splice. The specimen behaved as predicted to reach both yield and rupture capacity based on the embedment length of concrete.

The E-glass fiber rebar tested to capacities higher than predicted by ACI 440, but the failure mode of bar pullout from concrete was not observed. The shortest embedment length specimen, 457 mm (18-in), failed due to the presence of bending and shear forces from a slightly eccentric load induced by the misaligned bar. The longer two specimens failed at almost the same load around 267 kN (60 kip) which proves the bond between the concrete and E-glass fiber bars was stronger than ACI predicted and again compares to a published ultimate tensile strength of the GFRP bar at 345.7 kN (77.7 kip).. Since the bars both failed around the same load it is possible that the mechanical coupler used for testing damaged the bars causing higher stresses and ultimately failure at the connection and not in the concrete. A summary of the pullout tests conducted on the steel and E-glass fiber bar is shown in Table A.3.

Table A.3: Summary of Steel and E-glass Fiber Embedment Length Test

Rebar Material	Development Length Tested mm(in)	Bar Diameter mm(in)	Embedment Material	ACI Predicted Capacity kN(kip)	Failure Load kN(kip)	Failure Mode
Steel	381(15)	12.7(0.5)	Self-Consolidating Concrete	50.7(11.4)	81.4(18.3)	Failure at welded connection
CFCC	381(15)	17.2(0.677)	Self-Consolidating	63.6(14.3)	122.8(27.6)	Bar pullout from concrete
E-glass fiber	457(18)	25.4(1.0)	Self-Consolidating Concrete	164(37.2)	166(37.5)	Bar shear/axial failure due to bar off center
E-glass fiber	610(24)	25.4(1.0)	Self-Consolidating Concrete	190(42.7)	270(60.7)	Bar pullout from mechanical coupler.
E-glass fiber	914(36)	25.4(1.0)	Self-Consolidating Concrete	239(53.7)	274(61.6)	Bar tension failure no concrete pullout

## APPENDIX B: CALCULATIONS FOR THE CFCC PULLOUT TEST

### Shear Design

Factored Shear Resistance	$V_R = \phi V_n$	AASHTO CFFT Guide Spec Draft, eq 2.11.2-1
Nominal Shear Resistance	$V_n = V_c + V_f + V_s$	AASHTO CFFT Guide Spec Draft, eq 2.11.2-2
Concrete Shear Strength	$V_c = 0.158 \cdot \sqrt{f'_c} \cdot A_c$	AASHTO CFFT Guide Spec Draft, eq 2.11.2-3
Concrete Compressive Strength	$f'_c := 5\text{ksi}$	Provided by AIT
Outer diameter of concrete	$D_o := 11.8\text{in}$	Based on definition of $A_c$ in AASHTO CFFT Spec Draft, section 2.11.2, states that $A_c$ may be calculated based on NA depth of $0.3D_o$ (p.31)
Concrete neutral axis	$NA_c := 0.3 \cdot D_o$ $NA_c = 3.54\text{ in}$ $\frac{11.8 - 3.54}{5.9} = 7.08$	
Determine Concrete Area	$A_c := 7.08\text{in} \cdot NA_c = 25.063 \cdot \text{in}^2$	
Determine Concrete Shear Strength (equation defined above)	$V_c := 0.158 \cdot \sqrt{\frac{f'_c}{\text{ksi}}} \cdot \text{ksi} \cdot A_c$	$V_c = 8.9\text{ kip}$
Tensile Hoop Stress, limited to	$f_{fe} = 0.004 \cdot E_{fh}$	AASHTO CFFT Guide Spec Draft, eq 2.11.2-5
Transverse Shear Required	$V_u \geq 0.5 \cdot \phi \cdot V_c$	AASHTO CFFT Guide Spec Draft, eq 2.11.3-1
Minimum Shear Tube Thickness	$t_{\min} = 0.0079 \cdot \frac{\sqrt{f'_c}}{f_{fuh}} \cdot D_o$	AASHTO CFFT Guide Spec Draft, eq 2.11.3-2
Spiral diameter	$d_{sp} := 7.5\text{mm}$	CFCC catalog
Ultimate Factored Shear Load	$V_u := 8.8\text{kip}$	Provided by AIT
Resistance factor for shear	$\phi := 0.75$	AASHTO CFFT Guide Spec Draft, 2.6.3.2
Minimum Shear Reinforcing	$V_{\min} := 0.5 \cdot V_c \cdot \phi$ $V_u = 8.8\text{ kip}$	$V_{\min} = 3.321 \cdot \text{kip}$ need reinforcing where $V_u$ is greater than $V_{\min}$
Elastic Modulus	$E_f := 22000\text{ksi}$	
Ultimate hoop stress	$f_{fuh} := 300\text{ksi}$	
Minimum thickness	$t_{\min} := 0.0079 \cdot \frac{\sqrt{\frac{f'_c}{\text{ksi}}} \cdot \text{ksi}}{f_{fuh}} \cdot D_o = 0.00069\text{ in}$	

**Shear Design**

Shear Resistance from Spiral  
(assuming spiral is perpendicular)  $V_f = \frac{A_{fv} \cdot f_{fv} \cdot d}{s}$  ACI 440, eq 9-2

Area of shear reinforcing  $A_{fv} := 2 \cdot (7.5\text{mm})^2 \cdot \frac{\pi}{4} = 0.137 \cdot \text{in}^2$

**Assume  $V_u = V_f$** 

Ultimate stress in FRP  $f_{fv} := 0.004 \cdot E_f = 88 \cdot \text{ksi}$  ACI 440, eq 9-3

**Distance of Max Compression to Max tension bar**

Using 6-12.5mm bars  $d_{12.5} := 11.8\text{in} - 0.75\text{in} - 7.5\text{mm} - \frac{12.5\text{mm}}{2} = 10.509 \text{ in}$

Using 6-15.2mm bars  $d_{15.2} := 11.8\text{in} - 0.75\text{in} - 7.5\text{mm} - \frac{15.2\text{mm}}{2} = 10.456 \text{ in}$

Using 6-17.2mm bars  $d_{17.2} := 11.8\text{in} - 0.75\text{in} - 7.5\text{mm} - \frac{17.2\text{mm}}{2} = 10.416 \text{ in}$

**Spacing needed for shear reinforcing**

Using 6-12.5mm bars  $s_{12.5} := \frac{A_{fv} \cdot f_{fv} \cdot d_{12.5}}{V_u} = 14.392 \text{ in}$

Using 6-15.2mm bars  $s_{15.2} := \frac{A_{fv} \cdot f_{fv} \cdot d_{15.2}}{V_u} = 14.319 \text{ in}$

Using 6-17.2mm bars  $s_{17.2} := \frac{A_{fv} \cdot f_{fv} \cdot d_{17.2}}{V_u} = 14.265 \text{ in}$

**Assume a 12" spiral length on either side for shear reinforcing,  
use a maximum 3" spacing**

**Development Length**

Bar diameter	$d_b := \begin{pmatrix} 12.5\text{mm} \\ 15.2\text{mm} \\ 17.2\text{mm} \end{pmatrix}$	From Tokyo Rope
Force equilibrium	$l_e \cdot \pi \cdot d_b \cdot u = A_f \cdot f_f$	ACI440 Ch. 11, eq 11-1 ACI440 Ch. 11, eq 11-2
Embedment length relationship (normaliized)	$\frac{u}{\sqrt{f_c}} = 4.0 + 0.3 \cdot \frac{C}{d_b} + 100 \frac{d_b}{l_e}$	ACI440 Ch. 11, eq 11-3
Development bar stress	$f_{fe} = \frac{\sqrt{f_c}}{\alpha} \left( 13.6 \cdot \frac{l_e}{d_b} + \frac{C}{d_b} \cdot \frac{l_e}{d_b} + 340 \right) \leq f_{fu}$	
Development length shall be no less than 20 bar diameters	$20 \cdot d_b = \begin{pmatrix} 9.843 \\ 11.969 \\ 13.543 \end{pmatrix} \cdot \text{in}$	ACI440 section 11.1
Bar location modification factor	$\alpha := 1.0$	ACI440 section 11.1.1
Minimum cover to center of bar, C Value	$C := 0.75\text{in} + 7.5\text{mm} + \frac{d_b}{2} = \begin{pmatrix} 1.291 \\ 1.344 \\ 1.384 \end{pmatrix} \cdot \text{in}$	
	$\frac{C}{d_b} = \begin{pmatrix} 2.624 \\ 2.247 \\ 2.044 \end{pmatrix}$	ACI440 section 11.1 ok cant be >3.5

**Development Stress**  $f_{fe} := 144\text{ksi}$   $f_{fe} \cdot 0.234\text{in}^2 = 33.696\text{-kip}$

Ultimate Tensile Stress in bar  $f_{fu} := 300\text{ksi}$

Stress to be developed  $f_{fr1} := \min(f_{fu}, f_{fe}) = 144\text{ksi}$

ACI440 section 11.3

Development length needed ACI440 eq 11-6

$$l_{d12} := \alpha \cdot \frac{\frac{f_{fr1}}{\text{psi}} - 340}{\sqrt{\frac{f_c}{\text{psi}} \cdot \text{psi}} \cdot \left( 13.6 + \frac{C_0}{d_{b0}} \right)} \cdot d_{b0}$$

$$l_{d15} := \alpha \cdot \frac{\frac{f_{fr1}}{\text{psi}} - 340}{\sqrt{\frac{f_c}{\text{psi}} \cdot \text{psi}} \cdot \left( 13.6 + \frac{C_1}{d_{b1}} \right)} \cdot d_{b1}$$

$$l_{d17} := \alpha \cdot \frac{\frac{f_{fr1}}{\text{psi}} - 340}{\sqrt{\frac{f_c}{\text{psi}} \cdot \text{psi}} \cdot \left( 13.6 + \frac{C_2}{d_{b2}} \right)} \cdot d_{b2}$$

$l_{d12} = 51.5\text{-in}$

$l_{d15} = 64.1\text{-in}$

$l_{d17} = 73.4\text{-in}$

**MODIFIED Development Length**

Development Stress	$f_{fe} := 144\text{ksi}$	Determined using strain compatibility
Bar Area	$A_b := \begin{pmatrix} 0.118\text{in}^2 \\ 0.179\text{in}^2 \\ 0.234\text{in}^2 \end{pmatrix}$	
Ultimate Tensile Stress in bar	$f_{fu} := 300\text{ksi}$	
Stress to be developed	$f_{fr1} := \min(f_{fu}, f_{fe}) = 144\text{ksi}$	

ACI440 section 11.3

Development length needed

ACI440 eq 11-6

$$l_{d12} := \frac{f_{fr1} - \pi \cdot 85 \cdot \frac{(d_{b0})^2}{A_{b0}} \cdot \sqrt{\frac{f_c}{\text{psi}} \cdot \text{psi}}}{\left(\frac{\pi \cdot d_{b0}}{A_{b0}}\right) \cdot \left(3.4 + 0.25 \cdot \frac{C_0}{d_{b0}}\right) \cdot \left(\sqrt{\frac{f_c}{\text{psi}} \cdot \text{psi}}\right)}$$

$l_{d12} = 28\text{-in}$

$$l_{d15} := \frac{f_{fr1} - \pi \cdot 85 \cdot \frac{(d_{b1})^2}{A_{b1}} \cdot \sqrt{\frac{f_c}{\text{psi}} \cdot \text{psi}}}{\left(\frac{\pi \cdot d_{b1}}{A_{b1}}\right) \cdot \left(3.4 + 0.25 \cdot \frac{C_1}{d_{b1}}\right) \cdot \left(\sqrt{\frac{f_c}{\text{psi}} \cdot \text{psi}}\right)}$$

$l_{d15} = 36.1\text{-in}$

Development length needed

$$l_{d17} := \frac{f_{fr1} - \pi \cdot 85 \cdot \frac{(d_{b2})^2}{A_{b2}} \cdot \sqrt{\frac{f_c}{\text{psi}} \cdot \text{psi}}}{\left(\frac{\pi \cdot d_{b2}}{A_{b2}}\right) \cdot \left(3.4 + 0.25 \cdot \frac{C_2}{d_{b2}}\right) \cdot \left(\sqrt{\frac{f_c}{\text{psi}} \cdot \text{psi}}\right)}$$

$l_{d17} = 42.6\text{-in}$

Verify development length

$$l_d \leq \frac{\phi M_n}{V_u} + l_a \quad \text{ACI440 eq 11-7}$$

Factored Nominal Moment

$\phi M_{n12} := 340\text{in-kip}$  From created interaction diagram  
 $\phi M_{n15} := 482\text{in-kip}$   
 $\phi M_{n17} := 602\text{in-kip}$

Ultimate shear at splice

$V_u := 8.8\text{kip}$  From AIT information

length beyond CL of support  
either depth of section or 12db  
whichever is greater

$$l_{a1} := \max(d_{12.5}, 12 \cdot 12.5 \text{mm}) = 10.509 \text{-in}$$

$$l_{a2} := \max(d_{15.2}, 12 \cdot 15.2 \text{mm}) = 10.456 \text{-in}$$

$$l_{a3} := \max(d_{17.2}, 12 \cdot 17.2 \text{mm}) = 10.416 \text{-in}$$

*For 6-12mm bars*

$$\frac{\phi M_{n12}}{V_u} + l_{a1} = 49.145 \text{-in}$$

*For 6-15mm bars*

$$\frac{\phi M_{n15}}{V_u} + l_{a2} = 65.228 \text{-in}$$

*For 6-17mm bars*

$$\frac{\phi M_{n17}}{V_u} + l_{a3} = 78.825 \text{-in}$$

All computed development lengths are less than max and therefore okay. The  $l_d$  values are all greater than 20db as well and therefore okay.

### APPENDIX C: MOMENT-%STRAIN PLOTS

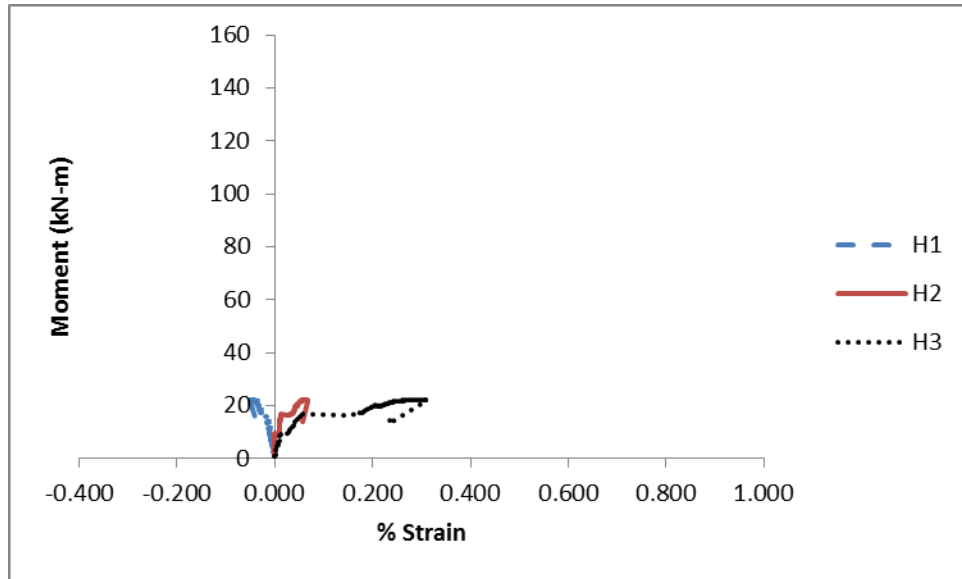


Figure C.1: Moment-% Strain plot for Tube B north end gauges.

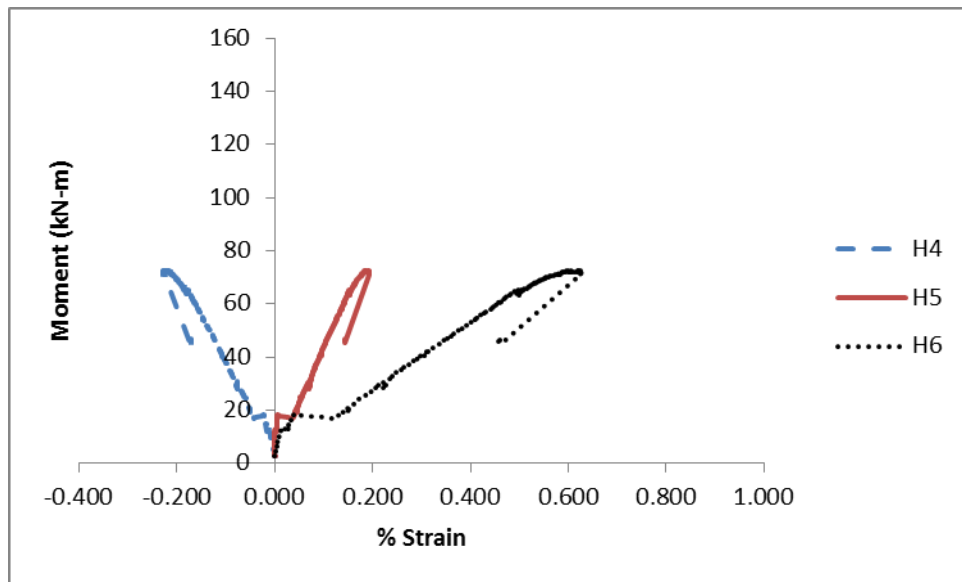


Figure C.2: Moment-% Strain plot for Tube B north end rebar gauges.

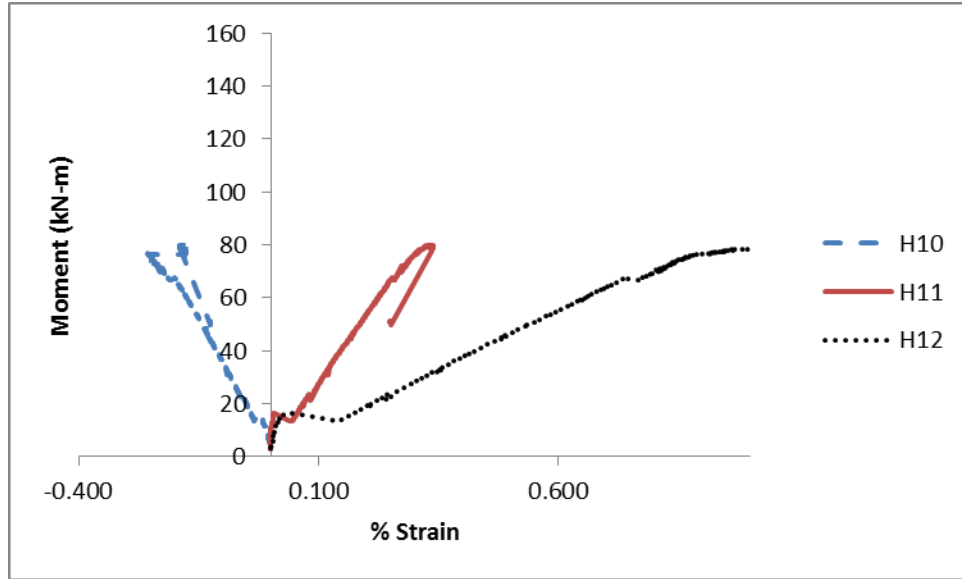


Figure C.3: Moment- % Strain plot for Tube B south end rebar gauges.

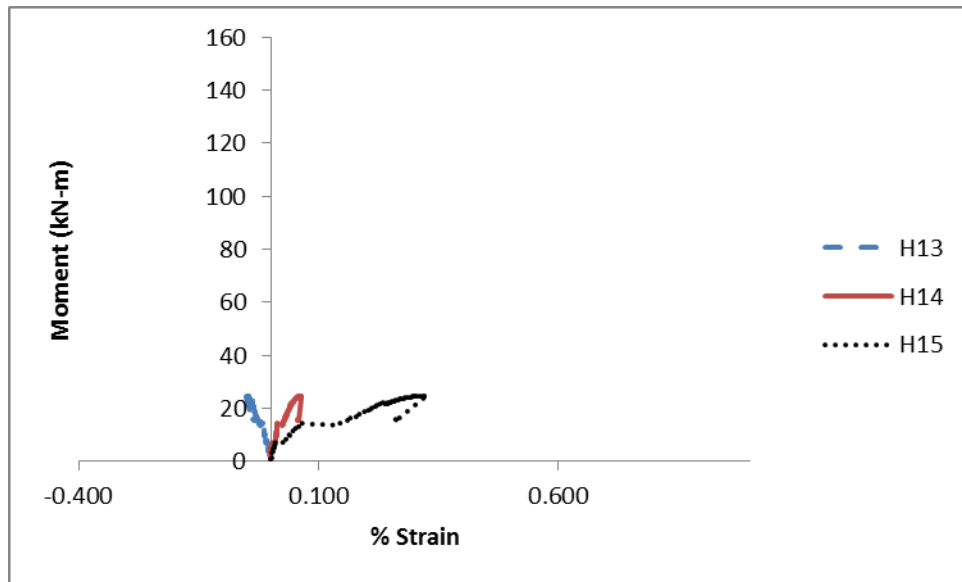


Figure C.4: Moment- % Strain plot for Tube B south end gauges.

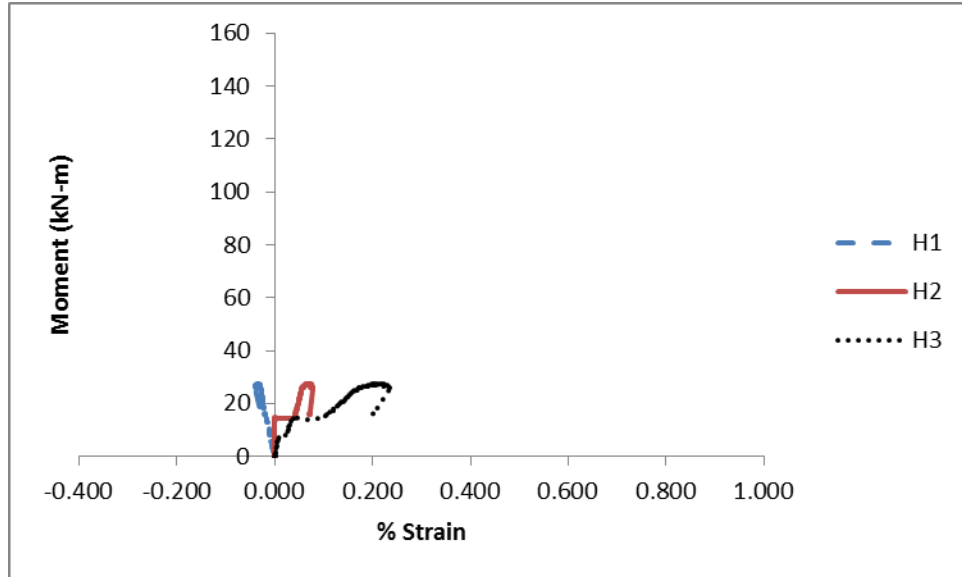


Figure C.5: Moment-% Strain plot for Tube C north end gauges.

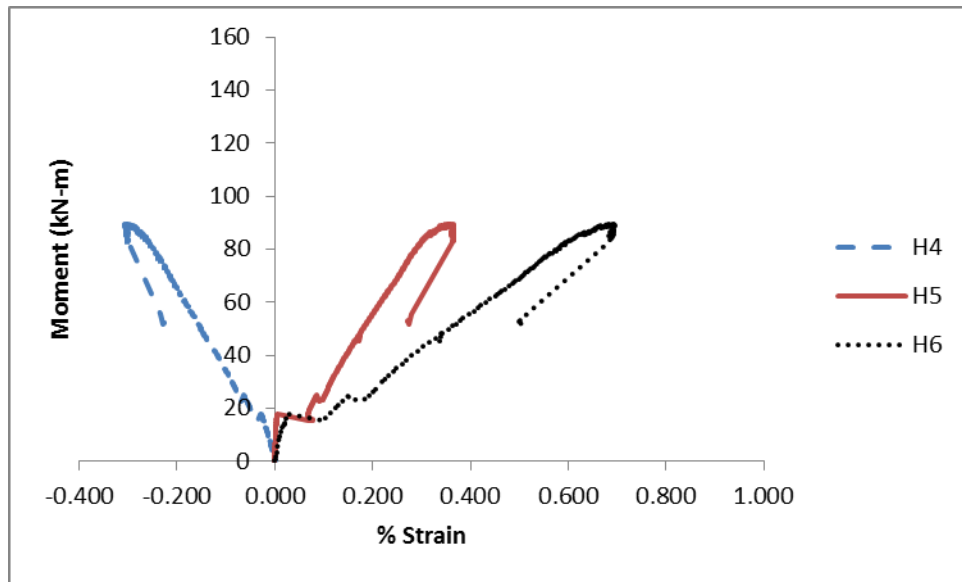


Figure C.6: Moment-% Strain plot for Tube C north end rebar gauges.

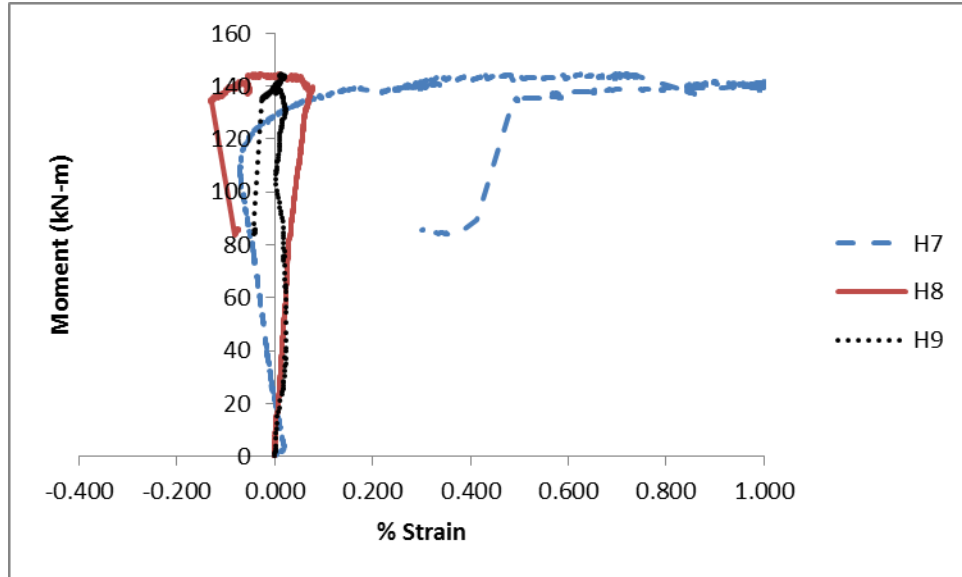


Figure C.7: Moment- % Strain plot for Tube C centerline (collar) gauges.

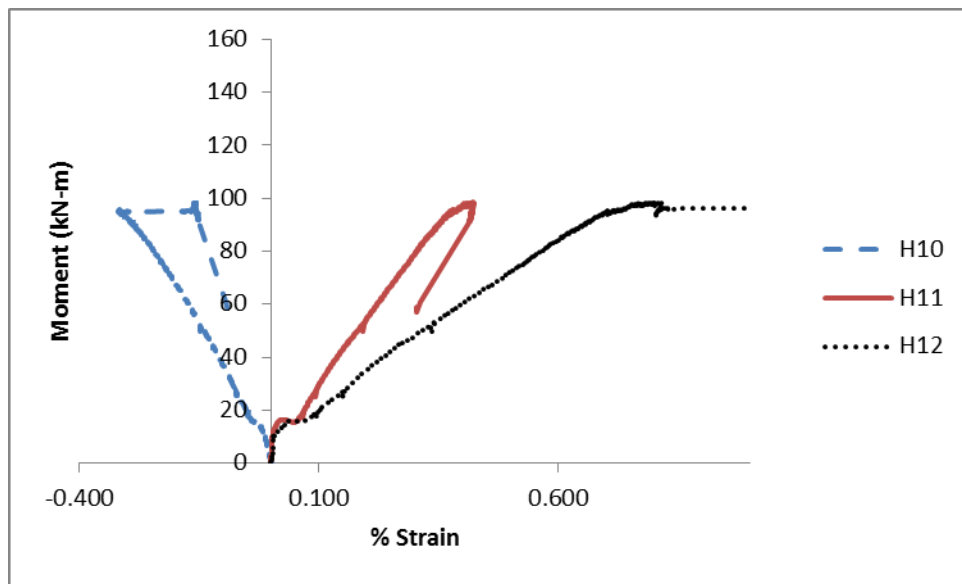


Figure C.8: Moment- % Strain plot for Tube C south end rebar gauges.

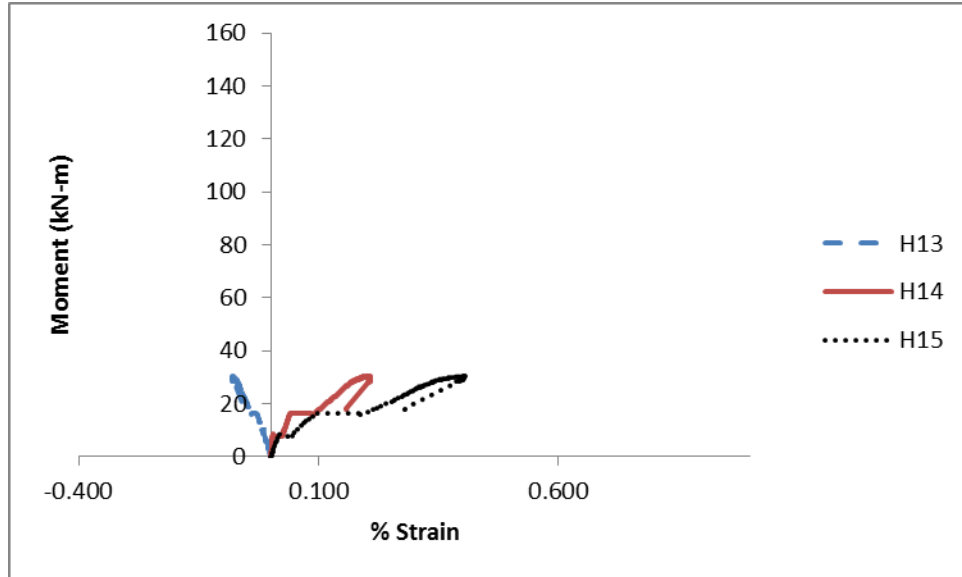


Figure C.9: Moment- % Strain plot for Tube C south end gauges.

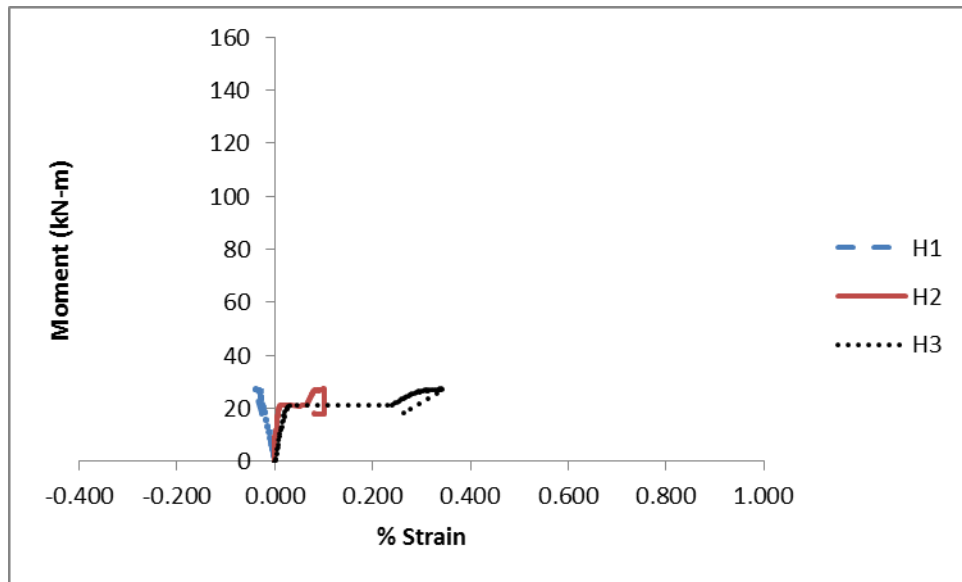


Figure C.10: Moment- % Strain plot for Tube F north end gauges.

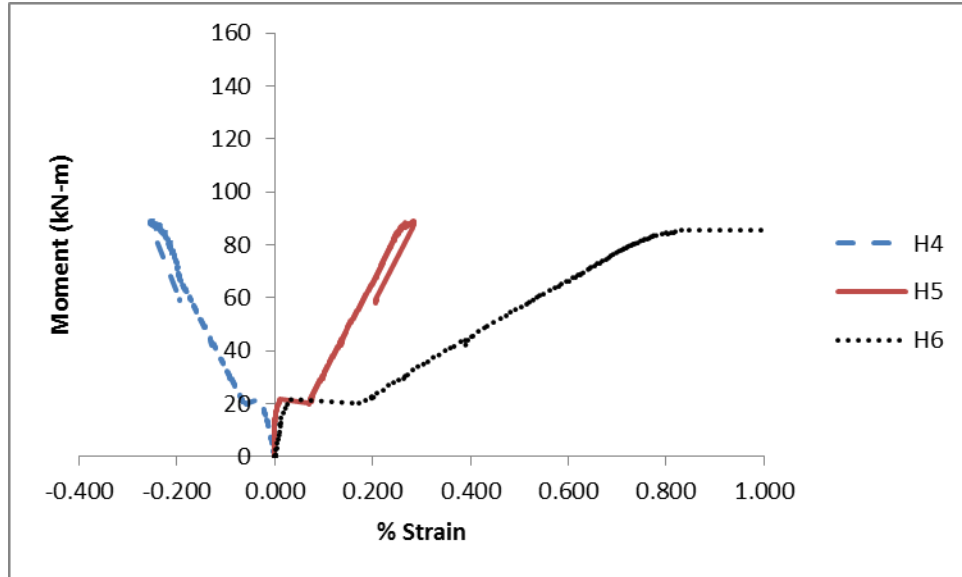


Figure C.11: Moment- % Strain plot for Tube F north end rebar gauges.

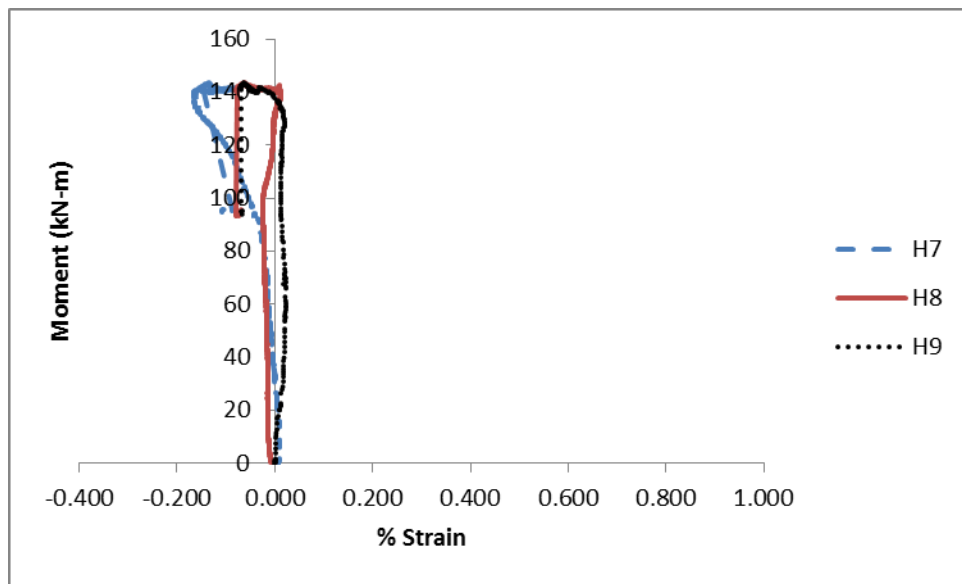


Figure C.12: Moment- % Strain plot for Tube F centerline (collar) gauges.

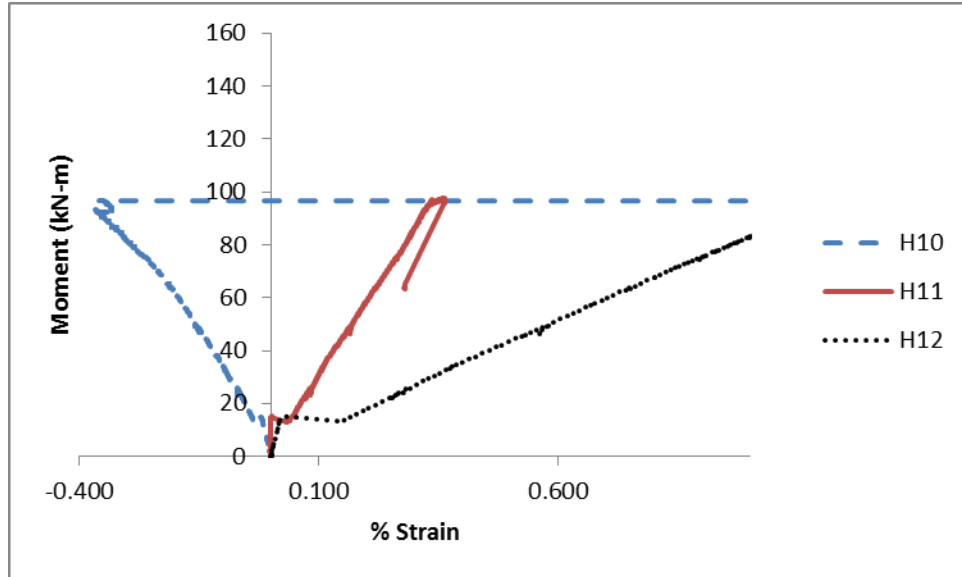


Figure C.13: Moment- % Strain plot for Tube F south end rebar gauges.

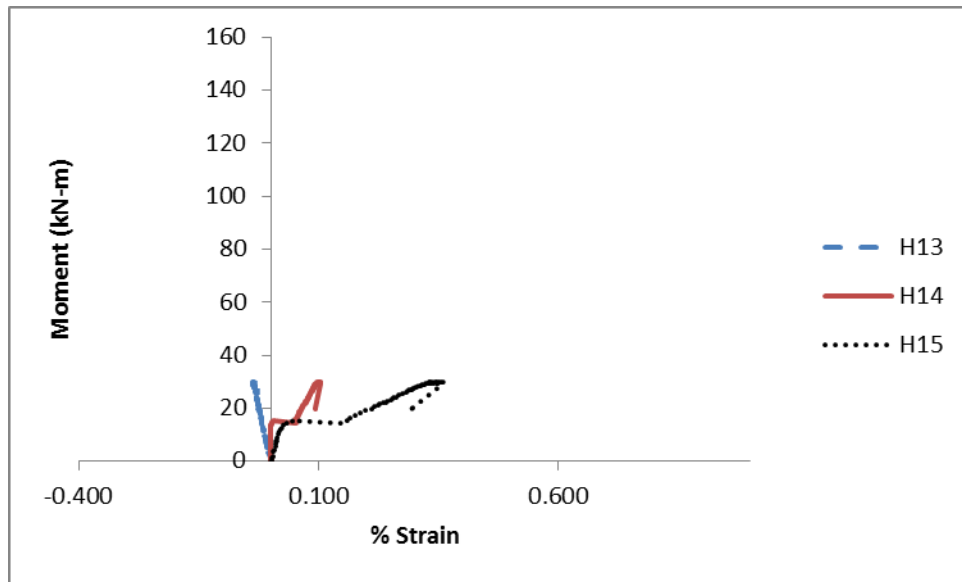


Figure C.14: Moment- % Strain plot for Tube F south end gauges.